2013

Frequency Selectivity of Synaptic Exocytosis in Hair Cells of the Bullfrog's Amphibian Papilla

Suchit H. Patel

FREQUENCY SELECTIVITY OF SYNAPTIC EXOCYTOSIS IN HAIR CELLS OF THE BULLFROG'S AMPHIBIAN PAPILLA

A Thesis Presented to the Faculty of

The Rockefeller University

in Partial Fulfillment of the Requirements for

the degree of Doctor of Philosophy

by

Suchit H. Patel

June 2013

FREQUENCY SELECTIVITY OF SYNAPTIC EXOCYTOSIS IN HAIR CELLS OF THE BULLFROG'S AMPHIBIAN PAPILLA

Suchit H. Patel, Ph.D.
The Rockefeller University 2013

Auditory organs act as spectral analyzers by decomposing acoustic stimuli into their frequency constituents. Individual auditory afferent neurons of the VIIIth cranial nerve respond best to a particular frequency of stimulation, and are thus frequency-tuned. Much of the tuning in the inner ears of mammals is ascribed to the frequency dependence of the traveling waves on the basilar membrane, the flexible structure that houses hair cells, the auditory receptors. However, in non-mammalian vertebrates, the basilar membrane does not conduct a traveling wave. In some animals, the membrane is absent entirely. Yet auditory fibers from these animals display comparable sharpness of tuning.

Though other tuning mechanisms have been characterized in these animals, they do not account for the observed sharpness found in auditory-nerve recordings. Hence, we explored the frequency response of the hair cell's synapse in the bullfrog's amphibian papilla, an auditory organ that lacks a basilar membrane. We monitored the synaptic output of hair cells by measuring changes in their membrane capacitance in response to sinusoidal electrical stimulation. Using perforated-patch recordings, we found that individual hair cells display frequency selectivity in synaptic exocytosis over the range of frequencies sensed by the organ. Moreover, this tuning varies from cell to cell in accordance with the cells' tonotopic position.

Using confocal imaging, we determined that hair cells tuned to high frequencies have a greater expression of the Ca^{2+} buffers parvalbumin 3 and calbindin-D28k than those tuned to low frequencies. We then used an extension of an existing model for synaptic release to explore how this gradient might influence the frequency response of the synapse. Increasing buffer concentration in the absence of other changes quenches free Ca^{2+} and thereby reduces the synaptic output. However, adjusting just one other release rate in conjunction could keep the system poised near a Hopf bifurcation, thereby keeping the system tuned with exquisite sensitivity to small stimuli at a particular frequency. Furthermore, the frequency range afforded by the model matched the hearing range of the organ.

Thus, hair cells of the bullfrog's amphibian papilla use synaptic tuning as an additional mechanism by which to sharpen their frequency selectivity, and a conspicuous gradient in Ca^{2+} buffering may help to keep the system poised near maximal sensitivity.

ACKNOWLEDGMENTS

To be able to study what one finds interesting solely because one finds it so is a true privilege. I would never have reached this point were it not for the support of so many colleagues, friends and family that have made the last few years such an enjoyable time. First, I would like to thank my parents for dedicating their lives to raising my sister and I in an environment that they embraced solely for our benefit. They pushed us to excel. Though my sister and I complain often of their lack of outward appreciation, it is obvious in the sacrifices they have made so that we could become greater than they are. That is a task I will find difficult to accomplish. Likewise difficult will be to emulate the caring and sincerity I have found in Jennifer, to whom I owe great thanks for being supportive of my enthusiasm when things worked and for keeping me sane when things didn't.

Next, I want to thank everyone that has led me down the road that brought me to this thesis. I was fortunate to have the tutelage of countless incredible teachers from my elementary education through college that fostered a sense of curiosity. My first experience with science—a silly experiment with raisins and Alka-Seltzer in seventh grade—still remains with me today. I want to thank my undergraduate advisors William Muller and Josefina Cubina for nudging me towards research. Moreover, I wish to thank Olaf Andersen for *accepting* me in the MD-PhD program. He, Jochen, Ruthie, Renee and Elaine make this program a fantastic place. Likewise, the Dean's office at Rockefeller has been nothing but exemplary in running things smoothly.

On a separate dimension, I must thank my fellow students and now colleagues for making this portion of my life enjoyable in ways I had not imagined. I am deeply humbled by the group of students and physicians I worked with at the Weill Cornell Community Clinic for their passion and their humanity. Likewise I owe thanks to Alessandra and Kaylan, and Jeff and the CTSC for helping me launch the Heart-to-Heart program and showing me that things besides science are also important and satisfying. In that regard, Jonathan Moreno has been an excellent co-pilot throughout my years here, for scientific and extracurricular discourse.

Though it took me four rotations to find the Hudspeth Lab, I am deeply satisfied and humbled that I discovered this marvelous group of people. I do not know whether it is by design or by chance, but within this lab I found an architecture surprisingly welcoming and unassuming. I am deeply indebted to Samuel Lagier and Jonathan A. N. Fisher for patiently teaching me how to conduct electrophysiology experiments, and how to deal with frustration when they do not work. Likewise, I am grateful to have found Daibhid Ó Maoiléidigh, an expert physicist and a good friend. The modeling work presented in these pages is more his work than mine. Josh Salvi was likewise very helpful with the immunolabeling work. A special thanks goes to Brian Fabella, the steward of the downstairs lab, for help with programming and technical work, and for keeping to the pact I made upon joining that decreed he could not leave the lab before I did. To my other daily conversation partners Kate, Fumiaki, Adria, Jason, I thank you for making my experience wonderful. To Aaron, Eliot and especially Sean, thank you for letting me try my hand at zebrafish work. Lastly, a sincere thanks

is due to everyone else in the group that provided an incredible environment for me to learn and grow.

I would be remiss if I did not also express my gratitude for the members of my faculty committee, Marcelo Magnasco, Leslie Vosshall, David Gadsby and Bill Bialek. They provided much needed enthusiasm when I was skeptical, and their insight helped me to pursue questions I had not considered. I would also like to thank Bill Roberts for making to the trip from Oregon to serve as my external examiner.

Of course, the chief engineer of my time here was Jim Hudspeth. I do not know how to convey my appreciation and sheer awe here. He has been a great mentor, and yet that is a word too thin. Jim's curiosity and enthusiasm is infectious. His breadth of knowledge, in science and in everything else, is immense. Yet he is incredibly approachable and his door has always been open. These were the factors that drew me into his lab in the first place, and I hope to take small tokens of each when I leave. I knew little math, no electrophysiology, and nothing about hair cells, and I told him so before joining. He said, "That's fine." I thank him for that leap of faith, for letting me make mistakes, for forcing me to be more intrepid in experimental pursuit, for proving that one can be an expert in many things, and for providing an excellent role model.

TABLE OF CONTENTS

LIST OF FIGURES

List of Abbreviations

BEF	Best excitatory frequency
BK	Large conductance Ca^{2+}-activated K^+ channels
BSA	Bovine serum albumin
CF	Characteristic frequency
DMSO	Dimethyl sulfoxide
EPSC	Excitatory postsynaptic current
MET	Mechanoelectrical transduction
NSF	N-ethylmaleimide-sensitive factor
PBS	Phosphate-buffered saline
RRP	Rapidly releasable pool
SNARE	Soluble NSF attachment protein receptor
TRP	Transient receptor potential
TRPM7	Transient receptor potential melastatin 7
VAchT	Vesicular acetylcholine transporter
VGLUT	Vesicular glutamate transporter

Chapter 1. Introduction

The ability to act in response to environmental signals around an organism is a fundamental problem for its survival and growth. Of all the sensory modalities, this problem is perhaps easiest to conceptualize for vision: the visual landscape is a rapidly changing array of patterns and movements. Here, the fundamental units of input that carry information about the environment are photons of different wavelengths. The first step to this problem's solution is for an organism to somehow capture this input—that is, transduce it into a communication modality that allows further processing. Complex sensory systems have evolved for this purpose that underscore the utility that organisms derive from this sensory modality.

Acoustic stimuli pose similar problems. The auditory landscape is a complex collection of sounds from different sources, in varying patterns and amplitudes that are constantly being presented to an organism. Even what seems at first glance to be a relatively simple selection of human speech proves to be an elaborate continuous array of frequencies modulated in a specific and meaningful temporal pattern (Figure 1.1). At the most basic level, the spectrogram presented in Figure 1.1, or at least some segment of it, is the information that must be captured if a human is to then react to it. Only when this information is transduced into a biological language that can be manipulated can the recipient determine an appropriate response. This is the task of the ear, the sensory transducer for hearing.

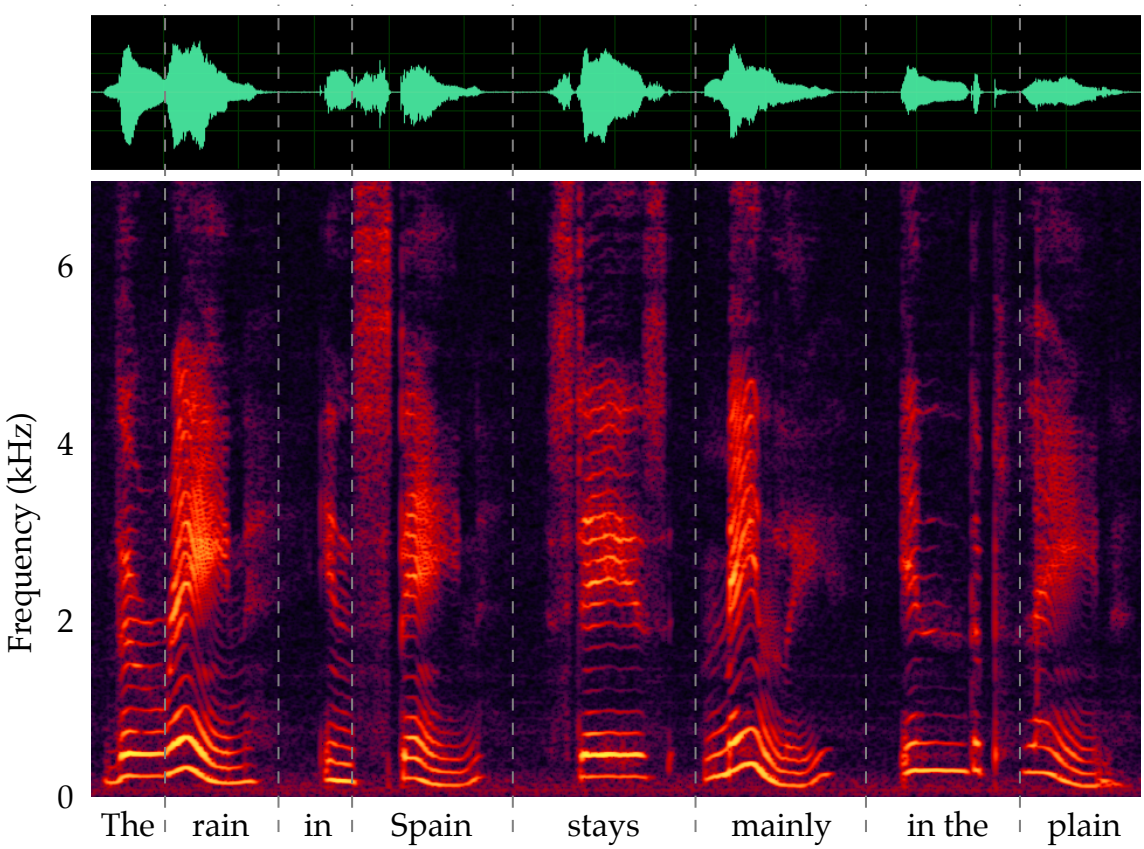

Figure 1.1 Spectrogram of human speech

In the upper panel is the envelope of the pressure wave from the speech sample shown at the bottom. Below that, the sample is decomposed into its constituent frequencies. Note the multiple harmonics of the fundamental frequencies for vowel sounds and their subtle temporal modulations, as opposed to the broadband distribution of consonants such as the first syllable of “Spain” or “plain.”

The vertebrate ear accomplishes this much like a piano in reverse by taking complex sound input and decomposing it into its frequency components. In mammals, sound in the form of pressure waves impinges on the tympanic membrane of the external ear. Vibrations of this elastic structure are conveyed via the middle ear ossicles to the cochlea, the spiral structure that houses hair cells. These auditory receptor cells are so named after the tuft of graded actin-filled stereociliary projections atop their apical surface known as the hair bundle. Vibrations at the oval window, the interface between the fluid filled cochlea and the most proximal middle ear bone, are ultimately conveyed to the hair bundles, causing the opening of mechanically gated ion channels located at their apical tips (Hudspeth and Jacobs, 1979; Hudspeth, 1982). The ensuing inward current of cations, usually K^+ from the specialized environment surrounding most vertebrate hair bundles (Corey and Hudspeth, 1979), results in graded depolarization of the cell in proportion to the stimulus delivered to the hair bundle (Hudspeth and Corey, 1977), thereby causing the opening of voltage-gated Ca^{2+} channels at the cell's base. The subsequent Ca^{2+} entry and Ca^{2+}-dependent fusion of glutamate-filled vesicles then stimulates the postsynaptic afferent neurons of the VIIIth cranial nerve to fire action potentials that convey information to the brain for further processing (reviewed in Fuchs, 1996).

Although the entry of all sound is through a common location in each ear, each afferent neuron, which typically carries auditory information from only one to a few hair cells, fires action potentials only in response to a narrow frequency of auditory stimuli, termed its best excitatory frequency (BEF). Thus, between the entry of sound at the inner ear and the firing of action potentials by each afferent neuron, there lies a phenomenological band-pass filter that limits the output of

the system—in this case, the firing characteristics of a given afferent neuron—to only a narrow range of frequencies. By extension, the *entire* cochlea (used here to represent the hearing apparatus of vertebrates) acts as a series of filters operating continuously in parallel, *each* tuned to its own narrow frequency band. These filters together span a broad range of frequencies so as to comprise the hearing range of each animal.

This principle is clear in the physical arrangement of the cochlea. Hair cells form a tonotopic axis. In amphibians, reptiles, birds, and mammals, the hair cells (and synapsing afferent neurons) at one end of the organ respond best to low frequencies; those at other end respond best to high frequencies. By recording the activity of single neurons in living animals, one can probe the threshold of sound intensity required to elicit a response to varying pure tones. In this way, auditory tuning curves are constructed (Figure 1.2). Qualitatively, such curves are informative in understanding to what input each neuron best responds. But quantitatively, they tell even more. The slopes on each side of the BEF show that the response attenuates faster than 40 dB/decade (Figure 1.2), making each auditory fiber responsive to an extremely narrow frequency band. In electrical circuits, such a band-pass filter would require a large array of components, forming a system of a dynamic order greater than ten. Yet the cochlea accomplishes this function.

What allows for such exquisite frequency discrimination over hearing ranges that often span nearly three orders of magnitude and amplitudes that range from the thermal floor to 120 dB, nearly twelve orders in intensity? No single biological mechanism explains the filtering entirely. Instead, multiple

Figure 1.2 Tuning curves of auditory afferents

In A are frequency-threshold curves normalized to their best frequency and overlaid on each other. The absolute threshold has not been normalized. Despite strikingly different tuning mechanisms in each animal's auditory end organ, each tuning curve exhibits a similar V shape. Q_{10dB} values, defined as the BEF divided by the width of the curve at 10 dB above the sound intensity at threshold, range from 1.9 for the cricket to 5.5 for mammals. B shows tuning curves measured from the VIIIth cranial nerve of the leopard frog *Rana pipiens*. Slopes on either side of the BEF of curves from the animal's amphibian papilla are approximately 35 dB/octave, indicating approximately 12 orders of filtering. A is adapted from Peng and Ricci (2011) and B from Zakon and Capranica (1981).

Figure 1.2 Tuning curves of auditory afferents

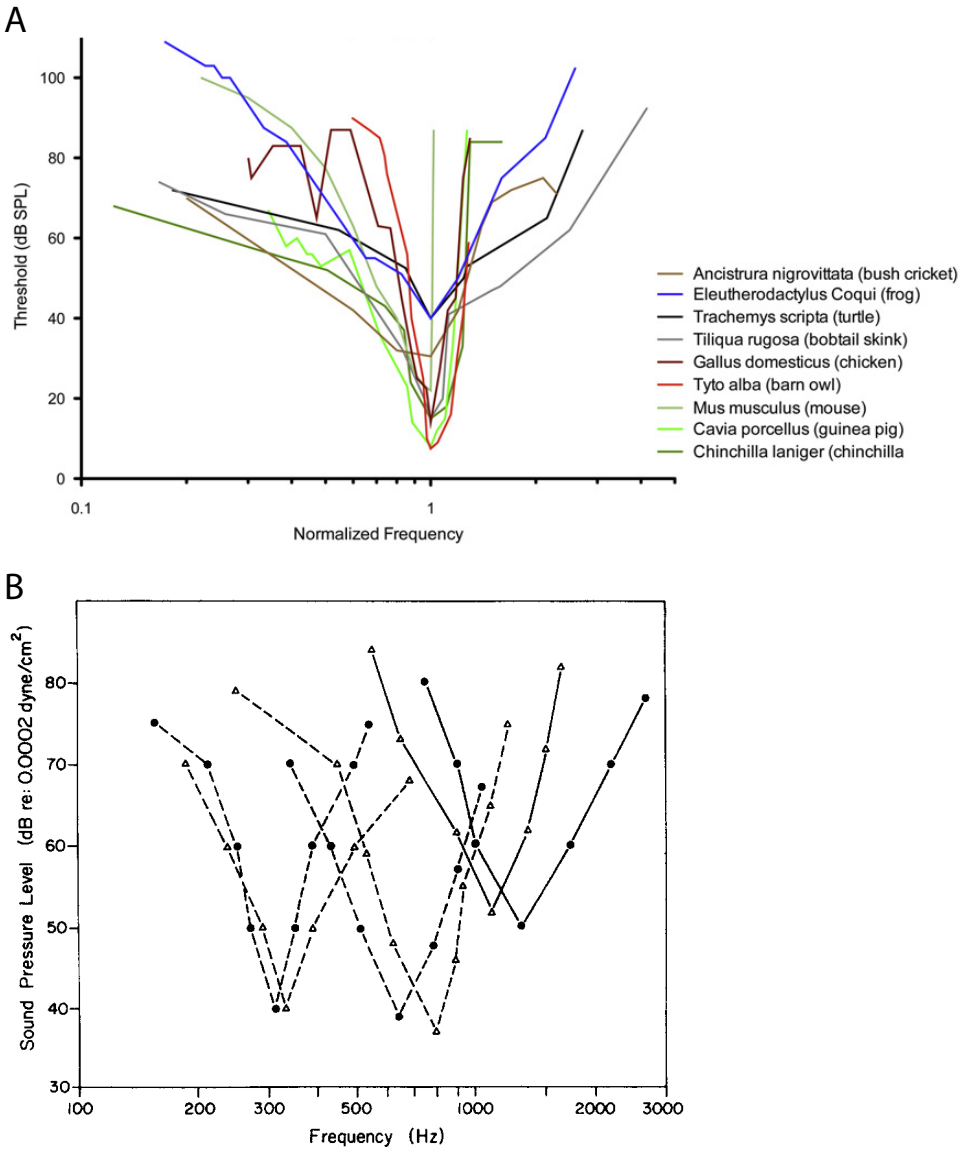

tuning mechanisms operate sequentially at several layers of the sensory cascade to bring about this phenomenological band-pass filter.

Across vertebrate ears, each cochlear apparatus employs each mechanism with varying significance, and presumably each permutation has evolved to fit the unique needs of a particular ear.

Known tuning mechanisms: Active traveling wave

In mammals, hair cells lie in the organ of Corti atop the flexible basilar membrane, which separates two of the cochlea's fluid-filled chambers. This basilar membrane exhibits a gradient in its stiffness (von Bekesy, 1960). At the basal end of the mammalian cochlea, the membrane is relatively stiff; at the apical end, it is relatively floppy. As a result, pressure waves in the cochlear fluid resulting from incoming vibrations at the oval window give rise to a traveling wave going from base to apex that peaks in a specific narrow position depending on the frequency of the input (Lighthill, 1981). This maximally stimulates the hair bundles of cells only at this position, which then drive the firing of afferent neurons, again only at this position.

In an active mammalian cochlea, the sharply tuned traveling wave accounts for nearly all of the tuning found at the level of auditory afferents (Ruggero et al., 2000). Though other tuning mechanisms are not as well characterized, the hair bundles of mammalian hair cells also exhibit a systematic variation in their length and stiffness that yields a gradient of resonant frequencies of hair-bundle oscillation (Lim, 1980, 1986). Hence, the hair bundle also likely contributes to some of the tuning. However, the traveling wave's tuning degrades rapidly upon hypoxia, and exactly *how* the *active* traveling wave

is shaped to be so narrow is an area of active research. Two forms of motility by hair cells have been implicated in the active process that powers this phenomenon. First, the hair bundle can undergo active movements, including spontaneous oscillations that provide nonlinear and frequency-selective amplification of sinusoidal stimuli (Martin and Hudspeth, 1999, 2001; Martin et al., 2003). Mammalian hair cells have an additional mechanism, termed electromotility, wherein the soma of an outer hair cell changes length in response to variations of its membrane potential (Brownell et al., 1985; Liberman et al., 2002). Both mechanisms likely cooperate to mediate the active process in the mammalian cochlea, and thus yield its exceptional sensitivity and frequency tuning (Hudspeth, 2008; Peng and Ricci, 2011).

Non-mammalian vertebrates, however, do not have such a sharply tuned, active traveling-wave system. Yet the comparison of tuning curves presented in Figure 2A reveals that tuning curves from auditory afferents are remarkably similar across different species. How is tuning accomplished in these animals? Multiple mechanisms are cascaded to sequentially filter the input. In birds, for example, the cochlear structure is somewhat similar to that of mammals in that hair cells also rest atop a flexible membrane. However, the evidence for a traveling wave is limited; observations in pigeons indicate the basilar membrane is broadly tuned (Gummer et al., 1987). Likewise, though the hair cells of the turtle's auditory papilla and those of the lizard also rest on a flexible partition, here too the mechanical response of the membrane to auditory stimuli is broadly tuned (Peake and Ling, 1980; O'Neill and Bearden, 1995). Instead, non-mammalian vertebrates employ two other principal mechanisms:

micromechanical tuning of hair bundles and electrical resonance of the hair cells' membrane potential.

Known tuning mechanisms: Mechanical resonance of hair bundles

Each hair bundle is a graded array of actin-filled projections that transduces mechanical oscillations into electrical current, a process termed mechanoelectrical transduction (MET). It accomplishes this through the opening of force-gated ion channels located at the apical tip of each stereocilium. Deflection of the bundle toward its tall edge produces a shear between neighboring stereocilia; as a result, the tip link, a proteinaceous element connecting the tip of a sterocilium with the shaft of its taller neighbor, is stretched, and induces the opening of an as yet unknown force-gated ion channel, resulting in depolarization of the cell's membrane potential (Howard et al., 1988).

As first demonstrated in alligator lizards (Holton and Hudspeth, 1983), each hair bundle oscillates best at a particular frequency. The relatively tall hair bundle from the apical end of the lizard's basilar papilla mechanically oscillates best at frequencies that correspond to the BEF of auditory nerve fibers innervating the same area, approximately 1 kHz. Conversely, the short hair bundles found at the basal end of the organ oscillate best at frequencies near 4 kHz, again corresponding to the BEF of afferents found at this end. Hence, the mechanical properties of the hair bundle are tuned to result in a best resonant frequency, which then drives the corresponding hair cell best at that frequency. In fact, the resonant frequency of the hair bundle varies tonotopically in a graded fashion along the length of the lizard's papilla, and overlaps with the tonotopic

variation in the BEFs of auditory afferents (Frishkopf and DeRosier, 1983). Recent work shows that the sharpness of tuning of the hair-bundle motion even accounts for the entire sharpness of tuning found in the hair cell's receptor potential though the mechanical tuning is only a second-order filter (Aranyosi and Freeman, 2004).

Known tuning mechanisms: Electrical resonance of hair cells

The ion channels governing the cell's response to MET current show a systematic variation in their properties across the tonotopic axis. The two main channels found in hair cells, somatic $Ca_V1.3$ L-type voltage-gated Ca^{2+} channels and large conductance Ca^{2+}-activated K^+ (BK) channels, vary systematically in their properties, giving rise to the tunable property of electrical resonance (reviewed in Fettiplace and Fuchs, 1999). When MET channels open due to hair bundle deflection, the resulting cation influx briefly depolarizes the hair cell. At the hair cell's synapse, this depolarization in turn causes the open probability of the $Ca_V1.3$ channels to increase, thereby resulting in Ca^{2+} influx. At the synapses of hair cells in the bullfrog's sacculus, both the $Ca_V1.3$ and BK channels are clustered in hotspots each representing about 90 Ca^{2+} and 40 K^+ channels (Roberts et al., 1990). Hence, as Ca^{2+} flows into the cell, the local Ca^{2+} concentration at each site increases rapidly. This Ca^{2+} entry depolarizes the cell, but also triggers opening of the local Ca^{2+}-sensitive BK channels with a slower time course. Ensuing K^+ efflux rapidly hyperpolarizes the cell beyond its resting potential. However, because the hair bundle is stimulated again on the next cycle of its mechanical stimulus, the cycle repeats. Even for a sustained, steady input of depolarizing current, the membrane potential oscillates as the cell undergoes

alternating depolarization from the steady current and voltage-gated Ca^{2+} conductance, and hyperpolarization due to the Ca^{2+}-gated K^+ conductance. The entire electrical phenomenon can be tuned to match the tonotopic position of the hair cell and the frequency of auditory stimuli the hair bundle transduces in its routine operation.

Electrical resonance results from the interplay of Ca^{2+} and K^+ channels. Thus, in principle, tuning of the resonant frequency could arise through variation in channel number, local Ca^{2+} buffer concentration and properties, or channel gating kinetics. Though there is evidence for variation in Ca^{2+} buffering, much of the tuning seems to lie in differential splicing of BK channel subunits, and control of the overall number of BK channel units (Fettiplace and Fuchs, 1999). The BK channels in high frequency cells exhibit faster gating kinetics, with shorter mean open times. Furthermore, high frequency cells have a greater total number of BK channels as well. The tuning seems to arise mainly from the gating kinetics of the channels themselves, as opposed to the Ca^{2+} sensitivity or the unitary conductance of each channel; the latter seem to be constant along the tonotopic axis (Art et al., 1995).

Electrical resonance provides a significant contribution to tuning in birds (Fuchs et al., 1988). In turtles, whose basilar membranes are broadly tuned, electrical resonance is also responsible for some tuning, as it is in the bullfrog's sacculus and in the low-frequency portion of the bullfrog's amphibian papilla (Crawford and Fettiplace, 1981; Ashmore, 1983; Pitchford and Ashmore, 1987). Mechanical resonance of hair bundles also makes a contribution in these animals. However, quantitatively, both of these resonant mechanisms account only for two orders of filtering each (Yu et al., 1991; Aranyosi and Freeman, 2004),

whereas the slopes of tuning curves of Figure 1.2 suggest sharper tuning. Hence, there seems to be a missing filter.

Where might this filter lie? It seems that much of the receptive cascade has already been characterized. The entry of sound through the middle ear is necessarily broadband since it serves as a common gate for all frequencies to enter the inner ear, though some attenuation of very high frequencies may occur (Overstreet and Ruggero, 2002; Ravicz et al., 2008). The macromechanical tuning of the flexible membrane on which hair cells lie has been characterized in most vertebrate auditory organs, and seems to be exceptionally tuned only in mammals. The resonant capability of hair bundles has been characterized, as have the tuned oscillations in membrane potential. If there is to be a missing filter, then, it may lie downstream of the cell's membrane potential. This leaves two major areas—the transformation of membrane potential into synaptic output, and the subsequent transformation of the synaptic output into firing of action potentials in auditory afferents.

Properties of the hair cell's ribbon synapse

The first of these processes has been studied in detail. Hair cells are one of two major cell types to possess ribbon synapses, characterized by an electron-dense body that seems to have several hundred synaptic vesicles tethered to it; the other major cell type is photoreceptors. Found in close apposition to the basal plasma membrane, the hair cell ribbon is a spheroid structure approximately 300 nm in diameter, though the shape and size vary greatly across various organisms (Gleisner et al., 1973; Moser et al., 2006).

Given the conspicuous nature of this synapse, as opposed to the conventional synapses found in neurons of the central and peripheral nervous system, several hypotheses for its function have been proposed. First, it should be noted that ribbon synapses release transmitter tonically; that is, their release rate increases monotonically in response to the graded depolarization of the hair cell's membrane potential, as opposed to all-or-none behavior driven by action potentials in neurons. Because of the high frequency of oscillations that occur in hair cells, and the hundreds of vesicles found at each ribbon, much work has focused on elucidating the ribbon's role in supporting prolonged signaling of the hair cell's membrane potential oscillations without fatigue. Initial studies of saccular hair cells from the leopard frog *Rana pipiens* showed that in response to prolonged depolarization lasting 1 s, well in excess of that which the cell is likely to undergo with natural stimuli, the synapse continues to release neurotransmitter at an impressively high rate (Parsons et al., 1994). Indeed the synaptic response is so great that the pool of vesicles found in apposition to the plasma membrane must turn over *entirely* at least five times over the course of the stimulus. This implied that the synapse must rapidly draw on vesicles from a much larger pool than might be in close proximity to the plasma membrane.

Subsequent work further quantified this high rate of release and sought to determine how it is maintained. Studies of the inner hair cells from cochleas of mice revealed that the high rate of release has at least two kinetically distinct components (Moser and Beutner, 2000). Immediately following a depolarizing stimulus, the cell shows a high release rate that corresponds with the number of vesicles found in the small space between the ribbon and the plasma membrane. However, after approximately 50 ms, the release rate is reduced, though it then

remains nearly constant for stimuli lasting up to at least 1 s. Based on this, the total vesicle pool near a ribbon can be divided into one collection termed the readily releasable pool (RRP)—those vesicles that are in close apposition to the plasmalemma and are released first—and another larger pool that includes all others found near the ribbon. Studies of saccular hair cells of the grassfrog also support this theory of a distinct RRP (Rutherford and Roberts, 2006) and confirm the multiphasic kinetics of vesicle release.

These results support the role of the ribbon as a structure to maintain fast release. Furthermore, if the ribbon is to maintain synaptic transmission at a fast rate of vesicle release, it must have vesicles available in the first place. Hence, refilling of the vesicle pool must occur at a rate fast enough to maintain synaptic release. This was supported by measurements suggesting fast vesicle replenishment in chick hair cells (Spassova et al., 2004) and more recently in hair cells of the bullfrog's amphibian papilla (Cho et al., 2011).

Tonotopic variation in synaptic physiology

The ribbon synapse can clearly support high rates of vesicle release. Yet if the synapse is to show a frequency-selective response that is tuned, it ought to show tonotopic differences in its physiology. Given the conspicuous tonotopic gradients in hair bundle properties, MET channel conductance (Ricci et al., 2003), Ca^{2+} buffering (Hackney et al., 2003), and the channels governing electrical resonance, are there systematic differences in *synaptic physiology* between low- and high-frequency cells? Experiments on the turtle's auditory papilla showed that high-frequency cells contain more than twice the number of ribbons found in low-frequency cells (Schnee et al., 2005). Ultrastructural studies revealed that

though the RRP at individual synapses is similar between both cell types, the overall number of vesicles in the RRP of the entire cell is greater in high-frequency cells. And though the exocytotic dependency on Ca^{2+} is similar in both cell types, low-frequency cells experience a greater Ca^{2+} load per synapse, assuming the cell's total Ca^{2+} current is equally distributed across its constituent synapses; they also seem to release at a faster rate than high-frequency cells.

Experiments comparing cells from the two ends of the frequency spectrum in gerbils revealed differences in the Ca^{2+} sensitivity of exocytosis (Johnson et al., 2008). High-frequency cells from the base of the cochlea show a linear relationship between Ca^{2+} influx and increases in the cell's capacitance (a surrogate measure of synaptic exocytosis), whereas low-frequency cells from the apex show a surprisingly supralinear relationship. Repetitive stimulation of the cells revealed that vesicle replenishment becomes rate-limiting for both cell types, but high-frequency cells maintain a greater rate of synaptic exocytosis than their low-frequency counterparts, reminiscent of the earlier studies in turtles.

In other mammals, the situation is more complex. In the mouse, the number of synapses per hair cell peaks in the midcochlear region, in which the cochlea is most sensitive to sound (Meyer et al., 2009). Accordingly, the peak Ca^{2+} current in response to depolarization, and the ensuing increases in the cell's capacitance are greater in this region when compared to more apical cells. However, when the synaptic response is scaled to the number of synapses per cell, the capacitance increase in response to depolarizing stimuli seems to be nearly identical between the two cell populations. Hence, no monotonic systematic difference is readily obvious. Perhaps this is not surprising given that

the mouse likely derives tuning from basilar membrane response; the synapse may serve only to convey information, not process its frequency content.

Frequency dependence of synaptic release

Based on the tonotopic differences in synaptic physiology in turtles, a model of synaptic function that probed the combined influence of the number of synapses per cell, density of vesicles at each ribbon, and the Ca^{2+} load experienced by each ribbon under physiological stimuli has suggested that hair-cell synapses may be optimized to best release transmitter in response to stimulation at the BEF (Schnee et al., 2005). If high-frequency hair cells maintain higher rates of release than low-frequency cells in response to prolonged stimuli, this may be since high-frequency stimuli require faster release kinetics to faithfully encode the oscillations of the membrane potential.

However, direct experimental observation of a tonotopic frequency preference of synaptic exocytosis has been limited. Certainly if synaptic tuning exists, it is likely to be found in non-mammalian vertebrates that lack the sharply tuned traveling wave. However, synaptic tuning in *auditory* organs has yet to be demonstrated. The sole support comes from recordings of capacitance changes in response to sinusoidal membrane potential stimuli in the sacculus of the leopard frog (Rutherford and Roberts, 2006). In this organ, a seismic sensor with hair cells broadly tuned near 50 Hz, hair cells show maximal exocytosis in response to 50 Hz stimuli, as opposed to 5 Hz or 200 Hz. Furthermore, the tuning mechanism seems to lie downstream to the Ca^{2+} current because the calcium current is nearly identical for the aforementioned frequencies employed in the study.

The results provide initial evidence that evolution has indeed configured at least one hair-cell synapse to be frequency selective. However, because the entire organ is broadly tuned to these low frequencies and thus lacks a tonotopic axis, it is impossible to explore *tonotopic* synaptic frequency preferences at frequencies relevant in audition. By extension, it is impossible to ask what the upper limit of the synaptic frequency preference might be. And it remains to be seen just how much of the overall tuning found in auditory afferents is accounted for by the putative synaptic tuning.

Properties of the amphibian papilla

In this thesis I describe efforts to resolve these questions utilizing the amphibian papilla of the American bullfrog *Rana catesbeiana*. Bullfrogs are vocal, vivacious amphibians that make numerous mating and territorial calls (Bee and Gerhardt, 2002). Much of the auditory spectrum of these calls is focused on frequencies between a few hundred Hertz and approximately 4 kHz. The fundamental frequencies within these calls are in the range of hundreds of hertz (Megela Simmons et al., 2008) and are transduced by the amphibian papilla, one of the animal's two principal auditory end organs.

The amphibian papilla is sensitive to auditory stimuli from approximately 150 Hz to 1.1 kHz (Lewis et al., 1982). Like other vertebrate auditory organs, it has hair cells arranged in a tonotopic axis that spans approximately 1 mm. At the caudal end, cells respond best to low frequencies, and this best frequency increases nearly linearly along the rostral projection of the organ. The organ is an attractive system in which to study frequency tuning for several reasons. The amphibian papilla displays several hallmarks of a sophisticated auditory organ

(Schoffelen et al., 2008). Auditory afferents spike at particular points in the stimulus cycle when driven by pure tone acoustic stimuli, a feature known as phase locking (Schmilz et al., 1992). Most striking in the barn owl—which can phase lock at frequencies approaching 10 kHz (Koppl, 1997)—this behavior is restricted to frequencies in the range of the amphibian papilla in the bullfrog, suggesting that synaptic transmission in this organ preserves temporal information with considerable fidelity.

The bullfrog also emits spontaneous otoacoustic transmissions, which are faint sounds emanating from its ear (van Dijk et al., 1989). Though varying from individual to individual, the frequencies of the transmissions lie in the range covered by the amphibian papilla, suggesting they are generated there by an active process (Hudspeth, 2008).

More importantly for the present subject, auditory tuning curves indicate sensitivity comparable to that found in other vertebrates (Figure 1.2B). The slopes on either side of the BEF indicate filtering in excess of a tenth order system (Yu et al., 1991). Though Q_{10dB} values cannot be strictly compared across organs of differing frequency ranges, they nonetheless are comparable to those found in other vertebrates at similar frequencies (Zakon and Capranica, 1981; Peng and Ricci, 2011). Several tuning mechanisms are responsible for accomplishing this sensitivity. The hair bundles display a graded tonotopic change in their height that likely yields a micromechanical tuning of their resonant frequency (Simmons et al., 1992). Within the caudal half of the amphibian papilla, hair cells also benefit from electrical resonance like that found in turtles (Pitchford and Ashmore, 1987; Smotherman and Narins, 1999). Electrical resonance has not been observed in the rostral, high-frequency end of the organ, though that may simply

be due to the rapid deterioration of hair cells from this region in experimental preparations. Lastly, hair bundles are embedded in a tectorial structure overlying the sensory epithelium. For over twenty years, this structure has been hypothesized to support a traveling wave that might focus mechanical stimulation to a small set of hair cells, though it remains to be experimentally observed (Hillery and Narins, 1984).

However, the amphibian papilla is rare amongst the auditory organs in that its hair cells are embedded in rigid cartilaginous connective tissue, as opposed to the flexible basilar membrane found in most other organs. Therefore, a traveling wave is not likely to exist along this structure. Yet the auditory afferents leaving the organ show sharp frequency tuning. The two *known* tuning mechanisms—electrical resonance and micromechanical tuning of hair bundles—are insufficient to account for the overall sharpness found in this organ. Thus, if synaptic tuning indeed exists in additional vertebrate hearing systems, the amphibian papilla is an organ in which it might well occur.

Synaptic physiology of the amphibian papilla

The papilla is an experimentally tractable system in which to pursue questions of synaptic physiology. It was here that the linear relation between the hair cell's Ca^{2+} influx and the postsynaptic current evoked by synaptic transfer was first shown (Keen and Hudspeth, 2006). By this point, presynaptic vesicle fusion had been shown to be linearly dependent on the presynaptic Ca^{2+}current (Johnson et al., 2005). That this linearity extends across the synapse suggests that the postsynaptic afferent faithfully receives, in the form of inward current due to

the opening of neurotransmitter-gated ion channels, the information encoded in the hair cell's Ca^{2+} current.

Furthermore, quantitative analysis of the excitatory postsynaptic currents (ESPCs) resulting from spontaneous vesicle release show that when the hair cell is hyperpolarized, the mean EPSC amplitude in the postsynaptic neuron is 50 pA, likely corresponding to the amount that can be elicited from a single quantum of neurotransmitter in one synaptic vesicle (Li et al., 2009). Yet when the hair cell is held near its resting potential or depolarized slightly, the mean amplitude is nearly two and half times this quantal amount, though the EPSC waveform shows no temporal elongation suggesting the neurotransmitter content equivalent to that of multiple vesicles was released nearly simultaneously by the hair cell. Thus, either the quantum of a single vesicle has enlarged somehow at resting potentials, or several vesicles have been released with sub-millisecond synchrony. Exactly which one of these two mechanisms prevails remains under investigation. Ultrastructural reconstruction utilizing electron microscopy of the hair cells of the middle frequency region of the papilla show that vesicles are tightly packed in the narrow ~100 nm space between the ribbon and the plasma membrane (Graydon et al., 2011). If the ribbon is a diffusion barrier to calcium ions, then in this space, the opening of a few Ca^{2+} channels at the membrane could rapidly saturate the buffers available and the resultant free Ca^{2+} may be enough to cause the fusion of several vesicles in the immediate space. Thus, the synchronous release theory may explain the multiquantal release, at least in the amphibian papilla.

The amphibian papilla also displays multiple kinetics in vesicle release for prolonged depolarizing stimuli; reconstructions of the ribbon support the idea

that the fastest component of release corresponds to the total number of vesicles found in close apposition to the plasma membrane, whereas the slower component corresponds to the pool found tethered to the ribbon itself (Graydon et al., 2011). Using two brief pulses of depolarization delivered to the papilla in rapid succession shows minimal additional release for the second pulse, an effect termed paired-pulse depression, likely corresponding to the rapid depletion of the RRP upon encountering the first pulse (Cho et al., 2011). This depression recovers with an impressively fast time course (15 ms for a fast component), suggesting that refilling of the RRP is extremely rapid, and would therefore support sustained release for long stimuli.

In sum, a breadth of knowledge has accumulated in the past decade on the synaptic physiology of the papilla, from kinetics of individual EPSC events to that of sustained vesicle release at larger timescales. Yet the synapse (and the animal as well) does not experience strong square pulses of stimuli. How it functions in response to acoustically evoked membrane potential waveforms remains to be elucidated.

Overview

In the following pages, I utilize the preparation of Keen and Hudspeth (2006) to explore synaptic frequency tuning. I have taken the approach taken by others before me of measuring capacitance changes as an indicator of vesicle release. Capacitance measurements are technically challenging mainly due to the level of experimental noise, but nonetheless they are tractable, and are correlated strongly with the exocytosis of synaptic vesicles in hair cells (Li et al., 2009). It is important to note that in the absence of a hypothetical mechanism that lends

synaptic tuning, the search for tuning ought to be pursued under conditions in which the cell is kept in its native state, and the stimuli employed mimic those it experiences *in vivo*. These two considerations deviate from the usual experimental paradigms that have been employed in many studies of synaptic function. That is not a criticism of the work to date. Instead, this is simply a shift in the experimental design to pursue a different line of investigation. As just discussed, much work has focused on evaluating the synapse as a machine that is able to release vesicles continuously at high rates. Strongly depolarizing stimuli without sinusoidal modulation, as have been commonly employed, suffice to reveal such aspects of synaptic function. But if one is to glean aspects of synaptic physiology as they are utilized *in vivo*, then sinusoidal stimuli are a fundamental necessity, as is keeping the cell in its native state. Experiments were designed to adhere to these constraints.

Chapter 2. Materials and Methods

Dissection procedure

To obtain recordings from hair cells, I employed an *in vitro* preparation of the amphibian papilla of the American bullfrog (*Rana catesbeiana*). In each experiment, the frog was sedated in cold water, doubly pithed, and decapitated. After removal of the lower jaw with scissors, the columella, the middle-ear connection between the tympanum and the frog's inner ear, was exposed from the ventral aspect and severed with a number 20 scalpel blade. Subsequently, the otic capsule was opened by removing cartilage and bone overlying its ventral aspect. This exposed the inner ear, which was kept moist by applying a few drops of freshly oxygenated artificial perilymph containing 120 mM NaCl, 2 mM KCl, 1.5 mM $CaCl_2$, 1 mM creatine, 1 mM sodium pyruvate, 5 mM HEPES and 3 mM glucose at pH 7.35 and 240 mOsm. The VIIIth cranial nerve was severed at its junction with the brainstem, the semicircular canals were cut and the intact ear, including the membranous labyrinth and remainder of the cranial nerve, was transferred into a dish containing artificial perilymph. To reduce Ca^{2+} toxicity, 100 μM amiloride was supplemented to block mechanotransduction (Jorgensen and Ohmori, 1988).

The papilla was then isolated from the other inner ear end organs by removing the sacculus and its otoconial sac, which revealed the posterior branch of the VIIIth nerve innervating the amphibian papilla, the basilar papilla, the lagena, and the posterior semicircular canal. The papilla was separated from the other organs with fine scissors and cut at its lateral edge where its roof meets the

sensory epithelium. This allowed reflection of the roof, with the papilla's nerve branch still attached to it, keeping a long section of the nerve relatively intact while still giving apical access to the sensory epithelium.

Subsequently, the organ was stretched on a tungsten wire with the epithelium's long axis overlying the wire and parallel to it. At the medial side of the organ, the epithelium was held down with three fine pins inserted into the cartilage equidistant from each other along the organ's rostrocaudal axis. The lateral side of the organ, now with the nerve and a small segment of the roof, was held down with a single pin that placed tension on the nerve and the sensory epithelium. Figure 2.1 shows the final arrangement of the organ prior to electrophysiological recording. The resultant forces often split the organ near its rostromedial region, exposing hair cells most frequently along the medial edge of the organ. To gain access to a greater potion of the organ, a hair knife was used to furrow small sections along the sensory axis. Though this necessarily destroyed hair cells at the furrow, the resulting gaps exposed healthy hair cells up to the mediocaudal region after debris was washed away with a few gentle rinses.

Electrophysiology

Perforated-patch recordings were obtained with conventional filament-containing borosilicate electrodes (1.2 mm outer diameter, 0.9 mm inner diameter) pulled with a horizontal puller (Model P-2000, Sutter Instruments). Pipettes were filled with 110 mM CsCl, 2 mM Na_2ATP, 2.5 mM $MgCl_2$, 10 mM HEPES, 1 mM EGTA at pH 7.3. Notably, this differs from the intracellular solution employed by Keen and Hudspeth in that the Mg^{2+} concentration exceeds

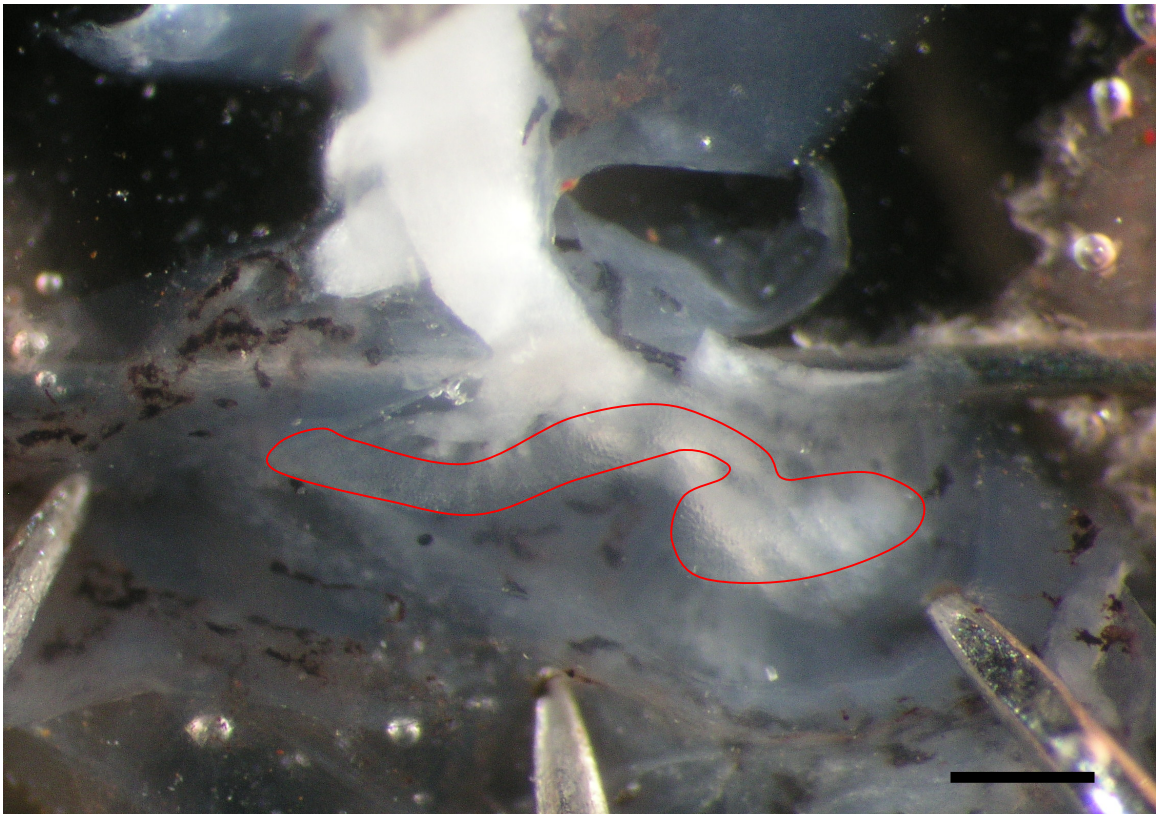

Figure 2.1 The amphibian papilla preparation

Shown above is the amphibian papilla preparation. In this view, caudal is to the left, rostral to the right. The sensory epithelium is oriented parallel to the gray tungsten wire (running horizontally near the center) and held down by fine pins, three of which are visible near the bottom. The epithelium, outlined in red, is visible just below the wire. Each speckle within the red region is a hair cell with its hair bundle oriented out of the plane of the page, toward the reader. The scale bar is approximately 100 μm.

that of ATP to ensure minimal free ATP. First, pipettes were backfilled by dipping the back of the pipette in this solution for 5 s. Capillary action along the filament drew the fluid to fill the tip. Subsequently, they were additionally filled with the same solution supplemented with freshly dissolved amphotericin-B (Sigma) at a concentration of 500 μg/ml. To maximize the perforating efficiency of the compound small aliquots of the compound were freshly dissolved for each experiment in dimethyl sulfoxide (DMSO) under low-light conditions, and this stock solution was then used to supplement the pipette solution. Since low-noise capacitance measurements were essential, pipettes were coated from their midpoint to within 100 μm of their tips with nail polish (Sinful Colors, Mirage Cosmetics) to reduce their transmural capacitance. Typically, electrodes displayed series resistances of 3 MΩ when filled with the intracellular solution only, and resulted in a stable perforated-patch recording configuration 10-15 min after seal formation with access resistances of 7-15 MΩ.

Cells were visualized by differential-intereference-contrast microscopy on an upright microscope with a 40X objective lens and 10X eyepiece. The Axopatch 200B amplifier (Axon Instruments) was used to obtain recordings, which were performed in the whole-cell voltage-clamp mode without compensation for series resistance or whole-cell capacitance. Stimuli were delivered and responses recorded with custom software written in LabView (National Instruments).

Synaptic responses were calculated as the capacitance change resulting from the fusion of synaptic vesicles and the ensuing growth of the cell's plasmalemma. For capacitance calculation, the Sine + DC technique was employed (Lindau and Neher, 1988) using a software lock-in amplifier built in

LabView. Data were recorded at a high frequency resolution (102 kHz) so that the software could extract the access resistance, membrane resistance and membrane capacitance in real time. Prior to seal formation, the pipette capacitance was neutralized by the amplifier's compensation so that the quadrature signal of the lock-in amplifier was brought to zero.

Once a seal was formed, each cell was held at -80 mV and driven with a 1,500 Hz sine wave 15 mV in amplitude to determine the capacitance. As the patch perforated and granted electrophysiological access to the cell, the recorded capacitance gradually increased from 1 pF (representing the pipette and the patch) to 12-16 pF, largely representing the whole cell's membrane capacitance. After this configuration had been attained, 1 s long sinusoidal stimuli of various frequencies, 5 mV in amplitude, and centered near the resting potential of either -55 mV or -45 mV, were interleaved in the capacitance recording. Seven frequencies of stimuli, with an inter-stimulus duration of 4 s, were presented in an array. The order of frequencies in each array, either spanning from 0 Hz to 1000 Hz, or a narrower set in some cells, was randomized to limit systematic contamination due to any steady drift of the baseline capacitance.

Measurement of cell position

After each recording, the cell's position was calculated as its distance from the organ's extreme caudal edge as determined by a calibrated eyepiece reticle.

Immunolabeling of Ca^{2+} buffers

For immunolabeling studies of soluble Ca^{2+} buffers, papillae were dissected into cold artificial frog perilymph and fixed for 1 hr at room

temperature in phosphate-buffered saline solution containing 4% formaldehyde and 0.1% Triton X 100. The tissue was then labeled and imaged as previously described (Castellano-Muñoz et al., 2010). Papillae were washed four times for 10 min each at room temperature in phosphate-buffered saline (PBS) containing 0.1% Triton X-100 and subsequently incubated for 30 min in the same solution supplemented with 5% bovine serum albumin (BSA) to block non-specific binding. The tissue was then incubated with primary antisera in PBS containing 0.1% Triton X-100 and 5% BSA for two hours at room temperature or overnight at 4°C. Polyclonal rabbit antisera against calretinin (Swant), parvalbumin 3 (Heller et al., 2002) and calbindin D28k (Swant) were used at respective dilutions of 1:5,000, 1:10,000 and 1:1,000. After primary labeling, the tissue was washed five times for 10 min each at room temperature. Secondary labeling was performed with donkey anti-rabbit IgG conjugated to Alexa 488 (Invitrogen) at a dilution of 1:500. Alexa 568-conjugated phalloidin was added during the incubation with the secondary antibodies at a concentration of 1:30 to label hair bundles. After washing five times for 10 min each at room temperature, each papilla was mounted between two coverslips with Vectashield (Vector Laboratories) for imaging.

Z-stacks were acquired at 0.5 μm intervals with a Fluoview FV1000 laser scanning confocal microscope with a 60X objective lens of numerical aperture 1.35 (Olympus). Images were collected from five or six equally spaced segments along the length of the amphibian papilla. In each section, data from 15-19 cells were analyzed. For studies of Ca^{2+} buffers, the pixel intensities were measured in the hair-cell cytoplasm immediately basal to the nuclei for papillae

immunolabeled for parvalbumin 3 and calbindin D-28k. All the measurements from a given papilla were conducted with identical settings of the confocal imaging system.

Modeling

For modeling studies, an existing model of synaptic vesicle release (Andor-Ardó et al., 2010) was simplified to reduce the number of states and to include steady-state dynamics relating to free Ca^{2+} and buffer concentrations, as well as voltage-dependent Ca^{2+} currents. The rationale and the corresponding equations are discussed in Chapter 4. Simulation and analysis were carried out in Mathematica (Wolfram Research).

Data Analysis

Data were analyzed with MATLAB (Mathworks) and Mathematica (Wolfram Research). Capacitance data were averaged for 200 ms immediately before and after each stimulus presentation; the difference between these two values was taken as the resulting capacitance change (ΔC_M). These data are shown for individual cells as a function of the frequency of stimulation. Data across cells was not averaged to prevent the pooling of data from cells possibly tuned to different frequencies. Negative capacitance changes, which sometimes occurred and were assumed to reflect the noise inherent in the recordings, were not indexed as zero but were averaged in the total data set for each cell. Capacitance changes from each stimulus presentation that exceeded ± 250 fF, or in which there was a simultaneous change in the series resistance, were rejected.

Confocal images from immunolabeling studies were analyzed with ImageJ (National Institute of Health).

Values are reported as means ± standard error of the mean unless otherwise specified. Capacitance data are averages of 5-25 presentations of stimuli at each frequency. For capacitance recordings, Student's t-test was used to analyze significance; for imaging data, one-way ANOVA was used. Significance was taken as $P < 0.05$.

Chapter 3. Frequency selectivity of synaptic exocytosis

Synaptic release has two principal hallmarks that can be measured: the changes in membrane capacitance of the presynaptic cell as a result of vesicle exocytosis and endocytosis, and the currents induced in the postsynaptic cell as a result of the opening of neurotransmitter-gated ion channels. The former has the disadvantage of not providing information in real time; voltage stimuli can not be delivered while measuring membrane capacitance. In the latter, the drawback is that two separate cells must be recorded simultaneously. Though such paired recordings offer the advantage of real-time measurement of postsynaptic potentials, presynaptic capacitance measurement is easily tractable in comparison. Capacitance recordings of hair cells are thus described in this chapter.

Experimental design

I began with measurements of membrane capacitance of individual hair cells to determine whether the synapse showed any preferential release. In the amphibian papilla, a single vesicle at the hair cell's ribbon synapse is approximately 38 nm in diameter; assuming a spherical surface area of 4.5 x 10^{-15} m^2 and a specific membrane capacitance of 10 $mF \cdot m^{-2}$ (Albillos et al., 1997), it has a membrane capacitance of approximately 45 aF (Li et al., 2009). The resolution of capacitance measurements is on the order of 15 fF (Lindau and Neher, 1988). Thus, if a change in the amount of release is to be discovered, at least several hundred additional vesicles must be released at some frequency

over another. Hair cells of the amphibian papilla contain 55 ribbons per cell, with 13 vesicles found in the RRP of each ribbon (Graydon et al., 2011). At modest release rates of several tens of vesicles released per ribbon per second when the cell is stimulated without deviating strongly from its resting potential, stimuli must last approximately one second to show a measurable difference in synaptic release.

Of course the capacitance of a cell is not solely the result of vesicle release; it is in a dynamic balance of vesicle fusion and endocytosis, both proceeding constantly. Indeed the only reason capacitance recordings show *anything* is because the time scale for endocytosis is much longer, with a time constant of nearly 5 s (Cho et al., 2011), whereas exocytosis proceeds rapidly within microseconds. With these constraints in mind, a protocol that would drive hair cells with a range of frequencies for one second at each frequency was utilized. In between these stimuli, when the capacitance was to be measured, each cell was held at -80 mV, thus minimizing stray Ca^{2+} entry from the opening of voltage-gated channels at rest. Concurrently, the cell was driven with a high frequency sine wave at 1500 Hz and 15 mV in amplitude to assay the capacitance (Figure 3.1A). Periodically, current-voltage relations were measured to ensure the cell's health remained stable, and initially, to assay the level of perforation and block of the cell's K^+ current with Cs^+ from the pipette.

In keeping with the considerations outlined in Chapter 1, namely that stimuli ought to mimic those the cells are likely to undergo *in vivo*, the amplitude of the stimulus waveform was chosen to be 5 mV. The receptor potential resulting from hair bundle deflection has not been directly measured in the amphibian papilla. However, these stimuli accord with the range of depolarizing

Figure 3.1 Capacitance recordings show frequency selective synaptic responses

Measurement of capacitance changes resulting from stimulation of a hair cell. (A) The upper trace depicts the voltage-clamp protocol employed during whole-cell recording in the perforated-patch configuration. A hair cell was held at -80 mV and exposed to a sinuosidal voltage change of ±15 mV at 1500 Hz to measure its membrane capacitance. In the segment labeled "Stimulus," the cell was depolarized to -55 mV and the capacitance probe was interrupted by a 1 s sinusoidal stimulus at one of seven randomly presented frequencies, usually a constant value (0 Hz), 25 Hz, 200 Hz, 400 Hz, 600 Hz, 800 Hz, or 1000 Hz. The whole-cell current is shown in the lower trace. (B) The upper trace depicts the cell's membrane capacitance one second before and after the stimulus. The capacitance recording was averaged over the 200 ms interval immediately before and after stimulation to calculate the capacitance change at the relevant frequency. Increasing frequencies are represented in spectral order. This hair cell, from the mid-frequency region of the papilla, displayed the greatest synaptic exocytosis during stimulation at 400 Hz (green). The exponential decay of the peak response has a time constant of 763 ms (black dashed line; R^2=0.81). The lower trace confirms that the access resistance remained stable. (C) Blocking the cell's inward calcium current with nifedipine abolished the capacitance response.

Figure 3.1 Capacitance recordings show frequency selective synaptic responses

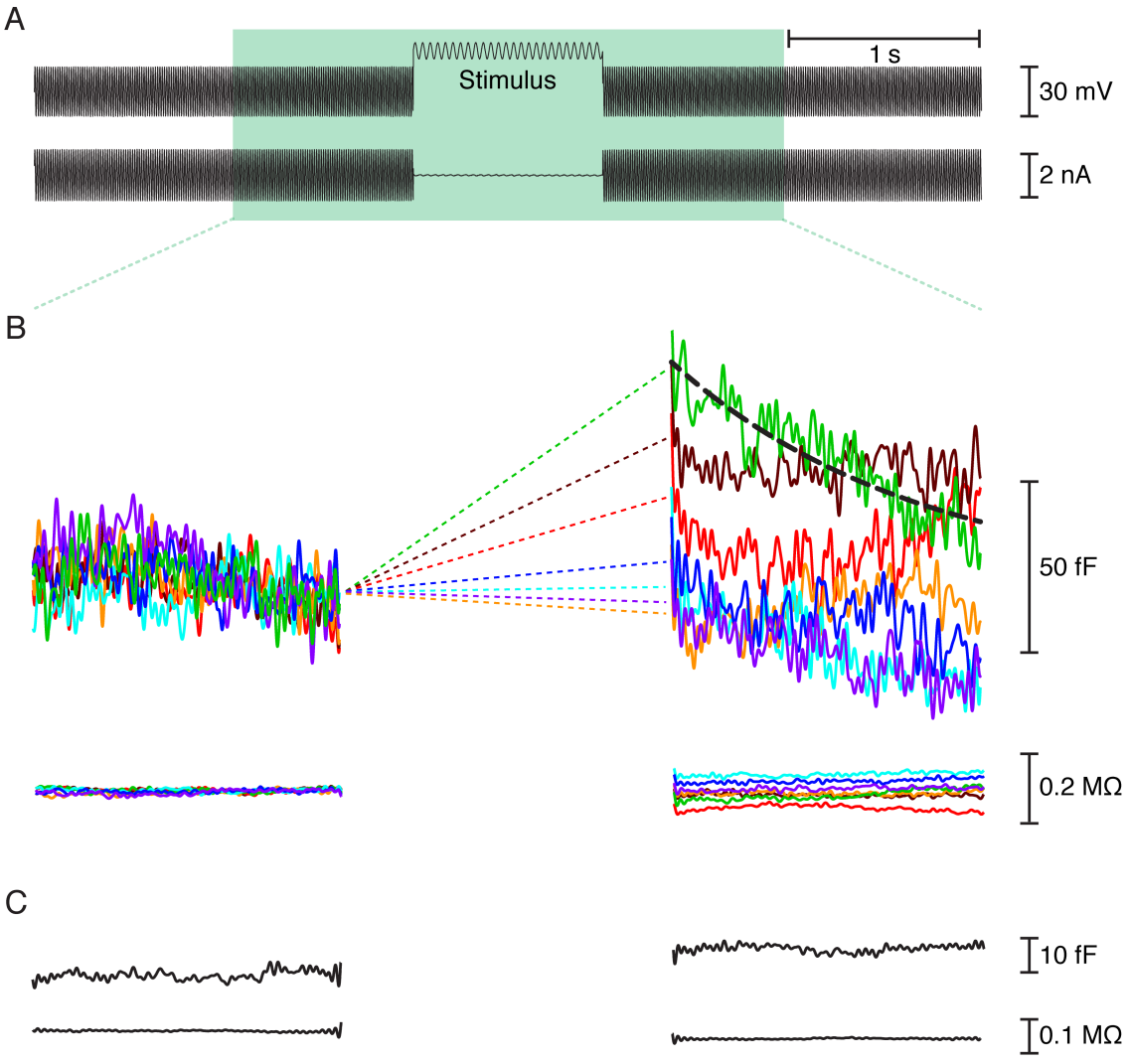

potentials that result from hair bundle deflection in the bullfrog's sacculus (Hudspeth and Corey, 1977), where it has been measured. As for the resting potential, stimuli were centered on a holding potential of -55 mV, near the measured resting potentials of papillary hair cells and where the quality factor (Q) of electrical tuning is greatest (Pitchford and Ashmore, 1987; Smotherman and Narins, 1999).

Synaptic exocytosis is frequency selective

After exposing hair cells from the papilla's middle frequency region, I stimulated cells with frequencies spanning the hearing range of the organ. A DC (0 Hz) stimulus was also utilized for comparison. In response, several cells showed preferential exocytotic responses at a particular frequency that were significantly greater than those observed at the flanking frequencies, providing the first observation of frequency-tuned exocytosis in this auditory organ. For example, the cell shown in Figure 3.1B showed the greatest synaptic response to stimuli at 400 Hz, as opposed to 200 Hz or 600 Hz. Other hair cells showed the greatest change at 200 Hz (Figure 3.2A) or 600 Hz (Figure 3.2B). Blocking the hair cell's dihydropridine-sensitive Ca^{2+} current with the blocker nifedipine, known to eliminate postsynaptic EPSCs in afferent neurons (Robertson and Paki, 2002; Keen and Hudspeth, 2006), eliminated the capacitance response, as shown in Figure 3.1C.

The amplitude of additional capacitance change at the best frequency over that at neighboring frequencies was 63 ± 8 fF. Based on the aforementioned quantitative properties of synaptic vesicles and counts of ribbons in hair cells, this amounts to an additional release of 1600 vesicles per cell, or 30 vesicles per

Figure 3.2 Hair cells show preferential synaptic responses to a range of frequencies

(A) Synaptic release from a rostral hair cell peaked for stimulation at 200 Hz. (B) A hair cell from the middle portion of the amphibian papilla was most responsive at 400 Hz. (C) A cell located farther toward the caudal end of the papilla responded best near 600 Hz. In these three and 13 other cells, the capacitance change at the best frequency significantly exceeded that at the flanking frequencies ($P < 0.05$).

Figure 3.2 Hair cells show preferential synaptic responses to a range of frequencies

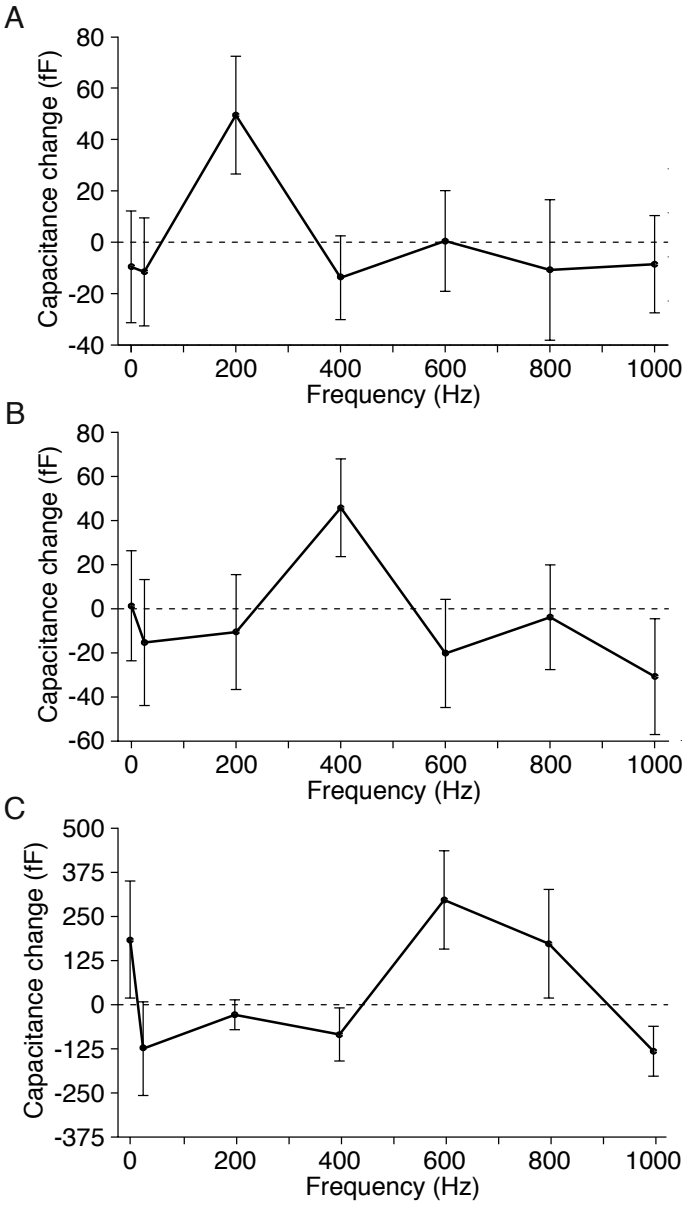

ribbon. Given that the ribbon has a RRP of 702 vesicles per cell, this means the RRP would need to refill only twice over the course of the 1 s. Hence, the response amplitude suggests that the frequency-tuned response arises from the RRP only, without the need to invoke the recruitment of additional vesicles from the ribbon-attached pool.

Synaptic tuning is tonotopic

Although the first to directly demonstrate frequency-tuned synaptic responses, the previous study of the saccular hair cells by Rutherford and Roberts (2006) was limited in that tonotopic variation in tuning could not be assayed in this organ. Thus, in the papilla, I next sought to ask whether tuning was tonotopic. Each cell's position relative to the extreme caudal edge of the organ was measured with an eyepiece reticle, and correlated with the frequency at which the cell displayed the greatest exocytotic response. Cells showed a clear trend in their best synaptic frequencies along the length of the organ. When plotted along with the distribution of the BEF of auditory afferents, there was a clear overlap between the distribution of the synaptic best frequency and that of the auditory nerves (Figure 3.3).

There was considerable variation in each cell's capacitance response across the frequency range of stimulation. Most ΔC_M responses were within ± 20 fF, though low-frequency noise and deterioration in the cell's health likely added considerable variability to each cell's observed response. In Figure 3.4 are shown responses from ten cells for which an identical frequency range was

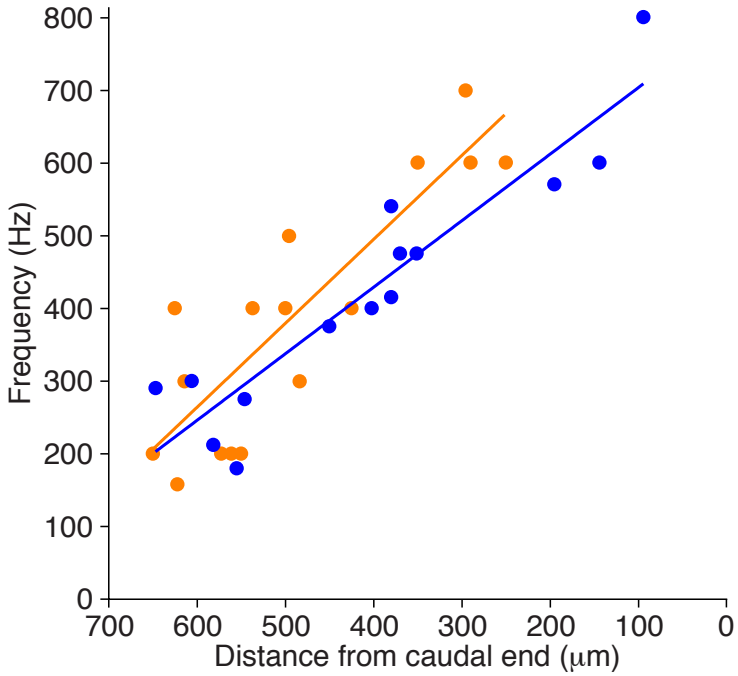

Figure 3.3 Tonotopic organization of synaptic tuning

The frequencies of greatest synaptic release for 16 hair cells (orange) are plotted against their distance from the caudal end of the amphibian papilla. The tonotopic map for auditory afferents (Lewis et al., 1982) is shown for comparison (blue). The coefficients of determination for the linear-regression fits are $R^2 = 0.76$ for the synaptic data and $R^2 = 0.86$ for the afferent responses.

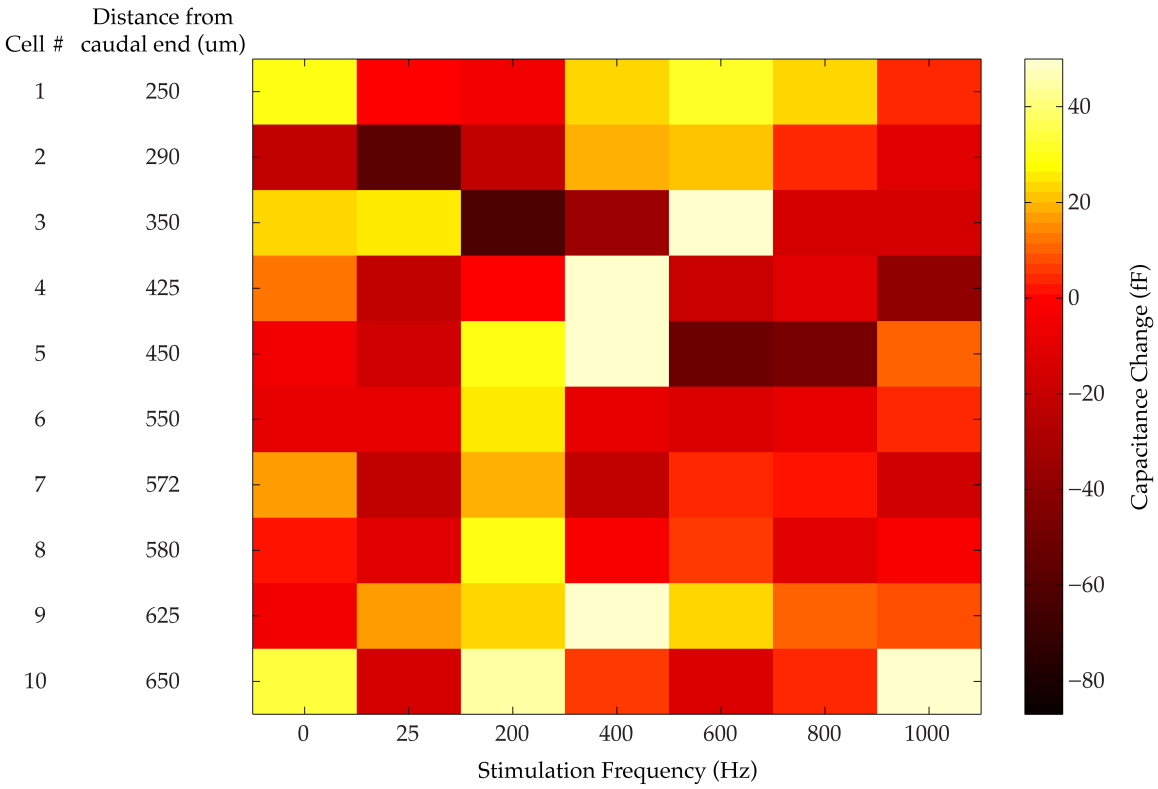

Figure 3.4 Capacitance responses to sinusoidal voltage stimulation of hair cells

From top to bottom are ΔC_M responses of ten cells arranged by position from the caudal end of the organ. Each cell was stimulated with an identical array of frequencies, shown at the bottom. Rostral cells have peak responses that cluster near 200 Hz, whereas caudal cells have the greatest responses near 600 Hz. In between are cells that respond best to 400 Hz.

employed during stimulation. Though there is considerable variability in the ensemble of data, the peak of the response clusters near 200 Hz for cells near the rostral end of the organ, and migrates toward 600 Hz for cells near the caudal end.

Synaptic tuning may account for two orders of overall sharpening

Hair cells displayed robust capacitance responses and Ca^{2+} currents for ten to fifteen minutes during recording. Owing to the limited lifetime of the preparation and the weak stimuli used, I was unable to define the shape of tuning curves further than identifying just the peak responses. But without information on how quickly the response decays as the stimulus frequency deviates from the optimal frequency, it was not possible to glean the quantitative contribution of this tuning to the overall sharpening found in auditory tuning curves.

The experimental limitations were circumvented in two ways. First, given that cells displayed tonotopic synaptic tuning, it was no longer necessary to assay the full spectrum of frequencies shown in Figure 3.1 for each cell. Hence, for some cells, a tighter distribution of frequencies was assayed during the cell's limited recording time to allow for better frequency resolution. Rostral cells were sampled with frequencies lower than those used for caudal cells. Second, the amplitude of the synaptic response was augmented by holding each cell at -45 mV. Though this procedure deviates somewhat from the cell's resting potential, it allows a significantly greater activation of the inward calcium current and therefore boosts the number of vesicles likely to be released. Using this method, I was able to delineate with greater resolution the decay of the tuned response

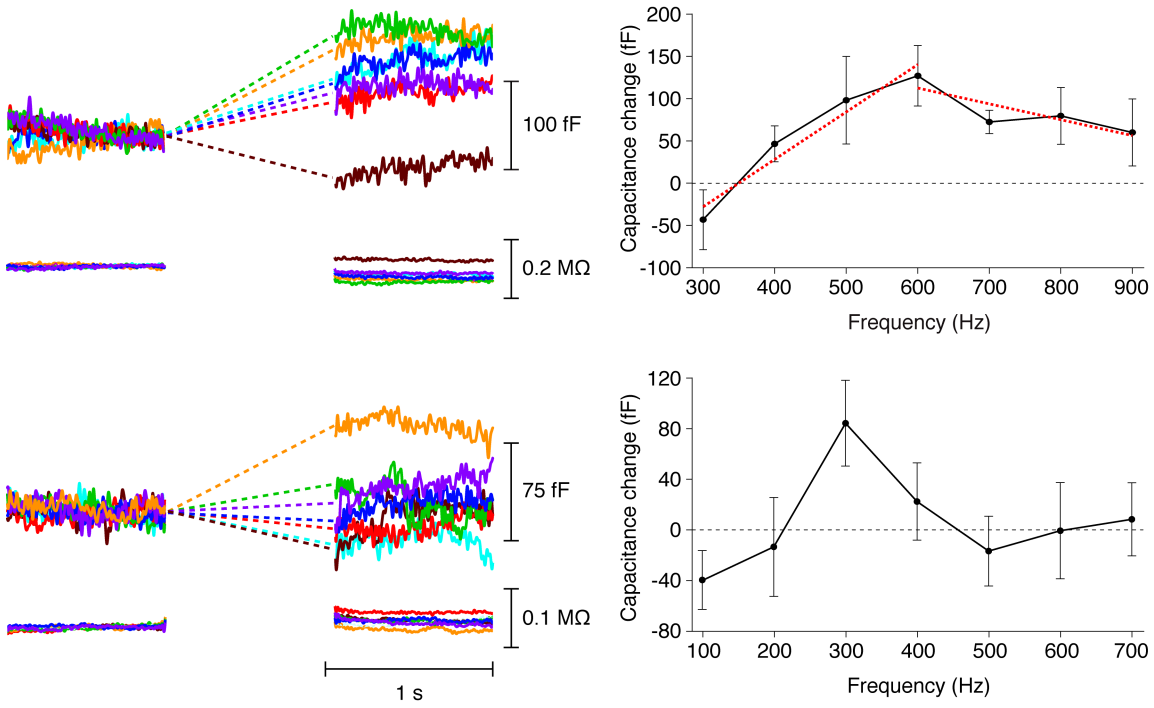

Figure 3.5 Synaptic tuning provides at least two orders of overall tuning

In the upper panel are data from a caudal cell showing the greatest response at 600 Hz. Above and below this frequency, the cell's response decays, and the data to the right has been fit with two linear fits (R^2 = .95 and .73 below and above the peak response, respectively). A rostral cell in the lower panel displays best response to 300 Hz. The frequency resolution, though 100 Hz, was not great enough to warrant fitting the slopes for this cell.

(Figure 3.5). In cells stimulated with this closer set of frequencies, responses decayed to less than half when the frequency was doubled (see upper portion of Figure 3.5). Below the peak response frequency, when the frequency was halved, responses decayed even faster in some cells. A first-order low-pass filter will decrease the response of a system by half as the frequency is doubled. Thus, based on the slopes of the decay, synaptic tuning accounts for at least two orders of the overall filtering found in auditory afferents.

Discussion

Capacitance recordings demonstrate that the hair cells of the amphibian papilla display tonotopic synaptic tuning, at least for frequencies up to 700 Hz. The synaptic tuning frequencies in these cells match those found at the level of the auditory afferent tuning curves from the same position. At least based on the amplitudes of the responses, the pool of vesicles found in close apposition to the plasma membrane may suffice to yield tuned responses.

Synaptic tuning is sharp enough to account for at least two orders of the overall tuning found in afferent tuning curves, though that is only a lower bound. A closer sampling of frequencies might show that the peak lies in an unsampled portion of the tuning curve, in which case the true tuning would be sharper still. Furthermore, it may be sharper regardless, particularly if stimuli that are 1 s in length appreciably saturate the system. To put it differently, the tuning mechanism may be quite sharp but involve a limited number of vesicles. *In vivo*, auditory stimuli, although frequent, are rarely longer than tens of milliseconds in a given epoch. Thus, a small output capacity might suffice. However, in probing the system with stimuli of long duration (an experimental

imposition), the mechanism's sharpness may degrade after the first few milliseconds, and therefore only two orders of sharpening are observed.

Does frequency tuning end at the synapse? Has the amount of tuning found in auditory afferents been accounted for? The answer is: perhaps. Yu et al. (1991) first posited that tuning in this organ is *not* solely the result of the second-order resonances found in electrical tuning and mechanical hair-bundle resonance. The synaptic tuning, as just outlined, may provide two orders, but possibly more if it could be measured with more natural stimuli. Likewise, hair-bundle tuning *in vivo* may exceed two orders. In isolation, the bundle is strongly influenced by thermal noise that limits its capacity for tuned amplification. However, coupling it with other nonlinear oscillators, such as neighboring hair bundles through the tectorial structures overlying most vertebrate hair cells, enhances its tuning, even if each bundle has a slightly different best frequency (Barral et al., 2010). Thus far, most measurements of hair-bundle tuning have focused on isolated, freestanding bundles (Frishkopf and DeRosier, 1983; Holton and Hudspeth, 1983). Hence, these would seem to provide only a lower bound on how much tuning might the bundle account for *in vivo*. If hair bundle tuning and synaptic tuning are both greater than order two, than perhaps the synapse does represent the final filter.

Without knowledge of a mechanism, it is difficult to ascertain whether the true synaptic tuning is actually sharper, or at which stimulus duration it degrades, if indeed it does so at all. Where might this tuning lie? Between the experimental input—oscillations of membrane potential—and the measured output of capacitance lies a complex cascade of systems that still remains to be fully understood. Though the kinetics of the L-type voltage-gated Ca^{2+} channels

found at the synapse has been characterized (Rodriguez-Contreras and Yamoah, 2001; Johnson and Marcotti, 2008; Zampini et al., 2010), exactly what follows Ca^{2+} influx remains under intense investigation. Upon entry, Ca^{2+} interacts with one of three main Ca^{2+} buffers in hair cells, namely calretinin, calbindin-D28k, and parvalbumin 3 (Shepherd et al., 1989; Edmonds et al., 2000; Heller et al., 2002). Immunolabeling studies of the mammalian cochlea and of the turtle's basilar papilla show striking gradients in the expression pattern of these buffers along the tonotopic axis (Hackney et al., 2003; Hackney et al., 2005), though how they influence frequency tuning has not been studied. Furthermore, in the tight space between the channels and the ribbon itself, the buffer undergoes rapid saturation, with resulting localized spikes in the free Ca^{2+} concentration that then stimulate vesicle fusion (Roberts, 1994; Graydon et al., 2011). How and to what extent buffer interactions in this zone influence frequency response remains unstudied.

Ultimately, the free Ca^{2+} must induce vesicle release. Hair cells are thought to lack the conventional synaptic calcium sensor synaptotagmin (Safieddine and Wenthold, 1999), though that has come under debate in recent studies (Johnson et al., 2010). Instead, they utilize a different Ca^{2+} sensor, otoferlin, originally identified in a recessive form of human deafness and shown to undergo Ca^{2+}-dependent interactions with the vesicle fusion proteins syntaxin1 and SNAP25 (Roux et al., 2006). Otoferlin's biochemical interactions with lipids, with Ca^{2+}, and the Ca^{2+}-dependency of its binding with syntaxin1 and SNAP25 have only recently been characterized (Ramakrishnan et al., 2009; Johnson and Chapman, 2010), though exactly *what* it does remains unclear. Most oddly, recent studies of exocytosis in mammalian inner hair cells in the presence

of botulinum toxin, which usually disables vesicle fusion at synapses by cleaving SNAP25, suggest that exocytosis proceeds in the absence of the usual complex of membrane fusion proteins (Nouvian et al., 2011).

In principle, the tuning found here could occur at any position within this cascade. The Ca^{2+} channel might display a frequency-tuned resonance that maximizes influx at a particular frequency. Tonotopic gradients in different splice isoforms of the various proteins may yield tunable kinetics of any of the respective processes, such as Ca^{2+} buffering or release kinetics. Likewise, cellular concentrations of modifiers, such as Mg^{2+} that binds the hair cells' Ca^{2+} buffers or interaction partners of the vesicle fusion apparatus, may also tune the overall kinetic response of the system. The hair cell's complement of synaptic proteins contains several classic regulators of vesicle priming and fusion, such as RIM and munc18 (Uthaiah and Hudspeth, 2010). However, it is also missing several regulators that are otherwise essential in most other systems, such as synapsin, which tethers vesicles to each other and to the cytoskeleton (Greengard et al., 1993) and complexin, which holds the vesicle fusion apparatus in an active state (the so called "primed" state) until the Ca^{2+} sensor synaptotagmin displaces it and rapid fusion ensues (Sudhof and Rothman, 2009). Notably, munc13, which is required for vesicle fusion in mice and in the nematode *Cænorhabditis elegans* (Augustin et al., 1999; Richmond et al., 1999), is also missing at the hair-cell ribbon. Hence, how vesicle docking and priming operates at the hair cell is not well understood, and thus precludes understanding how these processes might be tonotopically controlled to optimize the synaptic frequency response.

Alternatively, the tuning might arise as an emergent behavior of the interaction of the various components of this system, controlled by variation in

multiple parameters. A search for a potential mechanism guides the line of investigation in the next chapter. Joshua Salvi and I performed the immunolabeling studies and Daibhid Ó Maoiléidigh carried out the modeling work.

Chapter 4. Modeling Studies of Calcium Buffering as it Relates to Synaptic Tuning

Given that Ca^{2+}-induced vesicle release still remains incompletely understood, a search for a *biophysical* mechanism of synaptic tuning could prove to be daunting, particularly when the quest to understand just the fundamental steps in the process has already taken the better part of two decades. If the mechanism lies in the biochemical intricacies of the release process, even an exhaustive search may prove to be futile, particularly in the absence of a hypothesis. In light of these difficulties, I sought to understand the effectors of synaptic output, with the hope that such information might ultimately hint at the underlying processes that regulate synaptic tuning.

One illuminating study was published while the electrophysiology experiments were being performed. In the amphibian papilla of the grassfrog *R. pipiens*, a frequency-selective increase in capacitance is not observed when whole-cell recordings are employed (Quiñones et al., 2012). For stimuli similar to those used in the previous chapter but with a relatively coarser frequency resolution, caudal cells and rostral cells displayed frequency-tuned responses across the frequency range. These results raise the tantalizing possibility that soluble molecules, which would be washed out of the cell within seconds in a whole-cell recording, are important to the tuning mechanism.

One obvious candidate group is the Ca^{2+}-buffering proteins that influence the availability of free Ca^{2+} at the synapse. It is here that this chapter begins.

The Ca^{2+} buffers of the amphibian papilla

Where it has been studied, three principal Ca^{2+}-buffering proteins have been found in hair cells: calretinin, calbindin and parvalbumin. When immunolabeled for these three proteins, hair cells of the amphibian papilla showed strong and widespread expression of the latter two buffers (Figure 4.1). Labeling was noted in the cytoplasm and in the hair bundle. However, calretinin expression was limited to hair cells of the lateral edge of the epithelium.

Next, the relative expression level along the tonotopic axis was quantified by determining the intensity of labeling. Averaging the intensity of labeling just basal to the cell's nucleus revealed a conspicuous gradient in expression across the epithelium for both calbindin-D28K and parvalbumin 3. High-frequency cells showed nearly eightfold stronger labeling for calbindin-D28K and fourfold stronger labeling for parvalbumin.

Description of a release-site model with Ca^{2+} buffering

What role does this gradient play in synaptic tuning? An experimental approach to answer this question would measure the tuning curve of a single hair cell, perturb the Ca^{2+}-buffering capacity of the cell, and measure the tuning curve again. However, this is experimentally difficult. Each cell stays healthy for only a limited time. The baseline tuning curve can be measured only in perforated-patch conditions; once complete, breaking the patch under the recording pipette to wash out the buffer rapidly kills the cell as the perforating compound in the pipette fills the hair cell. Nor is the alternative of using a pharmacological blocker of the Ca^{2+} buffer possible, since such a compound has not been identified.

Figure 4.1 Tonotopic gradient of Ca^{2+} buffering in the amphibian papilla

(A) Immunofluorescence microscopy detected a relatively high concentration of parvalbumin 3 in hair cells at the caudal, high-frequency end of the amphibian papilla. (B) With identical settings of the confocal microscope, hair cells near the rostral, low-frequency end of the organ displayed a lower concentration of parvalbumin 3. (C) Parvalbumin 3 labeling increases tonotopically. (D-F) Calbindin-D28k occurs at a high concentration in caudal hair cells (D) relative to rostral ones (E) and also displays a tonotopic gradient (F). The coefficients of determination for the linear-regression fits are $R^2 = 0.97$ for parvalbumin 3 and $R^2 = 0.91$ for calbindin-D28k. The scale bar represents 10 μm for panels A-D.

Figure 4.1 Tonotopic gradient of Ca^{2+} buffering in the amphibian papilla

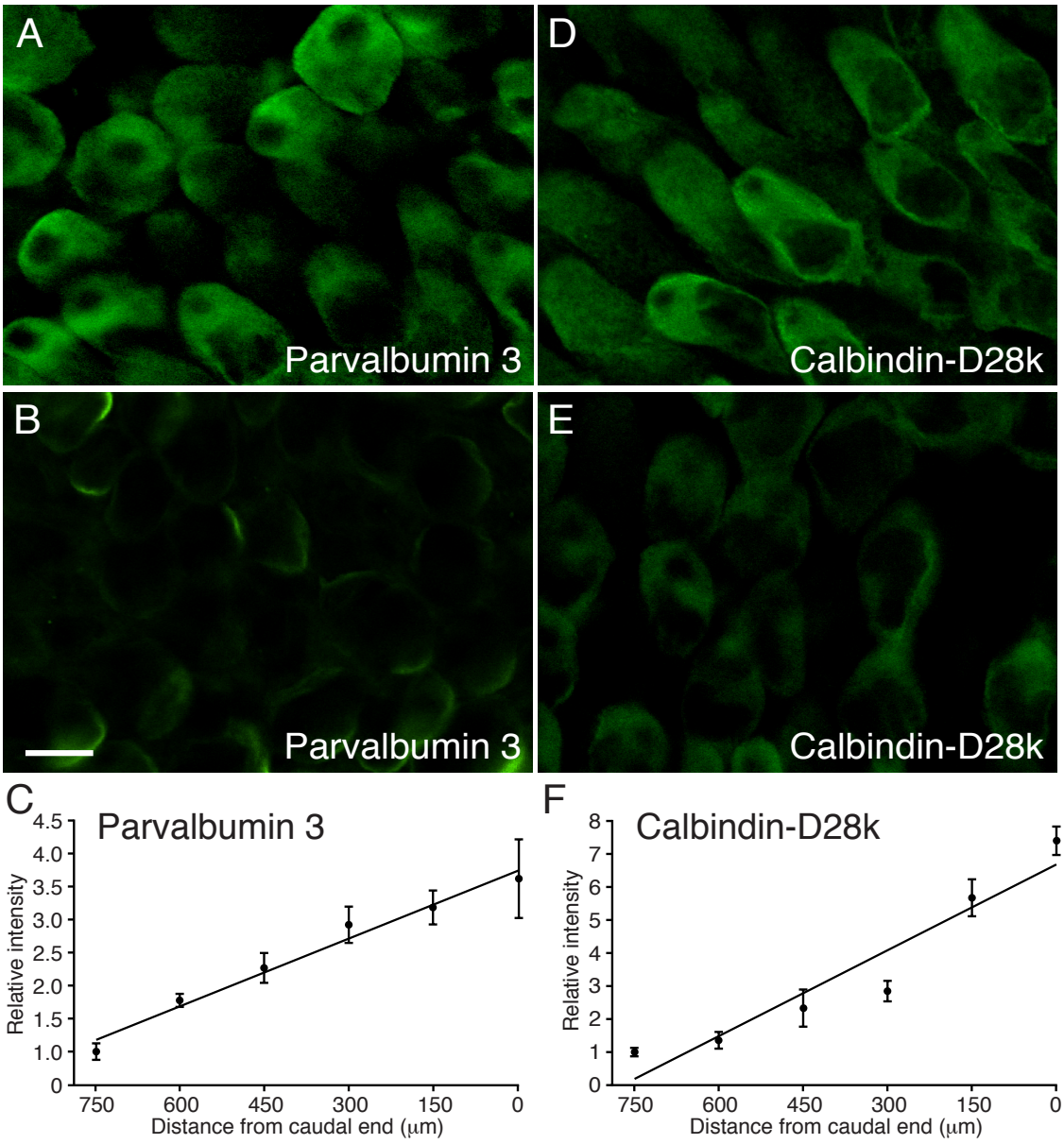

In light of these issues, we employed a modeling approach. A synaptic release-site model has already been developed that yields frequency tuning from a cyclical process (Andor-Ardó et al., 2010). The model describes the release process at each ribbon as occurring in a four-state cyclical system, and shows that sharp frequency-tuned release is possible when positive feedback is allowed. This was reduced to the minimum number of states required to describe release at a given site, namely, activated (i), and discharged (ii), and refilled (iii) (Figure 4.2). To incorporate the influence of free Ca^{2+}, the rate of refilled sites proceeding to a primed state was taken to be Ca^{2+}-dependent. Once activated, vesicles were discharged with a baseline release rate that was augmented by positive feedback with second order cooperativity. While more states and a greater cooperativity order might have added interesting dynamics, the goal here was to determine the minimum complexity necessary to shed light on a possible tuning mechanism that involves calcium buffering. To reduce complexity, each process was taken to have a forward component only. The intrinsic assumption, thus, is that vesicles do not spontaneously appear at the release site by endocytosis *at the release site*, and that once activated in the presence of Ca^{2+}, vesicles do not become "unactivated." Lastly, the process of refilling was modeled with a single rate constant that accounts for all the processes involved in that step, comprising endocytosis, vesicle trafficking, reattachment to the ribbon, and migration to the active region juxtaposed to the Ca^{2+} channels.

Input to the model, as calcium influx, was controlled by the activation of the voltage-dependent Ca^{2+} current. For this portion, the cell's total Ca^{2+} conductance, voltage of half-activation, width of the activation curve, and reversal potential of the current were taken from published literature

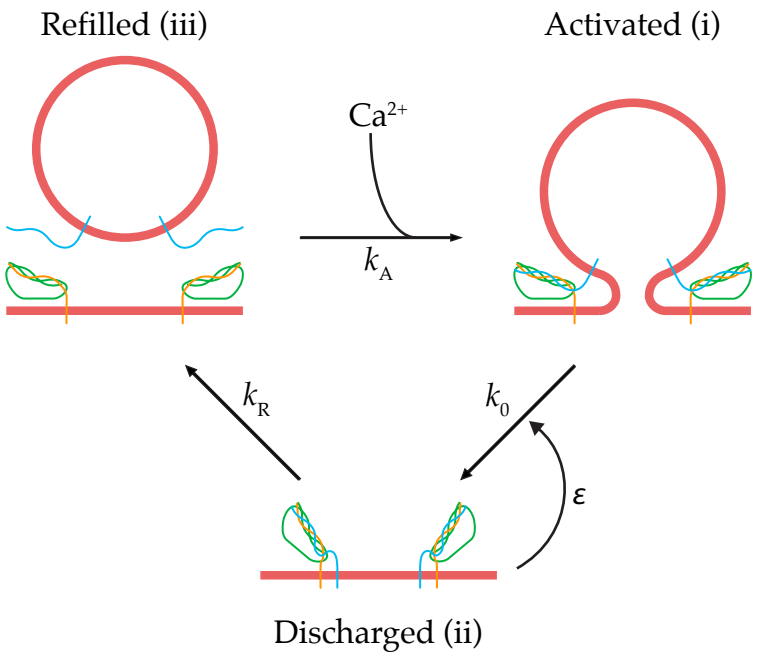

Figure 4.2 The simplified release site model

Each release site undergoes a cycle of irreversible steps. In the resting state (iii), the release site is ready to accept free Ca^{2+}, the binding of which induces the site to become activated (i). Once activated, the site rapidly mediates fusion with the plasma membrane and becomes discharged (ii). There is feedback cooperativity wherein the fusion of vesicles can induce additional fusion at the release site. Once the site is empty, it recovers to its resting, primed state with a recovery rate k_R. The total number of release sites equals the number of vesicles available in the cell's RRP.

(Graydon et al., 2011). In the absence of quantitative data on the absolute levels of buffer in the amphibian papilla, an estimate was made based on existing data of buffer expression levels in other hair cells (Edmonds et al., 2000; Heller et al., 2002; Hackney et al., 2003). The kinetic on and off rates for calbindin-D28K and parvalbumin 3 were also determined from published data (Schwaller, 2010). Since parvalbumin binds two Ca^{2+} ions, and calbindin-D28K four, a total buffering capacity corresponding to the total sites available was assumed, instead of keeping track of multiple buffering species. Diffusion of Ca^{2+} and buffer was not modeled; instead, a steady-state approximation was implemented by assuming the buffer- Ca^{2+} interactions reach equilibrium at a timescale faster than diffusion or the second-long stimuli employed in the capacitance recordings. While this is an approximation, the free calcium signal still followed the nonlinear gating of the corresponding conductance, but it did not undergo the onset and offset modulations afforded by buffer interactions.

The equations governing the system are

$$\dot{x}_1 = -k_0(1 + \varepsilon x_2^2)x_1 + k_A(1 - x_1 - x_2)C \qquad \text{(i)}$$

$$\dot{x}_2 = k_0(1 + \varepsilon x_2^2)x_1 - k_R x_2 \qquad \text{(ii)}$$

$$\dot{C} = -G(V - V_{Ca}) - k_B B C \qquad \text{(iii)}$$

$$\dot{C}_M = k_0(1 + \varepsilon x_2^2)x_1 C_V N - k_M C_M \qquad \text{(iv)}$$

in which C is the Ca^{2+} concentration, x_i is the fraction of sites in state i, k_0 is the vesicle-fusion rate in the absence of cooperativity, ε the cooperativity strength, k_A the rate constant for activation at a release site, k_R the rate constant for site recovery, B the buffer concentration, k_B the binding rate constant for Ca^{2+} buffer, V the membrane potential, V_{Ca} the Ca^{2+} reversal potential, C_M the membrane

capacitance, C_V the average vesicle capacitance, N the number of release sites per hair cell, and k_M the rate constant for membrane recovery. The function

$$G = \frac{g_{MAX}}{2ewN_A\left(1+e^{-\frac{V-V_0}{V_S}}\right)} \qquad \text{(v)}$$

accounts for the Ca^{2+} channels' voltage dependence, in which g_{MAX} is their maximum conductance, V_0 the voltage at which half are open, V_S their voltage sensitivity, e the electron charge, N_A is Avogadro's number, and w the hair cell's volume.

In Table 4.1 are the specific parameter values employed. The dynamics of the system are governed by equations i to iii; equation iv simply provides a way to relate the model's capacitance output to the experimental results of the previous chapter. Aside from the sourced parameters, k_M was determined by fitting the capacitance decay in electrophysiology data, and matches well the fast refilling rate of Cho et al. (2012)**.** The remaining parameters are constrained by the electrophysiology data.

Behavior of the release-site model

The measured tonotopic increase in buffer with increasing frequency presents an odd situation. In general, the resonant frequency of the synapse should grow as the rates associated with the process underlying synaptic tuning are raised. This would cause the system to cycle faster, and therefore the overall kinetics might be optimized for a higher frequency. Ca^{2+} influx increases at least one of these rates and thus one might expect a rise in buffer concentration to decrease the Ca^{2+}-dependent rates and consequently the resonant frequency.

Table 4.1 Model parameters

Parameter	Value	Units
ε	10^8	
V_{Ca}	90	mV
V_S	5	mV
V_0	-45	mV
g_{max}	3.6	nS
w	6.8×10^{-15}	L
k_R	7.6×10^4	s^{-1}
k_A	7.3×10^7	$M^{-1}\ s^{-1}$
k_B	5×10^7	$M^{-1}\ s^{-1}$
N	392	
C_V	34	aF
k_M	0.5	s^{-1}

However, if tonotopic changes in additional parameters other than the buffer concentration are allowed, then the system shows more interesting behavior.

For example, the system's state diagram (Figure 4.3) shows its behavior at a resting potential of -55 mV as a function of buffer concentration B and fusion rate k_0. The diagram outlines three distinct behaviors possible depending on the operating point of the system.

The simplest is the monostable behavior found outside the enclosed regions. Here, the rates are stable; that is, $\dot{k}_i$ are zero. However, it is important to note that the system is still cycling and releasing vesicles, even when not driven by an external stimulus. The monostable behavior stems from the fact that the average rate of release is stable. If one were to analyze the EPSC train from such a system, it would be stochastic. The distribution of inter-EPSC events is given by a convolution of the two Poisson distributions of the activation and refilling steps with the non-Poisson distribution of the release step. Ergo, the cycling time has a certain time-independent mean. The EPSC train will show a peak in its power-spectrum due to the cooperative step, since the cooperative step breaks independence. Moving along the abscissa by increasing the buffer concentration

Figure 4.3 State diagram of the release-site model

(A) A state diagram describes the release-site model at -55 mV as a function of the rate constant for vesicle fusion without cooperativity and the buffer concentration. Spontaneous vesicle release occurs in the red shaded region enclosed by a loop of supercritical Hopf bifurcations. Two steady states are possible in the blue shaded region demarcated by lines of saddle-node bifurcations (blue). The Hopf frequency rises as the buffer concentration increases along the black line. (B) In a plot of the Hopf frequency as a function of the buffer concentration, the resonant frequency equals f_H for points between the black circles at 171 Hz and 1200 Hz. (C) The change in capacitance as a function of frequency is much larger and more sharply tuned when the system operates near a Hopf bifurcation (green line; green dot in A) than when the buffer concentration is increased to move the system farther from the bifurcation (orange line; orange dot in A). (D) Each line outlines the behavior of the system in time for the corresponding operating point in (A). Inside the blue region of (A) the system has three possible states; two are unstable (dotted line) and one is stable (solid). While the behavior is monostable (violet) outside the fish, the rates spontaneously oscillate inside (red).

Figure 4.3 State diagram of the release-site model

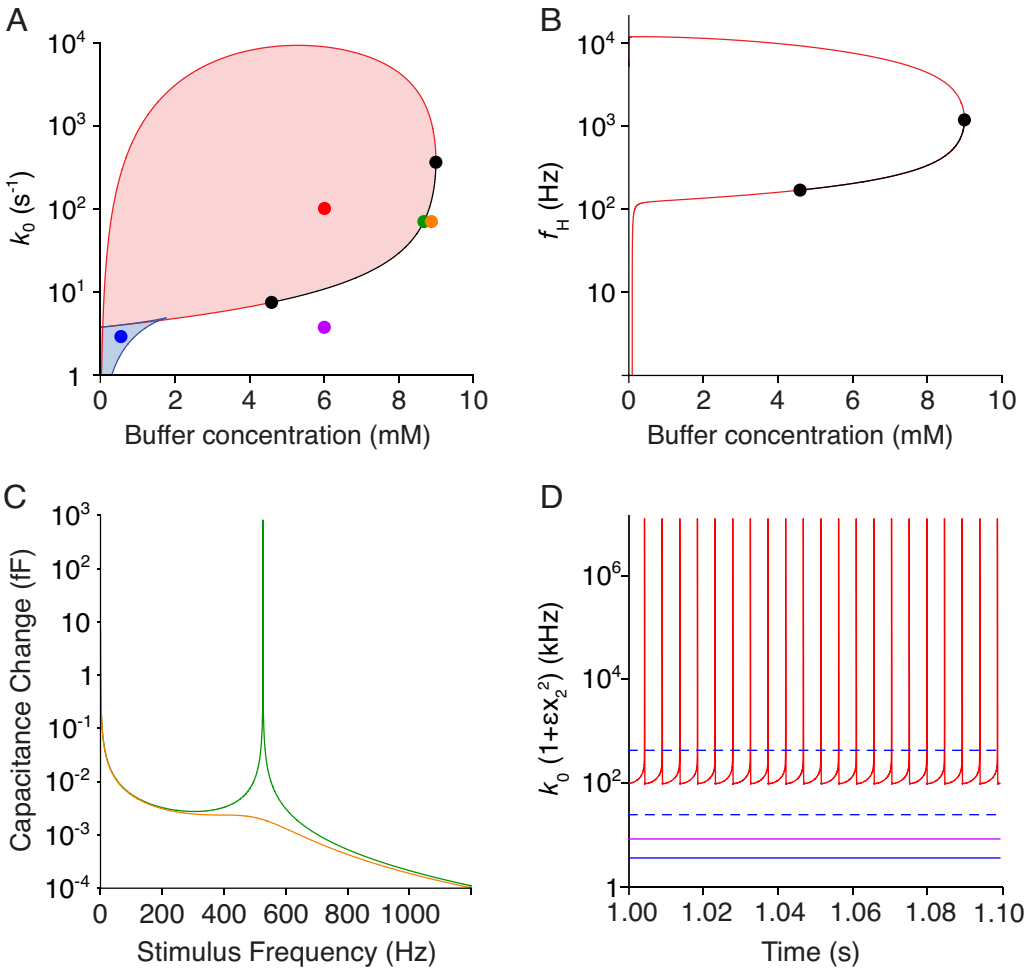

will progressively reduce the free Ca^{2+} available, and therefore increase the mean cycling time, as expected. Within the monostable region, the system shows resonant behavior in response to small stimuli, but this tuning is relatively weak.

In the bistable region, the behavior is similar to that in the monostable region except that two additional states are possible, each with its own cycling time. For most of these points, the two additional points created are unstable and in a real system where noise is non-zero, the system will trend toward the one stable point.

Within the large enclosed loop, however, is a region of spontaneous cycling. For certain values of B and k_0, the system shows spontaneous oscillations in the *rates* of the system. The rates for each transition oscillate from fast to slow. When it is in the fast phase, the mean cycling time shrinks and vesicles are released with greater probability. When it is in the slow phase, the mean cycling time extends, and few vesicles are released during this period. As a result, the Poisson-like distribution of EPSCs oscillates. Note that the *cycle time* of the release site does not necessarily match the oscillation period. *A priori*, there is no constraint that the two periods match and the specific choice of parameters seems to determine which is faster. In this case, the spontaneous oscillations are of a faster period than the cycling time, and therefore can influence the EPSC train significantly depending on their amplitude.

If the system is driven in this region here with a frequency that is close to the spontaneous oscillation frequency, the system's spontaneous oscillations can be entrained to the external driving frequency, and so the synaptic output becomes entrained as well. But this effect is only as strong as the driving force; alternatively, one must drive it strongly to yield a strong entrainment.

A loop of Hopf bifurcations encloses the spontaneously oscillating region. Along this line, there is a region that represents a supercritical Hopf bifurcation. At the line, the system is quiescent. The release site is still cycling with a mean time, but this time does not vary; the rates become stable in the absence of stimuli. But in response to even small stimuli, the system shows a tuned output such that small driving amplitudes incur large changes in the rate. On the positive phases of the driving, vesicles are released at an extremely high rate because the rates become very large, and on the negative phases almost no vesicles are released because the rates approach zero.

Varying B and k_0 can tune this Hopf frequency. Increases in buffer concentration independent of other changes will generally reduce the frequency. However, such increases act to keep the system close to the bifurcation point when a growth in k_0 increases the frequency. The combined influence of B and k_0 is such that the Hopf frequency increases from 171 Hz to 1200 Hz with *increasing* buffer and matches the hearing range of the organ (Lewis et al., 1982). If driven at a frequency near the Hopf frequency, the inter-event time *distribution* oscillates very strongly even for small driving stimuli because the underlying rates incur large variations, but it does not oscillate in the absence of stimuli. As a result, the period of the driving dominates the output of the system even though the output is stochastic, and thus the EPSC events will show a tuned response.

Deviating from the line by increasing the buffer reduces the tuned frequency, and rapidly degrades the tuned response (Figure 4.3C).

Discussion

The previous chapter outlined results that showed the synapse is frequency tuned. Here, I sought to understand how this might come about in the face of an apparent paradox wherein the Ca^{2+} buffering capacity, which ordinarily limits the synapse's output by cutting off Ca^{2+}, increases with tonotopic frequency position. The model confirms that increasing buffer reduces the frequency response ordinarily, but reveals that adjusting the release rate k_0 in tandem keeps the synapse near a Hopf bifurcation, thereby keeping the system sensitive and sharply tuned to oscillatory stimuli.

Figure 4.3 shows the tuned response drops precipitously as the operating point recedes from the Hopf line. In an idealized noiseless system such as that modeled here, this is not surprising. However, *in vivo*, the system has noise in each of the three processes modeled, as well as noise in the input of the membrane potential and due to the gating of the Ca^{2+} channels. If the channels are evenly distributed across the cell's ribbons, then at each ribbon, only a handful of channels are involved in evoking release, adding to the stochasticity of the overall process (Zampini et al., 2010). The overall effect of this noise is to degrade the tuning everywhere; with noise, the green curve in Figure 4.3C, which describes behavior near the Hopf bifurcation, will broaden and decrease in amplitude. However, without an estimate of the intrinsic noise involved in each of the processes represented in the model, an exact determination of the sharpness of tuning is not possible. It is simply the case that the system does not need to position itself *exactly* on the line along which the Hopf bifurcation occurs, but only near it for sharp tuning to occur.

The model also provides other insights into the tuning process. First, given that the buffer gradient may be crucial, eliminating it during whole-cell recording—and thereby forcing the system to a fixed low buffer concentration as commonly employed with low millimolar amounts of intracellular EGTA—would eliminate the tuned response, and may force the synapses into an oscillatory state. Thus, the model predicts that simultaneous whole-cell recordings of hair cells and afferent neurons might show oscillatory EPSC trains, particularly in the high-frequency region since maximal perturbation of buffer concentration will occur; capacitance recordings do not have the temporal resolution to observe the phenomenon. Such an experiment, at the moment, is complicated by the rapid deterioration of the high-frequency cells under ordinary experimental conditions. Indeed this has limited recordings of high-frequency cells in several preparations. Still, the prediction suggests yet another interesting experiment should future protocols allow for longer recording times from this cell population.

A more mechanistic exploration would focus on dynamic changes in buffer concentration or function while recording synaptic output. One possibility is to record changes in a cell's synaptic tuning in response to buffer changes. Perforated-patch experiments such as those of the previous chapter can record a tuning curve, rupture the patch to wash out the buffer, and record the curve again. However, despite reports of selective partitioning of the perforating compound in the inner and outer leaflets of the cell's membrane, several attempts with amphotericin-B and with nystatin, another perforating compound, both rapidly destroyed the cell membrane's integrity after they had penetrated into the cell.

An alternative would be to conduct a whole-cell recording of the cell while dynamically controlling the pipette's intracellular solution, and therefore, the amount of buffer in the cell. Though still somewhat technologically limited, a few reports exist of such experiments, in which controlled exchange of cell content occurs over a time constant of one minute (Bucurenciu et al., 2008). If such an experiment were possible on hair cells, then the model predicts that serially raising a low-frequency cell's buffering capacity would eliminate its tuning, and serially lowering a high-frequency cell's buffer would force it into an oscillatory regime.

An alternative might be to exploit the differential affinities of the buffers' binding sites to Ca^{2+} and Mg^{2+}. At physiological concentrations of Mg^{2+}, both calbindin and parvalbumin are already partially saturated by Mg^{2+}. Parvalbumin's affinity for Mg^{2+} is fairly high; even at rest, nearly all of it is bound with Mg^{2+}. Though the calcium affinity in both proteins is a thousand fold stronger than that for Mg^{2+}, saturating the cell with 10 mM Mg^{2+} by loading with the cell-permeant caged Mg^{2+} source DM-EDTA-AM (Ellis-Davies, 2006) effectively limits the cell's Ca^{2+}-buffering capacity.

Aside from these predictions, the model raises one fundamental question. For tuning to occur, the model's implies a gradient of the fusion rate k_0 in addition to that of buffer concentration. This might lie somewhere within the vesicle fusion apparatus. The effectors of this process are vast: the membrane fusion proteins, of the SNAP (Soluble NSF Attachment Protein) receptor group, collectively termed SNAREs, are still not fully understood. Modifiers of their function, such as the munc proteins discussed in the previous chapter, have not been characterized in hair cells across the frequency range. Still, that the fusion

rate is a key parameter implies that control comes from processes that occur after the binding of Ca^{2+}. Somehow, in the high-frequency cells, the process of fusion after Ca^{2+} binding might be faster. An alternative to tonotopic variations in SNARE components or modifiers (since one must consider both enhancers and inhibitors) might be spatiotemporal control of the vesicle population. Perhaps variations in the ribbon's shape and size, as well as the vesicles' arrangement around the ribbon, give rise to a phenomenological difference in the fusion rate. Naively, one possibility that the model does not exclude is simply increasing the size of the RRP in high-frequency cells. Though the *rate* of fusion is a key gradient in the model, the RRP was assumed to be equivalent across the tonotopic axis. The model might yield similar output if in high-frequency cells a larger RRP boosts fusion probability. For example, if the cooperativity stems from interactions of neighboring vesicles, high-frequency cells might exploit this through a tighter packing of a larger RRP. Ultrastructural reconstructions of ribbons from cells across the frequency range might thus show systematic changes of the ribbon and the associated vesicle pool that can guide future refinements of the model.

At any rate, the ribbon's physical parameters and the SNAREs therein are not likely to be the only tonotopically varying components of the synaptic apparatus. At the top of the cascade, a tonotopic variation in peak amplitude of the inward Ca^{2+} current has already been documented: rostral, low-frequency cells of the amphibian papilla show nearly twice the peak amplitude as caudal, high-frequency cells (Smotherman and Narins, 1999). However, it is not clear whether that variation results from changes in current density at each synapse, presumably due to variation in total channel number at each synapse, or simply

from scaling due to total synapse count per cell. In the case of the latter, this might just reflect the presence of more active zones in low-frequency hair cells. Without a count of ribbons per cell, the interpretation is not obvious.

Clearly, the model is a gross simplification of the overall release process. Multiple tonotopic changes that are not represented in the model are likely to take place that optimize the system for its best frequency. Hence, future studies should focus on identifying kinetic differences in synaptic function across the epithelium. For example, synaptic output in response to flash photolysis of caged Ca^{2+} might give insight into the rate parameter, since total Ca^{2+} input can be controlled by avoiding variations in Ca^{2+} gating in different cell populations. By doing so, kinetic parameters that underlie the tuning system can be elucidated, garnering a richer understanding of the mechanism as a whole.

Chapter 5. Conclusion

Robert Galambos and Hallowell Davis first reported the responses of individual afferent nerves of the cat's cochlea more than half a century ago (Galambos and Davis, 1943). Although later they discovered that their recordings were actually from the animal's cochlear nucleus and not the auditory nerve as they had originally claimed, the data nonetheless first demonstrated the sharp frequency selectivity of *individual* nerve responses in the auditory system. Two decades passed before Nelson Kiang demonstrated that "tuning" is exceptionally sharp in primary auditory fibers as well (Kiang, 1965). By this point, the place theory of Hermann Helmholtz (Helmholtz, 1877), which holds frequency discrimination is accomplished by selectively activating groups of afferent neurons on the basilar membrane based on the frequency of auditory input, had gained considerable support, supplemented with von Bekesy's diagrams of the membrane's tonotopically peaking traveling waves (von Bekesy, 1960). Thus, the hunt was on to determine how much of the tuning of the nerve fibers was to be found in the travelling wave. This line of investigation has only recently culminated as improved methodology has allowed for the recording of the profile of traveling wave in living mammalian cochleas at single points (Ruggero et al., 2000) and *very* recently, spatially as well (Ren et al., 2011; Fisher et al., 2012).

Soon after the mammalian tuning curves came those from the remaining terrestrial vertebrates: birds, amphibians, and reptiles (Sachs et al., 1974; Feng et al., 1975; Crawford and Fettiplace, 1980; Klinke and Pause, 1980). These animal

groups were subsequently found to lack tuned basilar-membrane traveling waves, and thus to rely on other mechanisms to achieve frequency tuning: hair bundle resonance, which might be quite sharp as it benefits from coupling to other hair bundles, and electrical resonance, which seems fixed at two orders. The discovery here of synaptic tuning, supporting the work of Rutherford and Roberts (2006) and the prediction of Schnee et al. (2005), adds another filter to the vertebrate sensory cascade, and explains at least some of tuning curves' sharpness. Whether synaptic tuning exists in other vertebrates will be determined in future studies. And if the mechanism does lie in a gradient of the Ca^{2+} buffer and a release parameter, certainly the other non-mammalian vertebrates seem to be well poised with their similar buffer gradients (Hiel et al., 2002; Hackney et al., 2003).

The phenomenon of synaptic tuning is surprising. That evolution has produced a synapse that distinguishes periods on the order of a millisecond in its stimuli is remarkable. The selective pressure to achieve sharp tuning, whether from a need to communicate in crowded niches or to maximize the detection of otherwise hidden prey, clearly has been strong. Frequency processing on these timescales at the level of individual cells has long been the domain of membrane properties and ion channels; synapses have rarely been included in this group. Biochemical processes usually regulate events on much slower timescales. And only in hair cells has this capacity been given to an additional entity—their conspicuous mechanical resonators. Yet perhaps for those very reasons it is *not* surprising. Certainly the cell has tuned other processors of input up to the synapse; why shouldn't the same occur at the synapse? Hearing seems to have pushed biology to the limit in many other respects, with thresholds of detection

starting at thermal noise and frequencies that approach 100 kHz. If the system has specialized itself to such an extent, then perhaps it is not so outrageous that it has co-opted an information transmission apparatus to do a bit of information processing as well.

If the origin of frequency-selective synaptic responses is attributed to a need for exceptional tuning, one last point is to be made: where does the tuning end? There do not seem to be many other areas left where tuning might be possible except in the generation of the afferent nerve's action potential. The auditory afferents of the mammalian cochlea show striking systematic variation in their firing properties. Those neurons that carry low-frequency information have a longer latency and adapt slower than high-frequency counterparts (Adamson et al., 2002). The underlying distribution of various K^+ channel subtypes is also tonotopically graded. The glutamate receptor subunits that regulate input to these neurons are also tonotopically graded, and this gradient seems to be under the control of brain-derived neurotrophic factor (BDNF) and neurotrophin-3 (NT-3), which themselves are systematically distributed in complementary gradients along the cochlea (Schimmang et al., 2003; Flores-Otero et al., 2007; Sugawara et al., 2007). In the mammalian cochlea, since tuning seems to be accomplished by the traveling wave, these specializations might only be to best respond to the different synaptic outputs of apical and basal cells, but if such patterns are recapitulated in other vertebrates, it seems possible that the generation of spikes can be frequency tuned. This was difficult to test in the amphibian papilla preparation utilized here, since my observations and those of Erica Keen both revealed spike amplitudes of ~10 mV when recording just postsynaptically to the hair cell, indicating that either the generation site is rather

distant, or that the neurons are leaky in the preparation. Hence, reverse correlation of spikes with input was difficult. Still, even the Hodgkin-Huxley model shows an intrinsic low-frequency resonance near 70 Hz, and thus suggests that fine control of the underlying ion channel dynamics might provide tunable responses, as it does for electrical resonance in hair cells. Future studies in this area may prove to be fruitful, and the hunt for the final filter might not be over.

APPENDIX ONE

Tabulated capacitance changes in hair cells in response to sinusoidal stimulation

Data from sixteen cells was used to plot the tonotopic dependence of synaptic tuning in Figures 3.3 and 3.4. Each of these cells showed a significantly greater change in capacitance to stimulation at a particular frequency over that at neighboring frequencies. On the following page is a table of each cell's position from the caudal end of the amphibian papilla and the mean capacitance change measured in that cell in response to sinusoidal stimulation at the respective frequencies (Table A3.1). Table A3.2 also shows data from several cells that failed to show significant frequency-tuned responses. For each cell indicated in the tables, the seven values of capacitance changes recorded correspond to the following frequencies:

Indicated Range	Frequencies Tested (Hz)
0-1000	0, 25, 200, 400, 600, 800, 1000
50-350	50, 100, 150, 200, 250, 300, 350
100-700	100, 200, 300, 400, 500, 600, 700
300-900	300, 400, 500, 600, 700, 800, 900

ΔC_M values are reported in fF.

Table A3.1 Capacitance changes in cells that showed frequency-tuned release.

Cell #	Distance from caudal end (μm)	Frequency Range	ΔC_M (1)	ΔC_M (2)	ΔC_M (3)	ΔC_M (4)	ΔC_M (5)	ΔC_M (6)	ΔC_M (7)
1	250	0-1000	29.45	-0.73	-5.55	24.01	30.88	22.80	3.94
2	250	0-1000	183.73	-117.79	-30.17	-84.41	301.85	180.35	-127.63
3	290	0-1000	-21.76	-58.12	-21.10	18.48	22.10	3.65	-11.18
4	295	300-900	109.00	-12.72	35.10	45.29	98.06	66.58	-5.85
5	350	0-1000	23.38	25.91	-61.49	-34.22	55.91	-16.16	-15.41
6	425	0-1000	12.50	-21.90	0.29	57.10	-20.20	-10.30	-38.50
7	450	0-1000	-4.13	-18.31	30.12	62.45	-51.81	-48.22	10.27
8	492	100-700	-40.36	-14.72	89.56	21.18	-18.25	2.56	11.15
9	495	100-700	-16.73	-113.87	-55.29	-49.05	21.43	-13.36	-138.36
10	512	100-700	12.01	-99.05	-10.66	54.51	-19.23	-76.48	-37.35
11	550	0-1000	-9.41	-8.48	26.40	-8.09	-13.39	-9.66	3.17
12	572	0-1000	15.91	-22.51	19.20	-22.33	3.68	2.67	-17.38
13	580	0-1000	2.65	-11.74	28.85	-2.06	6.38	-10.62	-2.00
14	625	0-1000	-4.53	17.03	22.61	56.29	24.17	10.41	8.36
15	625	50-350	-29.78	6.35	36.10	13.66	-15.76	-35.38	-2.43
16	650	0-1000	34.38	-15.79	45.29	5.22	-12.52	4.03	59.93

Table A3.2 Capacitance changes in cells that failed to show frequency-tuned release.

Cell #	Distance from caudal end (μm)	Frequency Range	ΔC_M (1)	ΔC_M (2)	ΔC_M (3)	ΔC_M (4)	ΔC_M (5)	ΔC_M (6)	ΔC_M (7)
1	477	100-700	-20.05	20.48	42.13	-46.90	29.81	54.42	41.08
2	495	100-700	-21.51	8.11	-8.82	0.28	-32.94	5.57	-26.82
3	500	100-700	55.51	22.33	54.79	7.28	56.51	16.11	50.88
4	525	0-1000	37.48	4.04	14.23	-7.66	-0.32	9.60	0.88
5	537	0-1000	162.10	-49.30	34.68	182.34	77.87	5.19	60.93
6	550	50-350	-48.17	-68.80	-34.94	-30.61	-7.39	-41.51	-58.47
7	600	0-1000	-33.26	-41.65	-47.07	-11.67	22.34	-2.25	57.86
8	612	0-1000	8.06	18.38	8.88	-14.37	-0.06	8.12	-4.39
9	612	0-1000	6.01	12.78	6.55	-28.43	-15.98	12.40	-13.65
10	662	50-350	-37.98	-23.63	-30.20	-2.65	-4.10	-22.52	-35.95
11	685	50-350	-6.96	-15.50	18.22	40.08	-10.32	28.95	1.01

APPENDIX TWO

The role of the transient receptor potential melastatin 7 (TRPM7) channel in synaptic transmission in hair cells

Work in progress in collaboration with Sean E. Low

Overview

In this section I describe preliminary work on an aspect of synaptic transmission unrelated to frequency selectivity. Recent work has identified TRPM7, a member of the transient receptor potential (TRP) superfamily of cation channels that possesses an enzymatically active kinase at its carboxyl terminus, as necessary for touch-evoked activation of escape behaviors in zebrafish (Low et al., 2011). Mutations in the gene encoding TRPM7 (*trpm7*) underlie the touch-unresponsive zebrafish mutant *touchdown*. In this line, the mechanosensitive Rohon-Beard (RB) neurons are present and respond to tactile stimuli, suggesting that TRPM7 is not required for sensory neuron survival or mechanosensation. Because the Mauthner cell, which is postsynaptic to the RB cells, does not respond in *touchdown*, and exposure to elevated concentrations of extracellular Ca^{2+} restores touch-evoked behaviors in the mutants, TRPM7 may modulate neurotransmitter release at central synapses in sensory neurons. A similar role has been proposed for mammalian TRPM7 at peripheral synapses (Krapivinsky et al., 2006; Brauchi et al., 2008).

Touchdown mutants are also unresponsive to water movement (unpublished observation, Low SE). Why this is so is not known. TRPA1, a related member from the TRP family, has previously been found in hair cells and proposed to play a role in hair cell mechanotransduction (Nagata et al., 2005), but this was later shown to be not the case (Kwan et al., 2006). Likewise has been the story with other members of the TRP family, namely TRPN1, TRPV4, and TRPML3 (Corey, 2006). Here I describe efforts to elucidate the role of TRPM7 in

hair cells in light of what is known about the channel's role in synaptic transmission and the possibility of it being the channel responsible for hair cell mechanotransduction.

S. E. Low performed the molecular-biological and behavioral experiments, I conducted the electrophysiology, and A. J. Hudspeth is carrying out electron-microscopy studies.

Introduction

The first transient receptor potential (TRP) gene was identified in the fruit fly *Drosophila* as encoding a putative ion channel, mutations in which resulted in a transient receptor potential in the animal's photoreceptors in response to sustained light stimuli (Montell and Rubin, 1989). Originally described almost twenty years prior to the gene's identification, the founding member of this class of proteins has only recently been confirmed as a pore-forming channel subunit (Cosens and Manning, 1969; Liu et al., 2007). Since the original discovery the identification of additional TRP channels within the genomes of worms, flies, mice, and humans has resulted in a superfamily with 33 members in mammals and approximately 60 predicted in the genome of the zebrafish (Montell, 2005). The collection has been divided into seven subfamilies based on sequence similarity (TRPM, TRPC, TRPP, TRPA, TRPV, TRPML and TRPN) (Montell et al., 2002). Structurally, these channels resemble voltage-gated K^+ channels, with each subunit possessing six transmembrane (TM) domains and four subunits assembling to form a functional channel. In contrast to voltage-gated K^+ channels, though, TRP channels are nonselective: they are permeable to multiple cations including Na^+, K^+, Ca^{2+} and Mg^{2+}. Furthermore, the channels are activated by a range of stimuli including light, temperature, pheromones, and mechanical stimuli. Hence, TRP channels have been linked to several sensory systems including vision, chemosensation, thermosensation, nociception, and mechanosensation (Clapham, 2003). In the case of TRPV1, the channel is a direct receptor for capsaicin, the active compound in hot peppers. TRP channels can

also act downstream of the initial transduction by way of an intracellular signaling cascade, as is the case for founding member TRP-1 (Montell and Rubin, 1989).

At least three members of the family serve mechanosensory roles. In a screen for osmotic avoidance and nose touch in *C. elegans*, the first was identified as *osm-9* (Colbert and Bargmann, 1995). The mammalian ortholog of *osm-9* proved to encode TRPV4, which responds to hypotonic stimuli (Liedtke et al., 2000). Indeed mammalian TRPV4 rescues the touch insensitivity of *osm-9* mutants (Liedtke et al., 2003). The second mechanosensory TRP channel was identified in *Drosophila*. A mutagenesis screen identified *nompC* as responsible for the apparently clumsy phenotype in this line of flies. The animal's mechanosensory bristle neurons lacked much of the mechanically activated current in homozygous mutants, and subsequent cloning localized the defect as arising from mutation in TRPN1. Thereafter, the zebrafish ortholog was found to be expressed in otic hair cells and necessary for the uptake of FM1-43, a fluorophore known to pass through the hair cell's mechanotransduction channels (Sidi et al., 2003). TRPN1 was also necessary for stimulus evoked microphonic potentials. Thus, *trpn1* encodes an essential component of vertebrate hair-cell mechanotransduction, though whether it is the mechanotransduction channel remains unclear. In *Xenopus*, TRPN1 localizes to the non-mechanotransducing kinocilium, suggesting that it is not an integral part of the MET apparatus at the tips of the hair cell's stereocilia (Shin et al., 2005). Lastly, the *Drosophila* mutant *painless*, so named for its abnormal response to noxious stimuli (Tracey et al., 2003), arises from a disruption in TRPA1 (Al-Anzi et al., 2006). Here, the channel is localized in the dendrites of multidendritic sensory neurons, an expression

pattern suggestive of a mechanosensory role. In *C. elegans*, TRPA1 is necessary for normal responses to repeated mechanical stimuli (Kindt et al., 2007). The channel also has been implicated as possibly the mechanotransduction channel of hair cells (Corey et al., 2004), but mice lacking the *trpa1* gene show normal transduction currents in hair cells, balance sense, and auditory brainstem responses (Kwan et al., 2006). TRPA1 is also not required for hair-cell mechanotransduction in zebrafish (Prober et al., 2008).

Recently, the zebrafish mutant *touchdown* was shown to have abnormal touch responses stemming from a truncation in TRPM7 (Elizondo et al., 2005), one of only two ion channels known to possess an enzymatically active kinase tethered to its carboxyl terminus. Though the kinase can phosphorylate the channel itself, it is dispensable for the channel's function (Matsushita et al., 2005). In *touchdown* mutants, the channel is found in the RB mechanosensory neurons, where the channel activity, but not kinase activity or specific cation selectivity, is necessary for normal touch-evoked responses (Low et al., 2011). Although the sensory neurons respond to tactile stimuli in the mutant, the immediately postsynaptic neuron that normally fires in response, the Mauthner cell, does not. Lastly, because elevated concentrations of extracellular Ca^{2+} restores the touch response, TRPM7 is postulated to play a role in synaptic transduction between the RBs and Mauther cells.

TRPM7's role in synaptic transmission is buttressed by its localization to synaptic vesicle membranes in mice and interactions with the synaptic-vesicle proteins synapsin and synaptotagmin (Krapivinsky et al., 2006). Presynaptic levels of the channel seem to influence the size of acetylcholine-induced EPSPs in cultured neurons, suggesting the channel plays a role in the amount of

neurotransmitter found in synaptic vesicles. In rat pheochromocytoma PC12 cells, in which TRPM7 also localizes to vesicle membranes, knockdown of TRPM7 reduces the frequency of spontaneous and stimulated vesicle-fusion events (Brauchi et al., 2008). Channel conductance seems to be necessary for fusion, whereas the kinase function affects vesicle mobility.

Because *touchdown* mutants also seem to be unresponsive to water movement, which is sensed by the zebrafish's lateral-line organ, we have explored the role of TRPM7 in this process.

Materials and Methods

Zebrafish husbandry and strains

Zebrafish were bred and raised according to guidelines approved by the Rockefeller University's Institutional Animal Care and Use Committee. Zebrafish were maintained in aquaria (Aquatic Habitats) at 28 °C. Naturally spawned eggs were collected, cleaned, staged and maintained in system water supplemented with 3.13 μM methylene blue to prevent fungal and bacterial growth. The *touchdown* allele tdo^{mi174} (hereafter *tdo*), in which TRPM7 is truncated after its second transmembrane domain, was identified in a screen conducted at the University of Michigan, Ann Arbor and is the mutant line employed here (Low et al., 2011). Homozygous *touchdown* mutants were identified at 50 hours post fertilization (hpf) by their hypopigmentation and lack of touch-evoked escape responses.

Behavior characterization

To assay lateral-line evoked escape behaviors, embryos were first anesthetized in system water supplemented with 765 μM benzoic acid ethyl ester and mounted dorsal side up in system water containing 1% low-melting point agarose at 42 °C. Solidified agarose was cleared away from the trunk and tail regions of embryos using a pair of fine forceps. House vacuum, applied with a fluid-filled borosilicate glass capillary tube positioned approximately 500 μm behind the tail, was controlled by a VC-6 perfusion valve control system (Warner Instruments). Lateral-line evoked behaviors were imaged at 1 kHz using a

Motion Scope camera (Redlake Imaging) mounted to an Olympus SZX7 stereomicroscope that magnified the sample 10X. Images acquisition and analysis was performed with ImageJ.

Molecular biology

Capped RNA encoding wild-type zebrafish TRPM7 that was fused to eGFP (TRPM7-eGFP) was synthesized from the T7 site of pcGlobin2 using the mMESSAGE mMACHINE T7 kit (Ambion). RNA was diluted to a concentration of 200 ng/μl in diethylpyrocarbonate-treated water (DEPC-H_2O) containing 282 μM phenol red and was then injected into one-cell stage embryos using a Nanoinject II system (Drummond Scientific).

Selective restoration of TRPM7 expression within hair cells was targeted by placing TRPM7-eGFP expression under the control of the myosin6b promoter. One-cell stage embryos were injected with 10 pg of a plasmid containing *myo6b:trpm7-eGFP* diluted in 4.6 nl of water that contained 282 μM phenol red.

Embryos were assayed 4–6 hrs after injection for the retention of phenol red, and at 24–30 hpf for eGFP fluorescence.

Microphonic recordings

Wild-type and *tdo* zebrafish larvae at 52-60 hpf were anesthetized with 765 μM benzoic acid ethyl ester in standard Evans solution containing (in mM) 134 NaCl, 2.9 KCl, 2.1 $CaCl_2$, 1.2 $MgCl_2$, 10 glucose, and 10 Hepes at pH 7.8. Larvae were secured on their sides in a 35 mm Petri dish coated with Sylgard by two tungsten pins, 50 μm in diameter, that were inserted in the tail and

dorsorostral to the heart. Larvae were then observed with a microscope using differential-interference-contrast optics with a 60X, 0.9 NA objective lens.

Stimuli were presented and data acquired with programs written in LabVIEW (National Instruments). Anteroposteriorly oriented neuromasts were mechanically stimulated along their axis of sensitivity with a glass probe attached near the cupula's tip. A sinusoidal stimulus with an amplitude of 5 μm was delivered with a piezoelectric stimulator. Probes were manufactured by melting the tip of electrodes pulled from thin-walled borosilicate glass by passing the electrodes through a bunsen burner flame.

Recordings were obtained at room temperature with a capacitatively coupled amplifier (P55, Grass Technologies) at a gain of 10,000X. Borosilicate-glass recording electrodes displayed resistances of 2–3 MΩ when filled with the bathing solution. These were placed within 1 μm of a neuromast's aperture. Signals were acquired at 50-μs sampling intervals and digitally low-pass filtered at 500 Hz. The displayed records represent averages of 200-300 stimulus presentations.

Posterior lateral line ganglion recordings

Methods similar to those previously published (Trapani and Nicolson, 2010) were employed to record the extracellular activity of neurons from the posterior lateral line ganglion. Embryos were mounted and visualized as for microphonic recordings. Prior to recording, the bath solution was replaced with standard Evans solution without benzoic acid ethyl ester and supplemented with 30 μM tubocurarine to block muscle contraction. Access to the membranous sac

that encloses the ganglion was obtained by increasing pressure of the recording pipette against the sac until the membrane ruptured. Pipette entry was verified by the visualization of sac inflation upon application of positive holding pressure to the pipette. Once inside, spontaneous spikes of varying amplitudes in the range of 0.1 to 0.25 mV were observed. The pipette was moved slowly inside the sac to press against a particular neuron's cell body. Upon the application of slight negative pressure, the spontaneous activity became less frequent, and the amplitude increased to approximately 0.5 mV and became homogeneous, suggesting activity was recorded from a few neurons of the posterior lateral line. The protocol was optimized by recording activity in wild-type larvae of 52-60 hpf. Identical procedures were followed to obtain recordings from *tdo* mutants.

The activity of the ganglion was recorded with an Axoclamp 200B amplifier (Molecular Devices) operating in fast current-clamp mode at 200X gain with the low-pass filter set to 2 kHz. Data were acquired with LabView and further band-pass filtered digitally between 10 Hz and 1 kHz.

Whole-mount *in situ* hybridization

In situ hybridization was performed using methods similar to those previously described (Westerfield, 1993). The DNA template was prepared by cutting 1.2 μg of plasmid DNA using a restriction enzyme digest and was precipitated with phenol/chloroform as follows. Following a 1 hr digest, 2 mg of proteinase K (New England Biolabs) and 0.5% sodium dodecyl sulfate were added and the mixture was incubated at 50 °C for 30 minutes. The template was extracted with phenol/chloroform, precipitated at -80 °C for 30 minutes, and

centrifuged at 4 °C for 20 minutes at 14,000 rpm. The precipitated template was resuspended in DEPC-H_2O and used for probe synthesis using SP6 and T7 polymerases (Promega) and DIG-labeled RNA mix (Roche). Riboprobes were sheared to 600 base pairs by alkaline hydrolysis. Probe length was verified by gel electrophoresis prior to use.

After 22 hpf, embryos were reared in system water supplemented with 200 μM 1-phenyl-2-thiourea to prevent the development of pigmentation and fixed at 72 hpf with 4% paraformaldehyde in PBS for 1 hr at room temperature. Embryos were then dehydrated with an increasing percentage of methanol in PBS and stored at -20 °C for 30 minutes. They were rehydrated by decreasing the percentage of methanol in PBS containing 0.1% Tween and incubated at room temperature with 10 μg/ml proteinase K for 5 min to increase the penetration of riboprobes, and then re-fixed with 4% formaldehyde in PBS for 1 hr at room temperature.

Antisense and sense control riboprobes were hybridized for 16 hrs at 65 °C. Embryos were incubated overnight at 4 °C with anti-DIG antibody conjugated to alkaline phosphatase. Chromogenic detection was performed with a nitro blue tetrazolium and 5-bromo-4-chloro-3-indolyl phosphate (NBT/BCIP; Roche). The chromogenic reaction was quenched at various times for both antisense and sense control conditions. Staining for *trpm7* mRNA was considered specific when corresponding staining was absent in sense control.

Results

touchdown mutants do not respond to water movement

To assess the responsiveness of *touchdown* fish to water movement, we imaged the behavior of head-fixed fish in response to water jet stimuli. Wild-type fish of 2 dpf showed robust escape responses when a suction water jet was activated near their tail for 20 ms. Using identical positioning and stimuli, *tdo* fish displayed a complete lack of response, even when the jet was active for 1,000 ms (Figure A1.1).

Posterior lateral line activation is impaired in *touchdown* fish

We sequentially examined the functioning of the lateral-line sensory cascade to determine if an afferent sensory defect was present in *tdo* fish. Since posterior lateral line neuromasts appeared morphologically normal in *tdo* fish, we assayed mechanotransduction by the neuromasts' hair cells. In both wildtype and *tdo* fish, extracellular microphonic potentials evoked at lateral line neuromasts were intact (Figure A1.2). Thus, *tdo* fish did not seem to lack mechanotransduction.

We next examined the activation of postsynaptic afferent neurons by spontaneous neurotransmitter release at hair-cell synapses, which are known to drive the spontaneous spiking behavior of posterior lateral line afferent neurons (Trapani and Nicolson, 2011). In all ten attempts on ten fish from three wild-type clutches, extracellular loose-patch recording in the posterior lateral line ganglion showed clear spontaneous spiking of lateral-line afferents. However, we failed

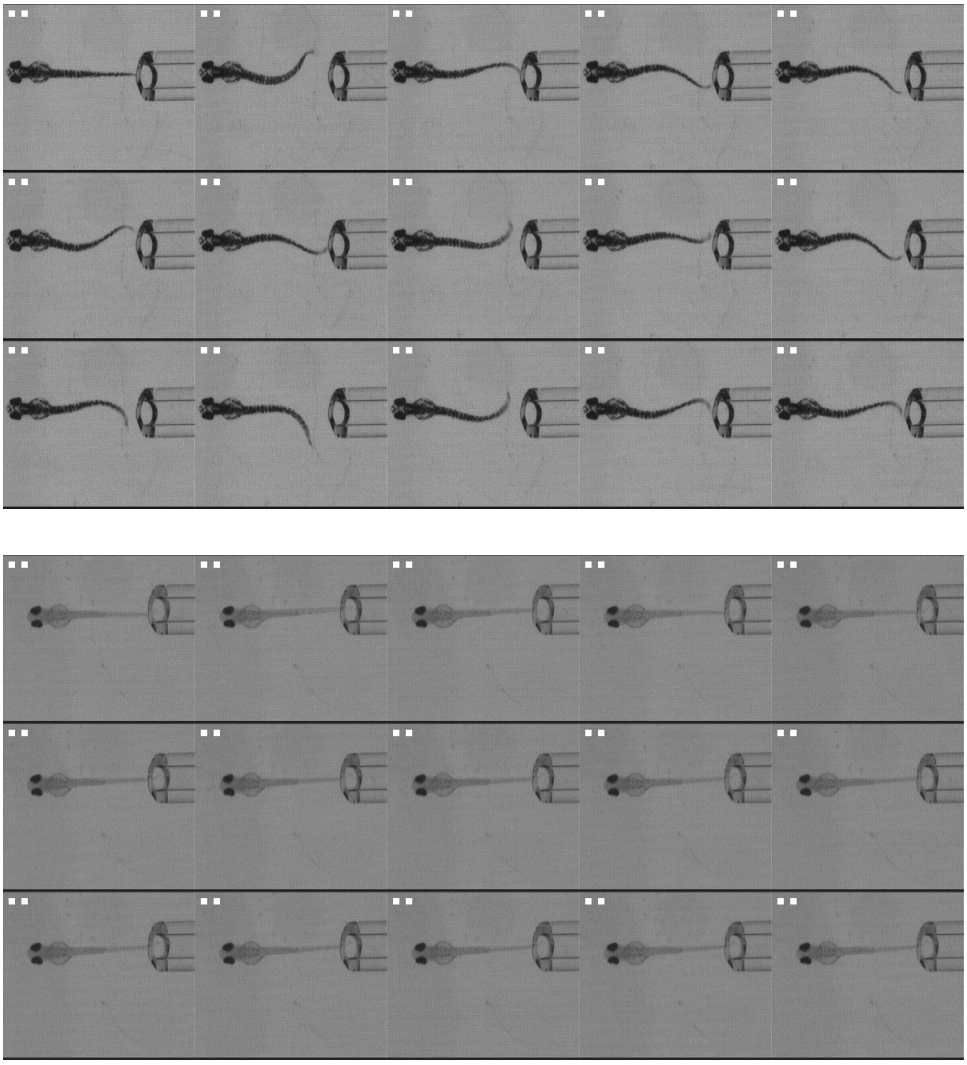

Figure A1.1 TRPM7 mutants do not respond to lateral line stimuli

In the upper panel is a representative response from a head-fixed wildtype 2 dpf larva to the activation of a water jet near its tail for 20 ms (pulsed between first and second frames). Note the conspicuous escape response, which is absent in the *tdo* larva of the lower panel when presented with the same stimulus. Each frame is advanced by 136 ms, for a total representation of two seconds.

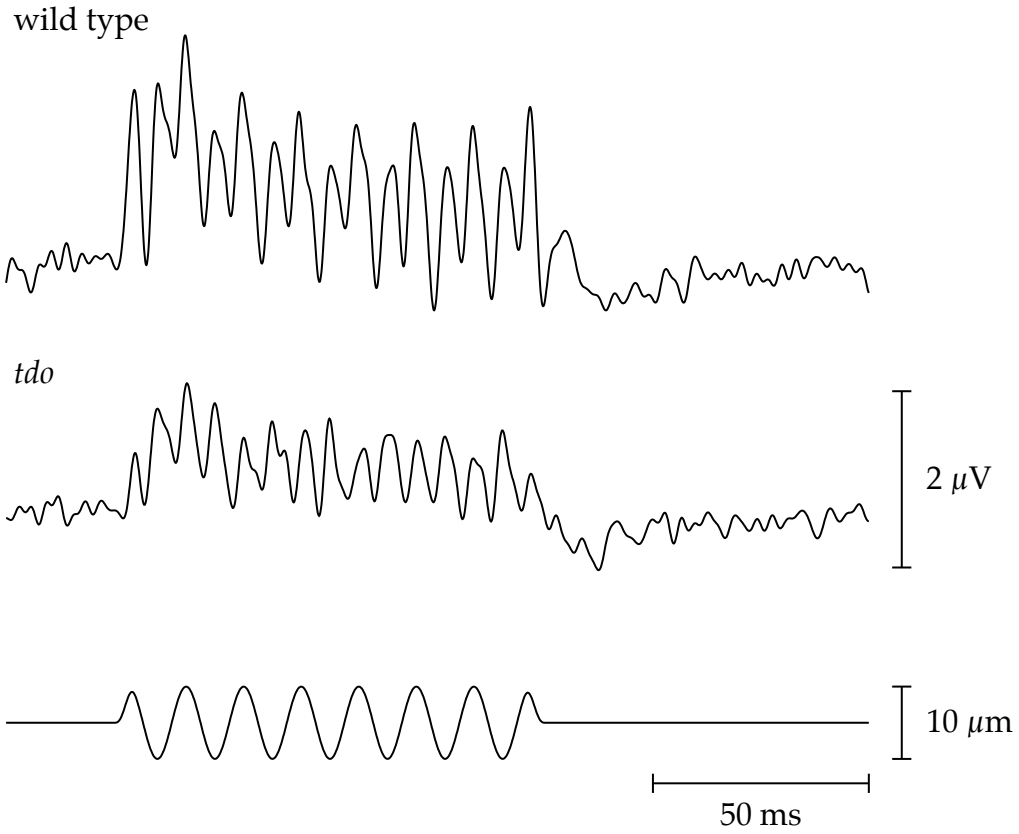

Figure A1.2 TRPM7 is not required for hair-cell mechanotransduction

In response to a 75 Hz mechanical stimulus delivered to lateral line neuromasts of 2 dpf wild type and *tdo* larvae, a microphonic potential is evoked at twice the stimulus frequency, confirming mecanotransduction by hair cells is present in *tdo* fish.

to observe any spiking in ganglia from *tdo* fish in an equivalent number of trials, indicating that synaptic transmission is impaired in *tdo* fish (Figure A1.3).

TRPM7 expressed in lateral-line hair cells rescues afferent neuron activity

Because posterior lateral line ganglion activity was absent in *tdo* fish, we determined if TRPM7 was expressed in either neuromast hair cells or posterior lateral line neurons of wildtype fish. Robust labeling with *in situ* hybridization against TRPM7 mRNA transcript was observed in lateral line neuromasts (Figure A1.4) but not in the ganglion.

We next asked whether rescue of TRPM7 expression rescues afferent neuron activity. We injected *tdo* larvae with mRNA encoding TRPM7 and measured ganglion activity. Five of six injected larvae showed rescue of spontaneous ganglion activity, while all six uninjected controls showed no rescue (Figure A1.3). Consistent with the mosaic expression of injected RNA, we found that the frequency of spontaneous spiking was somewhat reduced in RNA rescued fish. Furthermore, in one of three *tdo* embryos injected with a plasmid driving *trpm7* under the control of the *myo6b* promoter, which drives the hair-cell specific expression of myosin 6b, ganglion activity was also restored.

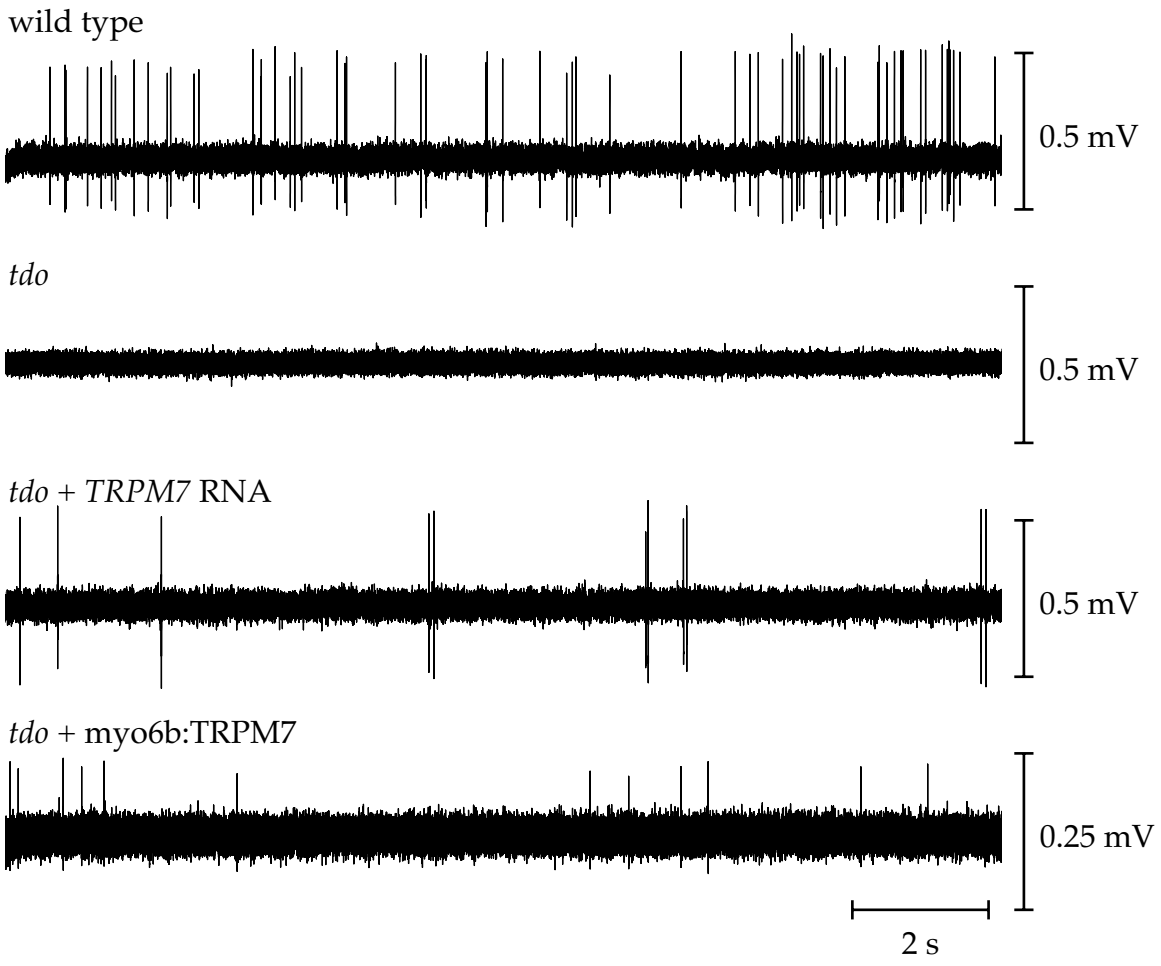

Figure A1.3 TRPM7 is necessary for posterior lateral line neuron activity

Extracellular recordings of spontaneous hair-cell evoked activity in afferent neurons is robust in 2 dpf wild-type larvae, but absent in *tdo* fish. Rescue of TRPM7 expression by RNA injection, as well as by a plasmid driving the hair-cell specific expression of TRPM7, restores spontaneous activity.

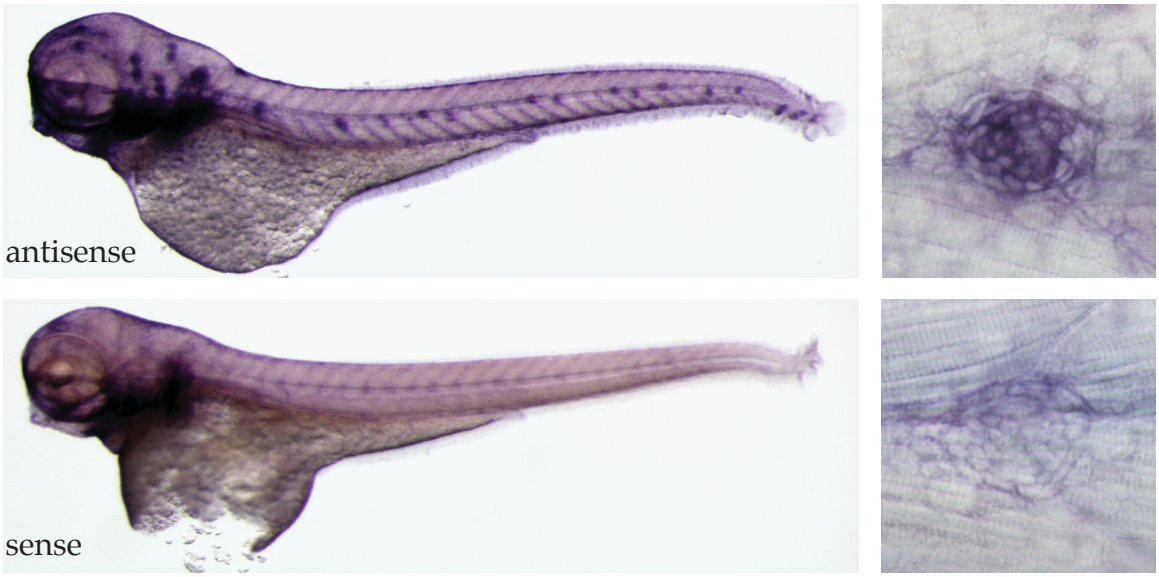

Figure A1.4 TRPM7 is expressed in lateral-line hair cells

An antisense probe against TRPM7 mRNA shows strong punctate labeling along the animal's length (upper panel). A closer examination shows labeling in the central portion of neuromasts where hair cells are located (upper right), whereas the sense control does not (lower panels).

Discussion

Our results suggest TRPM7 is required for synaptic transmission in hair cells of the posterior lateral line. Preliminary studies indicate that hair-cell specific expression of TRPM7 is sufficient to restore synaptic transmission. Our data are consistent with recent work that has identified the channel as necessary in mammalian synaptic transduction, though this is the first preliminary evidence of its necessity at a ribbon synapse (Krapivinsky et al., 2006).

An exact mechanistic understanding of TRPM7's role in synaptic transmission still remains to be formed. It has been suggested that TRPM7 in synaptic vesicles provides necessary counterions to release neurotransmitter that is bound within synaptic vesicles to an ion exchange matrix (Montell, 2006). This seems unlikely for two reasons. First, synaptic transmission is extremely rapid, operating on the order of 200 μs between Ca^{2+} entry into the presynaptic cell and the onset of neurotransmitter-gated currents in the postsynaptic cell (Llinas et al., 1981). This seems too rapid to depend on the gating of 40 pS TRPM7 channels that would provide counterions necessary to release neurotransmitter from a bound state inside of vesicles upon fusion. The counterion theory might still be correct; however, an ion channel is an unlikely source for the ions. Ions from the extracellular medium seem to be a more likely source; only in kiss-and-run fusion, in which a narrow fusion pore opens to permit exit of vesicle contents, might an intracellular source of ions be important. In the case of the hair cell, the synapses of which seem specialized for temporal fidelity, TRPM7 gating necessary for glutamate liberation seems particularly unlikely.

Second, where such an ion exchange mechanism has been postulated, the neurotransmitter involved has been acetylcholine (Rahamimoff and Fernandez, 1997; Reigada et al., 2003), which carries a positive charge. TRPM7's conductance could provide cations to counter this charge; however, in hair cells the neurotransmitter is glutamate. The positive charge of the amino group on glutamate is offset by the negative charge of the extra carboxylic group; the isoelectric point is at pH 3.2, above which the molecule is negative. Hence, cations provided by TRPM7 would not release bound glutamate.

If it does not provide counterions, what is TRPM7 doing at synaptic vesicles? Several functions are possible. The kinase domain may play a role in tethering vesicles to the ribbon or to other cytoskeletal components, as has been postulated in PC12 cells (Brauchi et al., 2008). This might be revealed by electron micrography of the synapse, and is being pursued. Alternatively, the kinase might regulate the vacuolar-type H^+-ATPase that is necessary for the filling of both acetylcholine and glutamate vesicles (Edwards, 2007). Yet another possibility is that the kinase regulates the vesicular glutamate and acetylcholine transporters VGLUT and VAchT. If TRPM7 regulates one of the two transporters, vesicle filling might be impaired in the truncated mutant; synergy between transporters has been demonstrated in which the depletion of one neurotransmitter transporter affects the synaptic release of a different neurotransmitter (Gras et al., 2008). However, if either is the case, it seems odd that in the zebrafish's mechanosensitive RB neurons, the kinase domain is not necessary for sensory transduction, and that vesicle fusion frequency was unaffected by the overexpression of a kinase-impaired version of TRPM7 in PC12 cells, though vesicle mobility does appear to be enhanced without the kinase

domain in the latter study (Brauchi et al., 2008). One method to separate a vesicle-fusion role from a vesicle-filling role is to evaluate capacitance changes in the presynaptic cell; if increases in capacitance occur in response to depolarization, then fusion might be conserved, and the defect might lie in vesicle filling or in the liberation of neurotransmitter from vesicles.

If instead the channel conductance is the important factor, the channel's role may be more complex. TRPM7 conducts a large outward current at +100 mV and a small inward current at voltages below -40 mV under physiological ionic conditions (reviewed in Bates-Withers et al., 2011). The resting internal concentration of Mg^{2+} blocks the channel almost entirely. The inward current, however, can be enhanced twofold when the *extracellular* pH is reduced to 6.0, and tenfold at pH_e 4.0 (Jiang et al., 2005). The current is likely carried by monovalent ions that compete for divalent binding sites in the channel's pore.

In light of this, TRPM7 might serve a cation exchange role in vesicle filling. The vacuolar-type H^+-ATPase produces the electrochemical gradient that drives transport of neurotransmitters into secretory vesicles. In the case of acetylcholine, VAchT exchanges protonated cytosolic acetylcholine for two luminal H^+ ions. Anionic glutamate transport by VGLUT is less understood, though it is thought to involve movement of n H^+ ions and thus, n+1 charge. Regardless, both require that the H^+-ATPase establish a proton gradient. Consider a synaptic vesicle of diameter 50 nm. If the H^+-ATPase couples the hydrolysis of cytosolic ATP to ADP to the transport into the vesicle of two to four protons as has been measured (Kettner et al., 2003; Cross and Muller, 2004), the maximum potential possible across the vesicle membrane resulting from the 50 zJ liberated from one ATP is ~160 mV. Assuming all other ions are found in

neutral equilibrium, the Nernst equation predicts this potential to correspond to a 500-fold proton concentration difference; if cytosolic pH is near 7.3, the vesicle then maximally acidifies to pH 4.6. Given the small vesicle volume, this amounts to a mean count of 1 H^+ ion, which would be inefficient for the VAchT or VGLUT transporters. However, if TRPM7's pH-activated monovalent conductance can allow the passive exit—driven by the potential created by H^+-ATPase—of other cations, such as Na^+ or K^+ (present at approximately 100 mM when the vesicle is formed and thus about 4,000 ions in the vesicle) the vesicle can then be further acidified beyond the equilibrium capacity of the H^+-ATPase.

Such a mechanism does not require kinase function or divalent selectivity and is consistent with published data in mammalian neurons, PC12 cells, dopaminergic neurons in the zebrafish (Krapivinsky et al., 2006; Brauchi et al., 2008; McNeill, 2009), and our results thus far in the *tdo* fish. Quantitative data on the affinities of the various transporters, as well as that of TRPM7 for the respective ions, are necessary before a more informed argument can be made. Still, such a model predicts that fusion of vesicles occurs normally (assuming filling is not a prerequisite), but that neurotransmitter content is diminished when TRPM7 channel activity is abolished. Three experimental approaches can help to test the model: capacitance recordings to assay fusion, vesicle pH assessment using vesicle-targeted pHluorin (a pH-sensitive green fluorescent protein variant), and pulse-chase experiments with radiolabeled neurotransmitter to assay the content of synaptosomes. If the model is accurate the latter two should be abnormal, but the first not so, in TRPM7 channel-dead mutants.

Various alleles of TRPM7 (kinase-dead, channel-dead, and monovalent-selective) are presently being investigated for their capacity to restore lateral-line neuron activity, water-current evoked behavior, and normal synaptic architecture at the ribbon. Furthermore, the use of pHluorin is also being explored to study whether the pH of vesicles is perturbed in *touchdown* mutants. Electron microscopy of hair-cell synapses is underway. Together, these experiments will provide a basis for targeted evaluation of TRPM7's role in synaptic transduction.

APPENDIX THREE

Frequency-selective exocytosis by ribbon synapses of hair cells in the bullfrog's amphibian papilla

Patel SH, Salvi D, Ó Maoiléidigh D, and Hudspeth AJ

Manuscript in revision

Frequency-selective exocytosis by ribbon synapses of hair cells in the bullfrog's amphibian papilla

Suchit H. Patel, Joshua D. Salvi, Dáibhid Ó Maoiléidigh, and A. J. Hudspeth

Howard Hughes Medical Institute and Laboratory of Sensory Neuroscience
The Rockefeller University, 1230 York Avenue, New York, NY 10065, USA

Abbreviated title: Tuned exocytosis in hair cells

Acknowledgments

The authors thank J. A. N. Fisher and S. Lagier for helpful advice; B. Fabella for excellent technical assistance; K. Leitch for expert aid with immunohistochemistry and imaging; and the members of our research group for valuable comments on the manuscript. This research was supported by National Institutes of Health grants DC000241 and GM07739. D. Ó M. is a Research Associate and A. J. H. is an Investigator of Howard Hughes Medical Institute.

Abstract

The activity of auditory afferent fibers depends strongly on the frequency of stimulation. Although the bullfrog's amphibian papilla lacks the flexible basilar membrane that effects tuning in mammals, it contains auditory nerve fibers that display comparable frequency selectivity. Seeking additional mechanisms of tuning in this organ, we monitored the synaptic output of hair cells by measuring changes in their membrane capacitance during sinusoidal electrical stimulation at various frequencies. Using perforated-patch recordings, we found that individual hair cells displayed frequency selectivity in synaptic exocytosis within the frequency range sensed by the amphibian papilla. Moreover, each cell's tuning varied in accordance with its tonotopic position. Using confocal imaging, we observed a tonotopic gradient in the concentration of proteinaceous Ca^{2+} buffers similar to that in the cochleas of several other vertebrates. A model for synaptic release reveals that this gradient may serve to maintain the sharpness of tuning. We conclude that hair cells of the amphibian papilla use synaptic tuning as an additional mechanism for sharpening their frequency selectivity.

Introduction

The auditory organs of tetrapod vertebrates employ complex mechanical and neural mechanisms to discriminate acoustic signals at frequencies ranging from below 10 Hz to over 100 kHz (Peng and Ricci, 2011). Frequency tuning may be represented as the action of sequential filters, each of which successively attenuates the response to sounds differing from the characteristic frequency at which a cell is most sensitive. The rate at which the response declines as a function of frequency specifies the equivalent number of linear, first-order filters necessary to attain a particular sharpness of tuning.

The frequency selectivity of the mammalian cochlea results primarily from the properties of an active traveling wave upon the basilar membrane (von Békésy, 1960). This traveling wave peaks in only a narrow region—and thereby stimulates only a limited set of hair cells—that depends on the frequency of auditory input (Ruggero et al., 2000). Although this mechanism is absent or rudimentary in nonmammalian tetrapods (Gummer et al., 1987; Manley et al., 1988; O'Neill and Bearden, 1995), the frequency selectivity of their afferent neurons is of comparable quality (Crawford and Fettiplace, 1980; Manley, 2001; Temchin et al., 2008; Yu et al., 1991). Tuning in these animals benefits from mechanical resonance of the receptor organs and of individual hair bundles (Aranyosi and Freeman, 2004; Frishkopf and DeRosier, 1983; Holton and Hudspeth, 1983). Electrical resonance, a phenomenon in which a hair cell's membrane potential oscillates at particular frequencies, also makes a contribution (Fettiplace and Fuchs, 1999). Because these processes represent only second-order filters, however, they cannot explain completely the observed sharpness of tuning found in auditory afferents, which resembles that of a tenth-order system (Eatock et al., 1993; Fuchs et al., 1988; Yu et al., 1991; Smotherman and Narins, 1999). Additional mechanisms must contribute to the frequency selectivity of nonmammalian auditory organs.

Because synaptic release by saccular hair cells peaks at specific frequencies (Rutherford and Roberts, 2006), the release of neurotransmitter by hair cells might provide an additional degree of tuning. We have therefore investigated the frequency responsiveness of synapses in a tonotopically organized auditory organ, the bullfrog's amphibian papilla.

Materials and methods

Electrophysiology

All procedures were approved by the Institutional Animal Care and Use Committee of The Rockefeller University. Amphibian papillae were dissected from bullfrogs (*Rana catesbeiana*) of either sex and hair cells were exposed as described (Keen and Hudspeth, 2006). Dissection and recording were performed in solution containing 112 mM Na^+, 2 mM K^+, 1.5 mM Ca^{2+}, 119 mM Cl^-, 3 mM **D**-glucose, 2 mM creatine, 1 mM pyruvate, and 5 mM HEPES at pH 7.3 and supplemented with 100 mM amiloride to minimize Ca^{2+} entry through mechanotransduction channels (Jorgensen and Ohmori, 1988). The preparation was visualized with differential-interference-contrast optics through a 40X objective lens of 0.8 numerical aperture. An eyepiece reticle was used to determine each cell's distance from the caudal end of the sensory epithelium.

Experiments were conducted at room temperature within 2 hr of dissection. Recordings were performed in the whole-cell mode with borosilicate recording pipettes coated with nail polish to reduce their transmural capacitance. Filled with 110 mM Cs^+, 2 mM Na^+, 2.5 mM Mg^{2+}, 113 mM Cl^-, 2 mM ATP, 1 mM EGTA, and 10 mM HEPES at pH 7.3, pipettes displayed resistances of 3-10 MW. For perforated-patch recordings, the back end of each filament-containing electrode was dipped into this solution for 5-10 s to fill the tip before the shaft was filled with the same solution augmented with 500 mg/ml amphotericin B (Sigma-Aldrich) freshly dissolved in dimethyl sulfoxide. A stable access

resistance of 7-15 MW developed 5-10 min after formation of a tight seal. Although the series resistance was not compensated, we corrected the holding potential for a liquid-junction potential of -4.3 mV. We rejected recordings in which the capacitance was unstable or in which the access resistance and cell capacitance showed clear correlation.

Experiments were controlled and data recorded with programs written in LabVIEW (National Instruments). Stimuli were delivered and recordings made with a voltage-clamp amplifier (Axopatch 200B, Molecular Devices). Using the lock-in technique (Lindau and Neher, 1988), we assayed each hair cell's capacitance with a 1.5 kHz sinusoidal signal 15 mV in amplitude and centered at -80 mV. Synaptic release was triggered by depolarizing the cell to -55 mV or -45 mV and imposing sinusoidal stimuli of 5 mV amplitude for one second at the indicated frequencies in random order. To eliminate artifacts resulting from the slowly activating I_h conductance, the extracellular medium was supplemented in some experiments with 50 mM ZD7288 (Tocris Bioscience).

Measurement of buffer gradients

Amphibian papillae dissected into cold saline solution were fixed for 1 hr at room temperature in phosphate-buffered saline solution containing 4% formaldehyde and 0.1% Triton X-100. The tissue was labeled and imaged as previously described (Castellano-Muñoz et al., 2010). Polyclonal rabbit antisera against parvalbumin 3 (Heller et al., 2002) and calbindin-D28k (Swant) were used at respective dilutions of 1:10,000 and 1:1,000. Secondary labeling was performed with donkey anti-rabbit IgG conjugated to Alexa 488 (Invitrogen) at a dilution of 1:500. Phalloidin conjugated to Alexa 568 (Invitrogen) was used to label hair bundles.

Z-stacks were acquired at 0.5 mm intervals with a laser-scanning confocal microscope (Fluoview FV1000, Olympus) bearing a 60X objective lens of numerical aperture 1.35. Images were collected from five or six equally spaced segments along the

length of the amphibian papilla. In each image, data from 15-19 cells were analyzed with ImageJ (National Institutes of Health). Pixel intensities were measured in the hair-cell cytoplasm immediately basal to the nuclei. Confocal imaging settings were held constant while imaging each papilla. To ensure that no artifactitious gradient was introduced by differences in tissue density or other variables, we also stained cells with 4,6-diamidino-2-phenylindole, which showed no significant gradient in fluorescence intensity along the papilla.

Data analysis

Data are presented as means ± standard errors of means for 5-25 presentations of stimuli at each frequency. One-tailed paired and unpaired Student's *t*-tests were used to determine the significance of capacitance data in which one mean value exceeded the others. Fluorescence data were analyzed by one-way ANOVA. Significance was defined as $P < 0.05$.

Release-site model

We simplified the release-site model (Andor-Ardó et al., 2010) by simplifying the parameters, minimizing the level of cooperativity, and reducing the number of states to three: (1) activated, (2) discharged, and (3) loaded. We extended the model by including the dynamics of both Ca^{2+} concentration and of membrane capacitance and by allowing all rate constants to differ. The system is described by

$$\begin{aligned}
\dot{x}_1 &= -k_0\left(1+\varepsilon x_2^2\right)x_1 + k_A\left(1-x_1-x_2\right)C \\
\dot{x}_2 &= k_0\left(1+\varepsilon x_2^2\right)x_1 - k_R x_2 \\
\dot{C} &= -G\left(V-V_{Ca}\right) - k_B B C \\
\dot{C}_M &= k_0\left(1+\varepsilon x_2^2\right)x_1 C_V N - k_E C_M ,
\end{aligned}$$

in which x_i represents the fraction of sites in state i, k_0 the vesicle-fusion rate without cooperativity, e the cooperativity strength, k_A the rate constant for binding to a release site, C the Ca^{2+} concentration, k_R the rate constant for site recovery, B the buffer

concentration, V the membrane potential, V_{Ca} the Ca^{2+} reversal potential, k_B the binding rate constant for Ca^{2+} buffer, C_M the membrane capacitance, C_V the vesicle capacitance, N the number of release sites per hair cell, and k_E the rate constant for endocytosis. Top dots represent temporal derivatives. The function

$$G = \frac{g_{MAX}}{2ewN_A\left(1 + e^{-(V-V_0)/V_S}\right)}$$

accounts for the Ca^{2+} channels' voltage dependence; g_{MAX} is their maximum conductance, e the electron charge, w the hair cell's volume, N_A Avogadro's number, V_0 the voltage at which half the channels are open, and V_S their voltage sensitivity.

Results

Frequency selectivity of synaptic exocytosis

The amphibian papilla responds to sounds at frequencies from 150 Hz to 1200 Hz (Lewis et al., 1982). To examine the frequency dependence of transmitter release in this organ, we delivered sinusoidal voltage stimuli within this frequency range to individual hair cells held under perforated-patch voltage-clamp conditions. We recorded the ensuing changes in membrane capacitance owing to the increase in surface area associated with exocytotic release of neurotransmitter.

When subjected to 5 mV sinusoidal voltage commands centered at -55 mV, the approximate resting potential, a hair cell responded with a small increase in the capacitance of its plasmalemma (Fig. 1). We observed in 16 instances a striking preference for a particular stimulation frequency that varied between hair cells. Most cells showed a predilection for frequencies between 200 Hz and 600 Hz, the range of characteristic frequencies for the segment of the sensory epithelium from which we recorded (Fig. 2A-D). The increase in the response at a cell's best frequency relative to those at the two flanking frequencies averaged 63 ± 8 fF. Frequency-selective release diminished as each hair cell deteriorated during 10-15 minutes of recording.

Likely owing to the modest synaptic release recorded at a holding potential of -55 mV in our usual recording protocol, we could define only the peaks of tuning curves. To better delineate the sharpness of tuning, we enhanced exocytosis by stimulating hair cells held at a more positive potential of -45 mV. Although deviating somewhat from physiological conditions, this procedure augmented synaptic responses and allowed discrimination of responses at greater frequency resolution. We found that responsiveness declined by more than half as the driving frequency doubled, implying at least first-order low-pass filtering (Fig. 2E, F). Filtering was even steeper for the high-pass response.

Spatial distribution of frequency selectivity

To assess possible tonotopic organization, we next related the frequency selectivity of synaptic release to the positions of hair cells in the amphibian papilla. The optimal stimulus frequency varied in a systematic way along the sensory epithelium (Fig. 3). Rostral hair cells responded best to stimulation at frequencies as low as 150 Hz, whereas caudal cells exhibited peak responses up to 700 Hz. The best-frequency positions determined by synaptic responsiveness corresponded well with those measured previously from afferent fibers (Lewis et al., 1982).

Tonotopic variation in the concentration of Ca^{2+} buffers

Because Ca^{2+} buffers influence synaptic function in hair cells (Roberts, 1994), we used immunolabeling to determine which proteinaceous buffers occur in the bullfrog's amphibian papilla. Although only a few hair cells in the rostrolateral region of the papilla expressed calretinin, both parvalbumin and calbindin-D28k occured widely (Fig. 4). We measured the intensity of immunofluorescence in the cytoplasm of individual hair cells along the sensory epithelium and found parvalbumin and calbindin-D28k labeling to be respectively fourfold and eightfold as strong in high-frequency cells as in low-frequency cells (Fig. 4C, F). The bullfrog's amphibian papilla thus manifests a tonotopic gradient in Ca^{2+} buffer concentration.

Model of synaptic tuning

One possible mechanism for synaptic tuning involves cooperative vesicle release (Andor-Ardó et al., 2010). An extension of this model reveals that spontaneously oscillatory vesicle release should occur for a limited range of buffer concentrations separated from constant release by a loop of Hopf bifurcations (Fig. 4G). The zone immediately outside one segment of the loop corresponds to a regime in which synaptic release could be entrained by periodic increases in Ca^{2+} concentration—the signature of synaptic tuning—at frequencies that increase as the buffer concentration rises (Fig. 4H). In a real system, the extent of this zone would depend upon the level of noise. The capacitance change in response to sinusoidal voltage changes is large and shaply tuned only when the buffer concentration is chosen such that the system is near a Hopf bifurcation (Fig. 4I). Increasing buffer concentration without changing other parameters decreases resonant frequency (Fig. 4I).

Discussion

Individual hair cells of the bullfrog's amphibian papilla release neurotransmitter most effectively during voltage stimulation at frequencies in the range of acoustic stimuli to which the organ best responds. The distribution of best frequencies along the organ accords with the tonotopic map based on afferent-fiber activity (Lewis et al., 1982) and with the pattern of electrical resonance (Smotherman and Narins, 1999). Hair cells of the amphibian papilla therefore display a tonotopic gradient in the frequency responsiveness of transmitter release. The frog's sacculus, where hair cells are uniformly tuned to a narrow range of lower frequencies, exhibits similar behavior (Rutherford and Roberts, 2006).

What accounts for the difference between the present findings and an earlier investigation (Quiñones et al., 2012) that showed no frequency-selective exocytosis in the

amphibian papilla of the grass frog? First, the previous study pooled data from numerous cells in two large segments of the papilla, potentially obscuring sharp tuning curves. Second, the frequency resolution employed here exceeded that used in the earlier study and was therefore more likely to reveal sharp tuning. Finally, the earlier recordings were conducted in the conventional whole-cell recording configuration as opposed to the perforated-patch mode. This difference suggests that soluble proteins, perhaps including Ca^{2+} buffers, are of critical importance for the mechanism of frequency selectivity. Supporting this notion is the papilla's conspicuous gradient of the Ca^{2+}-buffering proteins parvalbumin 3 and calbindin-D28k. Our observations accord with those of buffer gradients in other hearing organs (Hackney et al., 2003; Hiel et al., 2002; Schnee et al., 2005), raising the possibility that synaptic tuning occurs elsewhere as well, particulary in non-mammalian systems lacking sharply tuned travelling waves (Gummer et al., 1987; Manley et al., 1988; O'Neill and Bearden, 1995).

The release-site model shows how buffer concentration might influence synaptic tuning. Although additional tonotopic gradients are likely, the frequency range of the model could be matched to that of the amphibian papilla by systematic variation of only the buffer concentration and the rate constant for vesicle fusion. In this model a rise in the buffer concentration would not increase the resonant frequency but rather ensure that the system operates near a Hopf bifurcation, thereby keeping the system sensitive and sharply tuned. It is a noteworthy prediction of this model that lowering the buffer concentration, for example by whole-cell recording, might bring a hair cell into a regime in which spontaneous release of transmitter by individual synapses becomes rhythmic. This effect might be apparent in recordings of postsynaptic activity.

Our results imply that tuning can result from interactions involving only the readily releasable pool of synaptic vesicles. If each vesicle contributes a capacitance of 34 aF (Graydon et al., 2011), then approximately 1000 vesicles are released during 1 s of stimulation by approximately 50 synaptic ribbons (Graydon et al., 2011). This increment

of about 20 additional vesicles released per synapse is well within a ribbon synapse's exocytotic capacity of several hundred per second (Parsons et al., 1994). Our experiments are unlikely to have wholly depleted the readily releasable pool of 15 vesicles per active zone (Graydon et al., 2011) which can refill in 15-200 ms (Spassova et al., 2004, Cho et al., 2011). Because natural tones are seldom present for longer than a few tens to hundreds of milliseconds, this pool likely mediates tuned synaptic responses *in vivo*.

The frequency dependence of synaptic release constitutes a bandpass filter. From recordings at closely-spaced frequencies in cells under somewhat stronger depolarization, we observed low-pass responses that decreased by half as the frequency doubled and high-pass responses that sometimes declined even more rapidly. These results may therefore account for at least two orders of the overall sharpening of auditory-nerve responses. It is possible that synaptic filtering *in vivo* may be sharper, for the accumulation of Ca^{2+} in the presynaptic cytoplasm during prolonged depolarization might saturate synaptic release and thus broaden the tuning. However, given the small synaptic responses near the cells' resting potentials with shorter stimuli, experimental resolution of the capacitance recording did not allow us to finely define the sharpness of tuning at the resting potential.

The afferent fibers of the amphibian papilla display frequency selectivity comparable to that of the auditory organs in other vertebrates, including mammals (Crawford and Fettiplace, 1980; Liberman, 1978; Schoffelen et al., 2008; Yu et al., 1991). Although electrical resonance contributes to frequency selectivity in the low-frequency region of the papilla (Smotherman and Narins, 1999), it is insufficient to account for the documented sharpness of tuning (Yu et al., 1991). The amphibian papilla lacks a flexible basilar membrane that could support traveling waves (Wever, 1973). Although the overlying tectorium might bear traveling waves (Hillery and Narins, 1984), its function in tuning remains hypothetical. Hence, other tuning mechanisms must account for the sharp tuning found in auditory afferents. We propose that the tonotopic

tuning of hair-cell synapses plays an important role in sharpening the frequency selectivity of the amphibian papilla.

References

Andor-Ardó, D., Hudspeth, A.J., Magnasco, M.O., and Piro, O. (2010). Modeling the resonant release of synaptic transmitter by hair cells as an example of biological oscillators with cooperative steps. Proc Natl Acad Sci USA 107, 2019-2024.

Aranyosi, A.J., and Freeman, D.M. (2004). Sound-induced motions of individual cochlear hair bundles. Biophys J 87, 3536-3546.

Castellano-Muñoz, M., Israel, S.H., and Hudspeth, A.J. (2010). Efferent control of the electrical and mechanical properties of hair cells in the bullfrog's sacculus. PLoS ONE 5, e13777.

Cho, S., Li, G.-L., and von Gersdorff, H. (2011). Recovery from Short-Term Depression and Facilitation Is Ultrafast and Ca^{2+} Dependent at Auditory Hair Cell Synapses. J Neurosci 31, 5682-5692.

Crawford, A.C., and Fettiplace, R. (1980). The frequency selectivity of auditory nerve fibres and hair cells in the cochlea of the turtle. J Physiol 306, 79-125.

Eatock, R.A., Saeki, M., and Hutzler, M.J. (1993). Electrical resonance of isolated hair cells does not account for acoustic tuning in the free-standing region of the alligator lizard's cochlea. J Neurosci 13, 1767-1783.

Fettiplace, R., and Fuchs, P.A. (1999). Mechanisms of hair cell tuning. Annu Rev Physiol 61, 809-834.

Frishkopf, L.S., and DeRosier, D.J. (1983). Mechanical tuning of free-standing stereociliary bundles and frequency analysis in the alligator lizard cochlea. Hear Res 12, 393-404.

Fuchs, P.A., Nagai, T., and Evans, M.G. (1988). Electrical tuning in hair cells isolated from the chick cochlea. J Neurosci 8, 2460-2467.

Graydon, C.W., Cho, S., Li, G.-L., Kachar, B., and von Gersdorff, H. (2011). Sharp Ca^{2+} nanodomains beneath the ribbon promote highly synchronous multivesicular release at hair cell synapses. J Neurosci 31, 16637-16650.

Gummer, A.W., Smolders, J.W., and Klinke, R. (1987). Basilar membrane motion in the pigeon measured with the Mössbauer technique. Hear Res 29, 63-92.

Hackney, C.M., Mahendrasingam, S., Jones, E.M.C., and Fettiplace, R. (2003). The distribution of calcium buffering proteins in the turtle cochlea. J Neurosci 23, 4577-4589.

Heller, S., Bell, A.M., Denis, C.S., Choe, Y., and Hudspeth, A.J. (2002). Parvalbumin 3 is an abundant Ca^{2+} buffer in hair cells. J Assoc Res Otolaryngol 3, 488-498.

Hiel, H., Navaratnam, D.S., Oberholtzer, J.C., and Fuchs, P.A. (2002). Topological and developmental gradients of calbindin expression in the chick's inner ear. J Assoc Res Otolaryngol 3, 1-15.

Hillery, C.M., and Narins, P.M. (1984). Neurophysiological evidence for a traveling wave in the amphibian inner ear. Science 225, 1037-1039.

Holton, T., and Hudspeth, A.J. (1983). A micromechanical contribution to cochlear tuning and tonotopic organization. Science 222, 508-510.

Jorgensen, F., and Ohmori, H. (1988). Amiloride blocks the mechano-electrical transduction channel of hair cells of the chick. J Physiol 403, 577-588.

Keen, E.C., and Hudspeth, A.J. (2006). Transfer characteristics of the hair cell's afferent synapse. Proc Natl Acad Sci USA 103, 5537-5542.

Lewis, E., Leverenz, E., and Koyama, H. (1982). The tonotopic organization of the bullfrog amphibian papilla, an auditory organ lacking a basilar membrane. J Comp Physiol A 145, 437-445.

Liberman, M.C. (1978). Auditory-nerve response from cats raised in a low-noise chamber. J Acoust Soc Am 63, 442-455.

Lindau, M., and Neher, E. (1988). Patch-clamp techniques for time-resolved capacitance measurements in single cells. Pflügers Arch Eur J Physiology 411, 137-146.

Manley, G.A. (2001). Evidence for an active process and a cochlear amplifier in nonmammals. J Neurophysiol 86, 541-549.

Manley, G.A., Yates, G.K., and Köppl, C. (1988). Auditory peripheral tuning: evidence for a simple resonance phenomenon in the lizard Tiliqua. Hear Res 33, 181-189.

O'Neill, M.P., and Bearden, A. (1995). Laser-feedback measurements of turtle basilar membrane motion using direct reflection. Hear Res 84, 125-138.

Parsons, T.D., Lenzi, D., Almers, W., and Roberts, W.M. (1994). Calcium-triggered exocytosis and endocytosis in an isolated presynaptic cell: capacitance measurements in saccular hair cells. Neuron 13, 875-883.

Peng, A.W., and Ricci, A.J. (2011). Somatic motility and hair bundle mechanics, are both necessary for cochlear amplification? Hear Res 273, 102-122.

Quiñones, P., Luu, C., Schweizer, F., and Narins, P. (2012). Exocytosis in the frog amphibian papilla. J Assoc Res Otolaryngol 13, 39-54.

Roberts, W.M. (1994). Localization of calcium signals by a mobile calcium buffer in frog saccular hair cells. J Neurosci 14, 3246-3262.

Ruggero, M.A., Narayan, S.S., Temchin, A.N., and Recio, A. (2000). Mechanical bases of frequency tuning and neural excitation at the base of the cochlea: comparison of basilar-membrane vibrations and auditory-nerve-fiber responses in chinchilla. Proc Natl Acad Sci USA 97, 11744-11750.

Rutherford, M.A., and Roberts, W.M. (2006). Frequency selectivity of synaptic exocytosis in frog saccular hair cells. Proc Natl Acad Sci USA 103, 2898-2903.

Schnee, M.E., Lawton, D.M., Furness, D.N., Benke, T.A., and Ricci, A.J. (2005). Auditory hair cell-afferent fiber synapses are specialized to operate at their best frequencies. Neuron 47, 243-254.

Schoffelen, R.L.M., Segenhout, J.M., and van Dijk, P. (2008). Mechanics of the exceptional anuran ear. J Comp Physiol A 194, 417-428.

Schwaller, B. (2010) Ca^{2+} buffers. In: Handbook of Cell Signaling (Bradshaw RA, Dennis EA, eds), pp955-962. Amsterdam: Elsevier.

Smotherman, M.S., and Narins, P.M. (1999). The electrical properties of auditory hair cells in the frog amphibian papilla. J Neurosci 19, 5275-5292.

Spassova, M.A., Avissar, M., Furman, A.C., Crumling, M.A., Saunders, J.C., and Parsons, T.D. (2004). Evidence that rapid vesicle replenishment of the synaptic ribbon mediates recovery from short-term adaptation at the hair cell afferent synapse. J Assoc Res Otolaryngol 5, 376-390.

Temchin, A.N., Rich, N.C., and Ruggero, M.A. (2008). Threshold tuning curves of chinchilla auditory-nerve fibers. I. Dependence on characteristic frequency and relation to the magnitudes of cochlear vibrations. J Neurophysiol 100, 2889-2898.

von Békésy, G. (1960). *Experiments in Hearing* (New York: McGraw-Hill).

Wever, E.G. (1973). The ear and hearing in the frog, Rana pipiens. J Morphol 141, 461-477.

Yu, X.L., Lewis, E.R., and Feld, D. (1991). Seismic and auditory tuning curves from bullfrog saccular and amphibian papillar axons. J Comp Physiol A 169, 241-248.

Figures and Legends

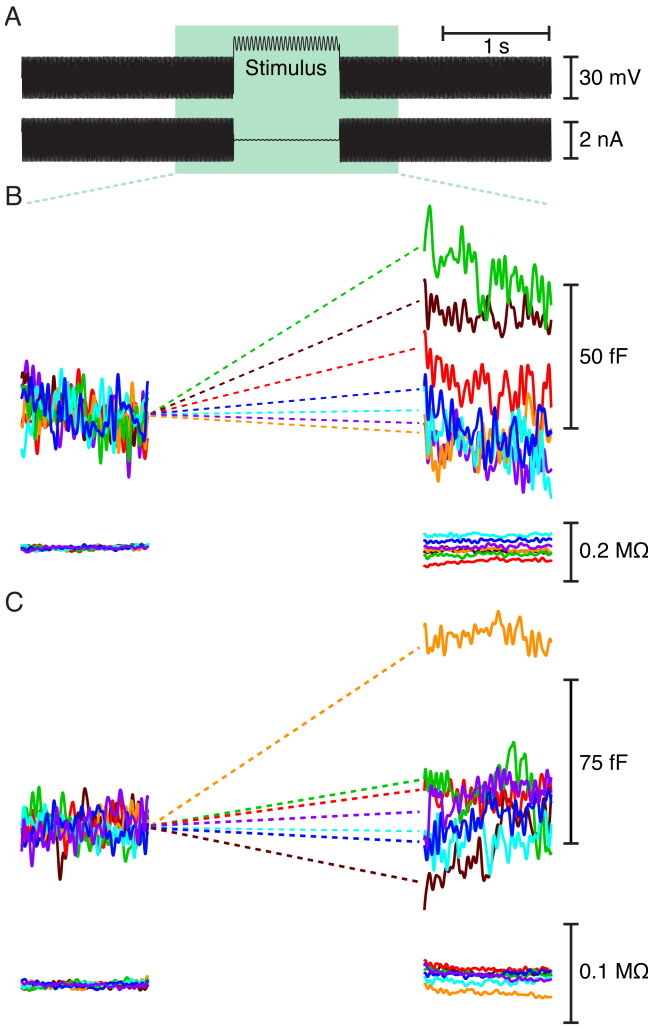

Figure 1. Measurement of capacitance changes resulting from exocytosis. (A) The upper trace depicts the voltage-clamp protocol employed during whole-cell recording in the perforated-patch configuration. A hair cell was held at -80 mV and exposed to a sinuosidal voltage change of ±15 mV at 1500 Hz to measure its membrane capacitance. In the segment labeled "Stimulus," the hair cell was depolarized to -55 mV and the capacitance probe was interrupted by a 1 s sinusoidal stimulus at one of seven randomly presented frequencies, usually 0 (constant value), 25, 200, 400, 600, 800, or 1000 Hz. The whole-cell current is shown in the lower trace. (B) The upper trace depicts the cell's membrane capacitance, which was averaged over the 200 ms interval immediately before

and after stimulation to calculate the capacitance change at the relevant frequency. Increasing frequencies are represented in spectral order. This hair cell, from the mid-frequency region of the papilla, displayed the greatest synaptic exocytosis during stimulation at 400 Hz (green). The lower trace confirms that the access resistance remained stable. (C) A rostral cell stimulated at a holding potential of -45mV shows greatest exocytosis at 300 Hz (orange). Responses to the frequencies used for this cell (100 to 700 Hz) are shown in spectral order.

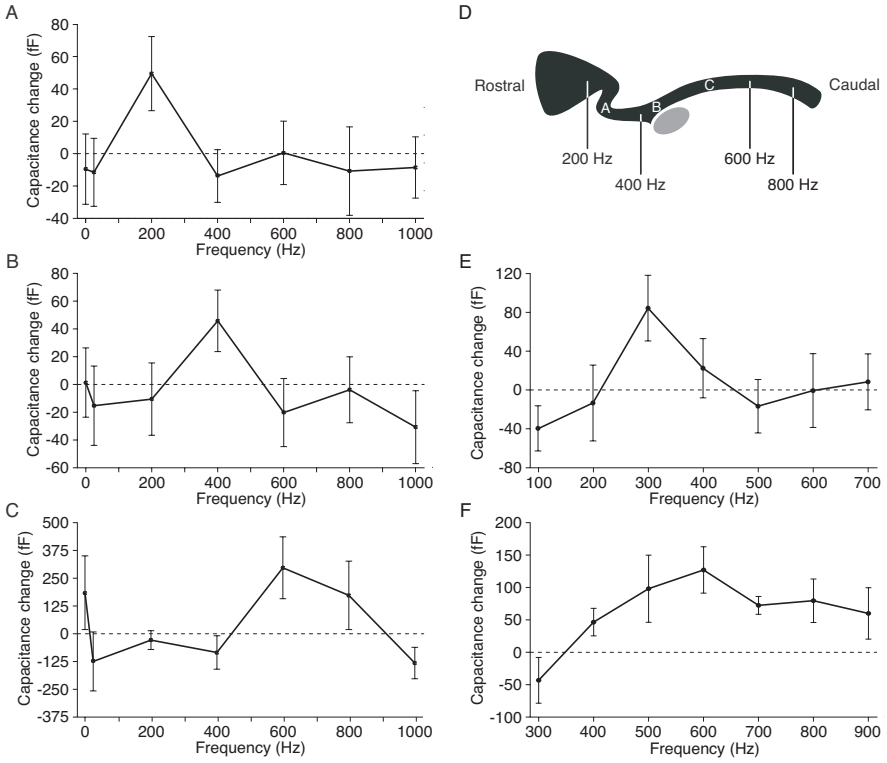

Figure 2. Frequency selectivity of exocytosis. (A) Synaptic release from a rostrally positioned hair cell peaked for stimulation at 200 Hz. (B) A hair cell from the middle portion of the amphibian papilla was most responsive at 400 Hz. (C) A cell located farther the caudal end of the papilla responded best near 600 Hz. In these three and 13 other cells, the capacitance change at the best frequency significantly exceeded that at the flanking frequencies ($P < 0.05$). (D) A schematic diagram of the bullfrog's amphibian papilla shows the locations of the three hair cells whose responses are depicted in panels A-C. The approximate positions of afferent fibers with various characteristic frequencies are indicated (Lewis et al., 1982). The gray ellipse represents the organ's cross-sectioned nerve. (E) When held at an elevated potential of -45 mV and stimulated at a more closely spaced set of frequencies, a hair cell from the rostral region of the papilla showed preferential responses that decayed as the stimulus deviated from the preferred frequency. (F) A hair cell from the middle portion of the papilla also displayed tuning when stimulated over a narrower range of frequencies.

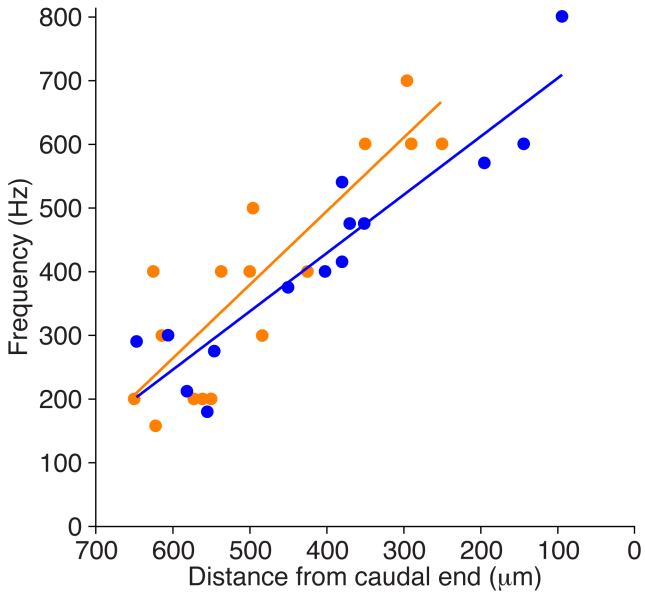

Figure 3. Tonotopic organization of synaptic frequency tuning. The frequencies of greatest synaptic release for 16 hair cells (orange) are plotted against their distance from the caudal end of the amphibian papilla. The tonotopic map for auditory afferents (Lewis et al., 1982) is shown for comparison (blue). The coefficients of determination for the linear-regression fits are $R^2 = 0.76$ for the synaptic data and $R^2 = 0.86$ for the afferent responses.

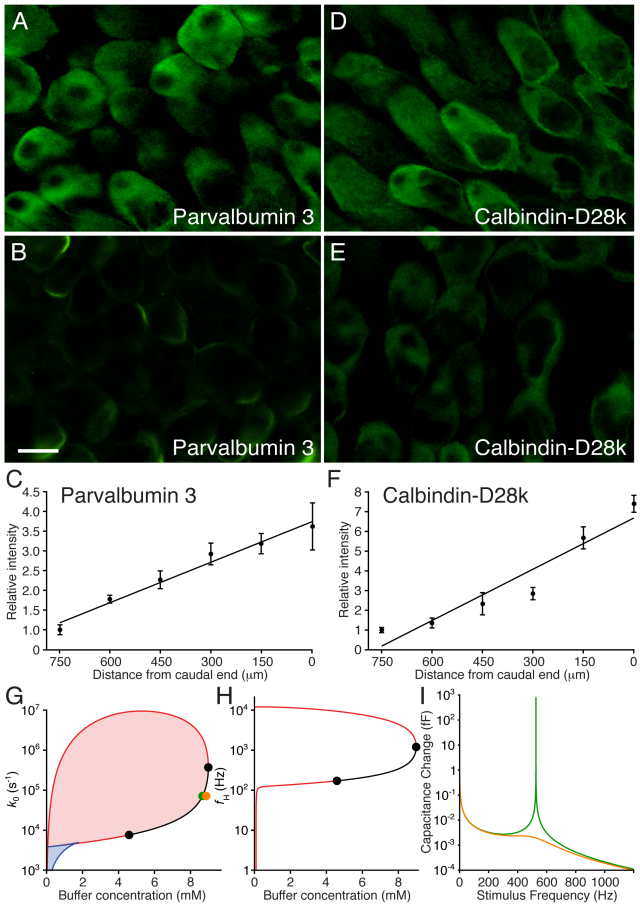

Figure 4. Tonotopic distribution of Ca^{2+} buffers. (A) Immunofluorescence microscopy detected a relatively high concentration of parvalbumin 3 in hair cells at the caudal, high-frequency end of the amphibian papilla. (B) With identical settings of the confocal microscope, hair cells near the rostral, low-frequency end of the organ displayed a lower concentration of parvalbumin 3. (C) parvalbumin 3 labeling increases tonotopically. (D-F) Calbindin-D28k occurs at a high concentration in caudal hair cells (D) relative to rostral ones (E) and also displays a tonotopic gradient (F). The coefficients of determination for the linear-regression fits are $R^2 = 0.97$ for parvalbumin 3 and $R^2 = 0.91$ for calbindin-D28k. The scale bar represents 10 mm for panels A-D. (G) A state diagram describes the release-site model at -55 mV as a function of the rate constant for vesicle fusion without cooperativity and the buffer concentration. Spontaneously oscillatory vesicle release occurs in the red shaded region enclosed by a loop of Hopf bifurcations.

Two steady states are possible in the blue shaded region demarcated by lines of saddle-node bifurcations (blue). Along the black line, the Hopf bifurcation is supercritical and the Hopf frequency rises as the buffer concentration increases. (H) In a plot of the Hopf frequency as a function of the buffer concentration, the resonant frequency equals f_H for points between the black circles at 171 and 1200 Hz. (I) The change in capacitance as a function of frequency is much larger and more sharply tuned when the system is near a Hopf bifurcation (green line and green dot in panel G) than when the buffer concentration is increased to move the system further from the bifurcation (orange line, orange dot in panel G). $V_{Ca} = 90$ mV, $C_V = 34$ aF, $N = 392$, $g_{MAX} = 3.6$ nS, $V_0 = -45$ mV, $V_S = 5$ mV, $w = 6.8$ pL (Graydon et al., 2011), $k_B = 5 \cdot 10^7$ $M^{-1} \cdot s^{-1}$ (Schwaller, 2010). $k_E = 0.5$ s^{-1} was derived from the decay of the peak capacitance traces shown in Fig. 1 and agrees with previous measurements (Cho et al., 2011). The parameters $e = 10^8$, $k_A = 7.3 \cdot 10^7$ M^{-1} s^{-1}, and $k_R = 7.6 \cdot 10^4$ s^{-1} are constrained by the data presented here.

REFERENCES

Adamson CL, Reid MA, Mo Z-L, Bowne-English J, Davis RL (2002) Firing features and potassium channel content of murine spiral ganglion neurons vary with cochlear location. J Comp Neurol 447:331-350.

Al-Anzi B, Tracey WD, Jr., Benzer S (2006) Response of Drosophila to wasabi is mediated by painless, the fly homolog of mammalian TRPA1/ANKTM1. Curr Biol 16:1034-1040.

Albillos A, Dernick G, Horstmann H, Almers W, Alvarez de Toledo G, Lindau M (1997) The exocytotic event in chromaffin cells revealed by patch amperometry. Nature 389:509-512.

Andor-Ardó D, Hudspeth AJ, Magnasco MO, Piro O (2010) Modeling the resonant release of synaptic transmitter by hair cells as an example of biological oscillators with cooperative steps. Proc Natl Acad Sci USA 107:2019-2024.

Aranyosi AJ, Freeman DM (2004) Sound-induced motions of individual cochlear hair bundles. Biophys J 87:3536-3546.

Art JJ, Wu YC, Fettiplace R (1995) The calcium-activated potassium channels of turtle hair cells. J Gen Physiol 105:49-72.

Ashmore JF (1983) Frequency tuning in a frog vestibular organ. Nature 304:536-538.

Augustin I, Rosenmund C, Sudhof TC, Brose N (1999) Munc13-1 is essential for fusion competence of glutamatergic synaptic vesicles. Nature 400:457-461.

Barral J, Dierkes K, Lindner B, Julicher F, Martin P (2010) Coupling a sensory hair-cell bundle to cyber clones enhances nonlinear amplification. Proc Natl Acad Sci U S A 107:8079-8084.

Bates-Withers C, Sah R, Clapham DE (2011) TRPM7, the Mg(2+) inhibited channel and kinase. Adv Exp Med Biol 704:173-183.

Bee MA, Gerhardt HC (2002) Individual voice recognition in a territorial frog (Rana catesbeiana). Proceedings of the Royal Society of London Series B: Biological Sciences 269:1443-1448.

Brauchi S, Krapivinsky G, Krapivinsky L, Clapham DE (2008) TRPM7 facilitates cholinergic vesicle fusion with the plasma membrane. Proc Natl Acad Sci U S A 105:8304-8308.

Brownell WE, Bader CR, Bertrand D, de Ribaupierre Y (1985) Evoked mechanical responses of isolated cochlear outer hair cells. Science 227:194-196.

Bucurenciu I, Kulik A, Schwaller B, Frotscher M, Jonas P (2008) Nanodomain coupling between Ca2+ channels and Ca2+ sensors promotes fast and efficient transmitter release at a cortical GABAergic synapse. Neuron 57:536-545.

Castellano-Muñoz M, Israel SH, Hudspeth AJ (2010) Efferent control of the electrical and mechanical properties of hair cells in the bullfrog's sacculus. PLoS ONE 5:e13777.

Cho S, Li G-L, von Gersdorff H (2011) Recovery from short-term depression and facilitation is ultrafast and Ca2+ dependent at auditory hair cell synapses. J Neurosci 31:5682-5692.

Clapham DE (2003) TRP channels as cellular sensors. Nature 426:517-524.

Colbert HA, Bargmann CI (1995) Odorant-specific adaptation pathways generate olfactory plasticity in C. elegans. Neuron 14:803-812.

Corey DP (2006) What is the hair cell transduction channel? J Physiol 576:23-28.

Corey DP, Hudspeth AJ (1979) Ionic basis of the receptor potential in a vertebrate hair cell. Nature 281:675-677.

Corey DP, Garcia-Anoveros J, Holt JR, Kwan KY, Lin SY, Vollrath MA, Amalfitano A, Cheung EL, Derfler BH, Duggan A, Geleoc GS, Gray PA, Hoffman MP, Rehm HL, Tamasauskas D, Zhang DS (2004) TRPA1 is a candidate for the mechanosensitive transduction channel of vertebrate hair cells. Nature 432:723-730.

Cosens DJ, Manning A (1969) Abnormal electroretinogram from a Drosophila mutant. Nature 224:285-287.

Crawford AC, Fettiplace R (1980) The frequency selectivity of auditory nerve fibres and hair cells in the cochlea of the turtle. J Physiol (Lond) 306:79-125.

Crawford AC, Fettiplace R (1981) An electrical tuning mechanism in turtle cochlear hair cells. J Physiol (Lond) 312:377-412.

Cross RL, Muller V (2004) The evolution of A-, F-, and V-type ATP synthases and ATPases: reversals in function and changes in the H+/ATP coupling ratio. FEBS Lett 576:1-4.

Edmonds B, Reyes R, Schwaller B, Roberts WM (2000) Calretinin modifies presynaptic calcium signaling in frog saccular hair cells. Nat Neurosci 3:786-790.

Edwards RH (2007) The neurotransmitter cycle and quantal size. Neuron 55:835-858.

Elizondo MR, Arduini BL, Paulsen J, MacDonald EL, Sabel JL, Henion PD, Cornell RA, Parichy DM (2005) Defective skeletogenesis with kidney stone formation in dwarf zebrafish mutant for trpm7. Curr Biol 15:667-671.

Ellis-Davies GC (2006) DM-nitrophen AM is caged magnesium. Cell Calcium 39:471-473.

Feng A, Narins P, Capranica R (1975) Three populations of primary auditory fibers in the bullfrog (Rana catesbeiana): Their peripheral origins and frequency sensitivities. Journal of Comparative Physiology A: Neuroethology, Sensory, Neural, and Behavioral Physiology 100:221-229.

Fettiplace R, Fuchs PA (1999) Mechanisms of hair cell tuning. Annu Rev Physiol 61:809-834.

Fisher JA, Nin F, Reichenbach T, Uthaiah RC, Hudspeth AJ (2012) The spatial pattern of cochlear amplificaiton.

Flores-Otero J, Xue HZ, Davis RL (2007) Reciprocal regulation of presynaptic and postsynaptic proteins in bipolar spiral ganglion neurons by neurotrophins. J Neurosci 27:14023-14034.

Frishkopf LS, DeRosier DJ (1983) Mechanical tuning of free-standing stereociliary bundles and frequency analysis in the alligator lizard cochlea. Hear Res 12:393-404.

Fuchs PA (1996) Synaptic transmission at vertebrate hair cells. Curr Opin Neurobiol 6:514-519.

Fuchs PA, Nagai T, Evans MG (1988) Electrical tuning in hair cells isolated from the chick cochlea. J Neurosci 8:2460-2467.

Galambos R, Davis H (1943) The response of single auditory-nerve fibers to acoustic stimulation. J Neurophysiol 6:39-57.

Gleisner L, Flock A, Wersall J (1973) The Ultrastructure Of The Afferent Synapse On Hair Cells In The Frog Labyrinth. Acta Oto-laryngologica 76:199-207.

Gras C, Amilhon B, Lepicard EM, Poirel O, Vinatier J, Herbin M, Dumas S, Tzavara ET, Wade MR, Nomikos GG, Hanoun N, Saurini F, Kemel ML, Gasnier B, Giros B, El Mestikawy S (2008) The vesicular glutamate transporter VGLUT3 synergizes striatal acetylcholine tone. Nat Neurosci 11:292-300.

Graydon CW, Cho S, Li G-L, Kachar B, von Gersdorff H (2011) Sharp Ca2+ Nanodomains beneath the Ribbon Promote Highly Synchronous Multivesicular Release at Hair Cell Synapses. J Neurosci 31:16637-16650.

Greengard P, Valtorta F, Czernik AJ, Benfenati F (1993) Synaptic vesicle phosphoproteins and regulation of synaptic function. Science 259:780-785.

Gummer AW, Smolders JW, Klinke R (1987) Basilar membrane motion in the pigeon measured with the Mössbauer technique. Hear Res 29:63-92.

Hackney CM, Mahendrasingam S, Jones EMC, Fettiplace R (2003) The distribution of calcium buffering proteins in the turtle cochlea. J Neurosci 23:4577-4589.

Hackney CM, Mahendrasingam S, Penn A, Fettiplace R (2005) The concentrations of calcium buffering proteins in mammalian cochlear hair cells. J Neurosci 25:7867-7875.

Heller S, Bell AM, Denis CS, Choe Y, Hudspeth AJ (2002) Parvalbumin 3 is an abundant Ca2+ buffer in hair cells. J Assoc Res Otolaryngol 3:488-498.

Helmholtz HL (1877) Die Lehre von den Tonempfindungen als physiologische Grundlage für die Theorie der Musik, Fourth Edition. London: Longmans, Green, and Co.

Hiel H, Navaratnam DS, Oberholtzer JC, Fuchs PA (2002) Topological and developmental gradients of calbindin expression in the chick's inner ear. J Assoc Res Otolaryngol 3:1-15.

Hillery CM, Narins PM (1984) Neurophysiological evidence for a traveling wave in the amphibian inner ear. Science 225:1037-1039.

Holton T, Hudspeth AJ (1983) A micromechanical contribution to cochlear tuning and tonotopic organization. Science 222:508-510.

Howard J, Roberts WM, Hudspeth AJ (1988) Mechanoelectrical Transduction by Hair Cells. Annual Review of Biophysics and Biophysical Chemistry 17:99-124.

Hudspeth A (1982) Extracellular current flow and the site of transduction by vertebrate hair cells. J Neurosci 2:1-10.

Hudspeth AJ (2008) Making an effort to listen: mechanical amplification in the ear. Neuron 59:530-545.

Hudspeth AJ, Corey DP (1977) Sensitivity, polarity, and conductance change in the response of vertebrate hair cells to controlled mechanical stimuli. Proc Natl Acad Sci USA 74:2407-2411.

Hudspeth AJ, Jacobs R (1979) Stereocilia mediate transduction in vertebrate hair cells (auditory system/cilium/vestibular system). Proc Natl Acad Sci USA 76:1506-1509.

Jiang J, Li M, Yue L (2005) Potentiation of TRPM7 inward currents by protons. J Gen Physiol 126:137-150.

Johnson CP, Chapman ER (2010) Otoferlin is a calcium sensor that directly regulates SNARE-mediated membrane fusion. J Cell Biol 191:187-197.

Johnson SL, Marcotti W (2008) Biophysical properties of CaV1.3 calcium channels in gerbil inner hair cells. J Physiol (Lond) 586:1029-1042.

Johnson SL, Marcotti W, Kros CJ (2005) Increase in efficiency and reduction in Ca2+ dependence of exocytosis during development of mouse inner hair cells. J Physiol 563:177-191.

Johnson SL, Forge A, Knipper M, Münkner S, Marcotti W (2008) Tonotopic variation in the calcium dependence of neurotransmitter release and vesicle pool replenishment at mammalian auditory ribbon synapses. J Neurosci 28:7670-7678.

Johnson SL, Franz C, Kuhn S, Furness DN, Rüttiger L, Münkner S, Rivolta MN, Seward EP, Herschman HR, Engel J, Knipper M, Marcotti W (2010) Synaptotagmin IV determines the linear Ca2+ dependence of vesicle fusion at auditory ribbon synapses. Nat Neurosci 13:45-52.

Jorgensen F, Ohmori H (1988) Amiloride blocks the mechano-electrical transduction channel of hair cells of the chick. J Physiol (Lond) 403:577-588.

Keen EC, Hudspeth AJ (2006) Transfer characteristics of the hair cell's afferent synapse. Proc Natl Acad Sci USA 103:5537-5542.

Kettner C, Bertl A, Obermeyer G, Slayman C, Bihler H (2003) Electrophysiological analysis of the yeast V-type proton pump: variable coupling ratio and proton shunt. Biophys J 85:3730-3738.

Kiang NY-S (1965) Discharge Patterns of Single Fibers in the Cat's Auditory Nerve. Cambridge: MIT Press.

Kindt KS, Viswanath V, Macpherson L, Quast K, Hu H, Patapoutian A, Schafer WR (2007) Caenorhabditis elegans TRPA-1 functions in mechanosensation. Nat Neurosci 10:568-577.

Klinke R, Pause M (1980) Discharge properties of primary auditory fibres in Caiman crocodilus: comparisons and contrasts to the mammalian auditory nerve. Exp Brain Res 38:137-150.

Koppl C (1997) Phase locking to high frequencies in the auditory nerve and cochlear nucleus magnocellularis of the barn owl, Tyto alba. J Neurosci 17:3312-3321.

Krapivinsky G, Mochida S, Krapivinsky L, Cibulsky SM, Clapham DE (2006) The TRPM7 ion channel functions in cholinergic synaptic vesicles and affects transmitter release. Neuron 52:485-496.

Kwan KY, Allchorne AJ, Vollrath MA, Christensen AP, Zhang DS, Woolf CJ, Corey DP (2006) TRPA1 contributes to cold, mechanical, and chemical nociception but is not essential for hair-cell transduction. Neuron 50:277-289.

Lewis E, Leverenz E, Koyama H (1982) The tonotopic organization of the bullfrog amphibian papilla, an auditory organ lacking a basilar membrane. J Comp Physiol A Neuroethol Sens Neural Behav Physiol 145:437-445.

Li G-L, Keen E, Andor-Ardó D, Hudspeth AJ, von Gersdorff H (2009) The unitary event underlying multiquantal EPSCs at a hair cell's ribbon synapse. J Neurosci 29:7558-7568.

Liberman MC, Gao J, He DZ, Wu X, Jia S, Zuo J (2002) Prestin is required for electromotility of the outer hair cell and for the cochlear amplifier. Nature 419:300-304.

Liedtke W, Tobin DM, Bargmann CI, Friedman JM (2003) Mammalian TRPV4 (VR-OAC) directs behavioral responses to osmotic and mechanical stimuli in Caenorhabditis elegans. Proc Natl Acad Sci U S A 100 Suppl 2:14531-14536.

Liedtke W, Choe Y, Marti-Renom MA, Bell AM, Denis CS, Sali A, Hudspeth AJ, Friedman JM, Heller S (2000) Vanilloid receptor-related osmotically activated channel (VR-OAC), a candidate vertebrate osmoreceptor. Cell 103:525-535.

Lighthill J (1981) Energy Flow in the Cochlea. J Fluid Mech 106:149-213.

Lim DJ (1980) Cochlear anatomy related to cochlear micromechanics. A review. J Acoust Soc Am 67:1686-1695.

Lim DJ (1986) Functional structure of the organ of Corti: a review. Hear Res 22:117-146.

Lindau M, Neher E (1988) Patch-clamp techniques for time-resolved capacitance measurements in single cells. Pflügers Archiv European Journal of Physiology 411:137-146.

Liu CH, Wang T, Postma M, Obukhov AG, Montell C, Hardie RC (2007) In vivo identification and manipulation of the Ca2+ selectivity filter in the Drosophila transient receptor potential channel. J Neurosci 27:604-615.

Llinas R, Steinberg IZ, Walton K (1981) Relationship between presynaptic calcium current and postsynaptic potential in squid giant synapse. Biophys J 33:323-351.

Low SE, Amburgey K, Horstick E, Linsley J, Sprague SM, Cui WW, Zhou W, Hirata H, Saint-Amant L, Hume RI, Kuwada JY (2011) TRPM7 is required

within zebrafish sensory neurons for the activation of touch-evoked escape behaviors. J Neurosci 31:11633-11644.

Martin P, Hudspeth AJ (1999) Active hair-bundle movements can amplify a hair cell's response to oscillatory mechanical stimuli. Proc Natl Acad Sci U S A 96:14306-14311.

Martin P, Hudspeth AJ (2001) Compressive nonlinearity in the hair bundle's active response to mechanical stimulation. Proc Natl Acad Sci U S A 98:14386-14391.

Martin P, Bozovic D, Choe Y, Hudspeth AJ (2003) Spontaneous oscillation by hair bundles of the bullfrog's sacculus. J Neurosci 23:4533-4548.

Matsushita M, Kozak JA, Shimizu Y, McLachlin DT, Yamaguchi H, Wei FY, Tomizawa K, Matsui H, Chait BT, Cahalan MD, Nairn AC (2005) Channel function is dissociated from the intrinsic kinase activity and autophosphorylation of TRPM7/ChaK1. J Biol Chem 280:20793-20803.

McNeill MS (2009) The Transient Receptor Potential Melastatin 7 is required for early melanophore survival and facets of both embryonic and larval motility in zebrafish. In: Neuroscience. Iowa City: University of Iowa.

Megela Simmons A, Simmons JA, Bates ME (2008) Analyzing acoustic interactions in natural bullfrog (Rana catesbeiana) choruses. Journal of Comparative Psychology 122:274-282.

Meyer A, Frank T, Khimich D, Hoch G, Riedel D, Chapochnikov N, Yarin Y, Harke B, Hell S, Egner A, Moser T (2009) Tuning of synapse number, structure and function in the cochlea. Nat Neurosci 12:444-453.

Montell C (2005) The TRP superfamily of cation channels. Sci STKE 2005:re3.

Montell C (2006) An exciting release on TRPM7. Neuron 52:395-397.

Montell C, Rubin GM (1989) Molecular characterization of the Drosophila trp locus: a putative integral membrane protein required for phototransduction. Neuron 2:1313-1323.

Montell C, Birnbaumer L, Flockerzi V, Bindels RJ, Bruford EA, Caterina MJ, Clapham DE, Harteneck C, Heller S, Julius D, Kojima I, Mori Y, Penner R, Prawitt D, Scharenberg AM, Schultz G, Shimizu N, Zhu MX (2002) A unified nomenclature for the superfamily of TRP cation channels. Mol Cell 9:229-231.

Moser T, Beutner D (2000) Kinetics of exocytosis and endocytosis at the cochlear inner hair cell afferent synapse of the mouse. Proc Natl Acad Sci USA 97:883-888.

Moser T, Brandt A, Lysakowski A (2006) Hair cell ribbon synapses. Cell Tissue Res 326:347-359.

Nagata K, Duggan A, Kumar G, Garcia-Anoveros J (2005) Nociceptor and hair cell transducer properties of TRPA1, a channel for pain and hearing. J Neurosci 25:4052-4061.

Nouvian R, Neef J, Bulankina AV, Reisinger E, Pangrsic T, Frank T, Sikorra S, Brose N, Binz T, Moser T (2011) Exocytosis at the hair cell ribbon synapse apparently operates without neuronal SNARE proteins. Nat Neurosci 14:411-413.

O'Neill MP, Bearden A (1995) Laser-feedback measurements of turtle basilar membrane motion using direct reflection. Hear Res 84:125-138.

Overstreet EH, Ruggero MA (2002) Development of wide-band middle ear transmission in the Mongolian gerbil. J Acoust Soc Am 111:261-270.

Parsons TD, Lenzi D, Almers W, Roberts WM (1994) Calcium-triggered exocytosis and endocytosis in an isolated presynaptic cell: capacitance measurements in saccular hair cells. Neuron 13:875-883.

Peake WT, Ling JA (1980) Basilar-membrane motion in the alligator lizard: Its relation to tonotopic organization and frequency selectivity. J Acoust Soc Am 67:1736-1745.

Peng AW, Ricci AJ (2011) Somatic motility and hair bundle mechanics, are both necessary for cochlear amplification? Hear Res 273:109-122.

Pitchford S, Ashmore JF (1987) An electrical resonance in hair cells of the amphibian papilla of the frog Rana temporaria. Hear Res 27:75-83.

Prober DA, Zimmerman S, Myers BR, McDermott BM, Jr., Kim SH, Caron S, Rihel J, Solnica-Krezel L, Julius D, Hudspeth AJ, Schier AF (2008) Zebrafish TRPA1 channels are required for chemosensation but not for thermosensation or mechanosensory hair cell function. J Neurosci 28:10102-10110.

Quiñones P, Luu C, Schweizer F, Narins P (2012) Exocytosis in the Frog Amphibian Papilla. J Assoc Res Otolaryngol 13:39-54.

Rahamimoff R, Fernandez JM (1997) Pre- and postfusion regulation of transmitter release. Neuron 18:17-27.

Ramakrishnan NA, Drescher MJ, Drescher DG (2009) Direct interaction of otoferlin with syntaxin 1A, SNAP-25, and the L-type voltage-gated calcium channel Cav1.3. J Biol Chem 284:1364-1372.

Ravicz ME, Cooper NP, Rosowski JJ (2008) Gerbil middle-ear sound transmission from 100 Hz to 60 kHz. J Acoust Soc Am 124:363-380.

Reigada D, Diez-Perez I, Gorostiza P, Verdaguer A, Gomez de Aranda I, Pineda O, Vilarrasa J, Marsal J, Blasi J, Aleu J, Solsona C (2003) Control of neurotransmitter release by an internal gel matrix in synaptic vesicles. Proc Natl Acad Sci U S A 100:3485-3490.

Ren T, He W, Gillespie PG (2011) Measurement of cochlear power gain in the sensitive gerbil ear. Nat Commun 2:216.

Ricci AJ, Crawford AC, Fettiplace R (2003) Tonotopic variation in the conductance of the hair cell mechanotransducer channel. Neuron 40:983-990.

Richmond JE, Davis WS, Jorgensen EM (1999) UNC-13 is required for synaptic vesicle fusion in C. elegans. Nat Neurosci 2:959-964.

Roberts WM (1994) Localization of calcium signals by a mobile calcium buffer in frog saccular hair cells. J Neurosci 14:3246-3262.

Roberts WM, Jacobs RA, Hudspeth AJ (1990) Colocalization of ion channels involved in frequency selectivity and synaptic transmission at presynaptic active zones of hair cells. J Neurosci 10:3664-3684.

Robertson D, Paki B (2002) Role of L-type Ca2+ channels in transmitter release from mammalian inner hair cells. II. Single-neuron activity. J Neurophysiol 87:2734-2740.

Rodriguez-Contreras A, Yamoah EN (2001) Direct measurement of single-channel Ca(2+) currents in bullfrog hair cells reveals two distinct channel subtypes. J Physiol (Lond) 534:669-689.

Roux I, Safieddine S, Nouvian R, Grati M, Simmler MC, Bahloul A, Perfettini I, Le Gall M, Rostaing P, Hamard G, Triller A, Avan P, Moser T, Petit C (2006) Otoferlin, defective in a human deafness form, is essential for exocytosis at the auditory ribbon synapse. Cell 127:277-289.

Ruggero MA, Narayan SS, Temchin AN, Recio A (2000) Mechanical bases of frequency tuning and neural excitation at the base of the cochlea: comparison of basilar-membrane vibrations and auditory-nerve-fiber responses in chinchilla. Proc Natl Acad Sci USA 97:11744-11750.

Rutherford MA, Roberts WM (2006) Frequency selectivity of synaptic exocytosis in frog saccular hair cells. Proc Natl Acad Sci USA 103:2898-2903.

Sachs MB, Young ED, Lewis RH (1974) Discharge patterns of single fibers in the pigeon auditory nerve. Brain Res 70:431-447.

Safieddine S, Wenthold RJ (1999) SNARE complex at the ribbon synapses of cochlear hair cells: analysis of synaptic vesicle- and synaptic membrane-associated proteins. Eur J Neurosci 11:803-812.

Schimmang T, Tan J, Muller M, Zimmermann U, Rohbock K, Kopschall I, Limberger A, Minichiello L, Knipper M (2003) Lack of Bdnf and TrkB signalling in the postnatal cochlea leads to a spatial reshaping of innervation along the tonotopic axis and hearing loss. Development 130:4741-4750.

Schmilz B, White TD, Narins PM (1992) Directionality of phase locking in auditory nerve fibers of the leopard frog Rana pipiens pipiens. Journal of Comparative Physiology A: Neuroethology, Sensory, Neural, and Behavioral Physiology 170:589-604.

Schnee ME, Lawton DM, Furness DN, Benke TA, Ricci AJ (2005) Auditory hair cell-afferent fiber synapses are specialized to operate at their best frequencies. Neuron 47:243-254.

Schoffelen RLM, Segenhout JM, van Dijk P (2008) Mechanics of the exceptional anuran ear. J Comp Physiol A Neuroethol Sens Neural Behav Physiol 194:417-428.

Schwaller B (2010) Ca2+ Buffers. In: Handbook of Cell Signaling (Second Edition) (Ralph AB, Edward AD, eds), pp 955-962. San Diego: Academic Press.

Shepherd GM, Barres BA, Corey DP (1989) "Bundle blot" purification and initial protein characterization of hair cell stereocilia. Proc Natl Acad Sci USA 86:4973-4977.

Shin JB, Adams D, Paukert M, Siba M, Sidi S, Levin M, Gillespie PG, Grunder S (2005) Xenopus TRPN1 (NOMPC) localizes to microtubule-based cilia in epithelial cells, including inner-ear hair cells. Proc Natl Acad Sci U S A 102:12572-12577.

Sidi S, Friedrich RW, Nicolson T (2003) NompC TRP channel required for vertebrate sensory hair cell mechanotransduction. Science 301:96-99.

Simmons DD, Bertolotto C, Narins PM (1992) Innervation of the amphibian and basilar papillae in the leopard frog: reconstructions of single labeled fibers. J Comp Neurol 322:191-200.

Smotherman MS, Narins PM (1999) The electrical properties of auditory hair cells in the frog amphibian papilla. J Neurosci 19:5275-5292.

Spassova MA, Avissar M, Furman AC, Crumling MA, Saunders JC, Parsons TD (2004) Evidence That Rapid Vesicle Replenishment of the Synaptic Ribbon Mediates Recovery from Short-Term Adaptation at the Hair Cell Afferent Synapse. J Assoc Res Otolaryngol 5:376-390.

Sudhof TC, Rothman JE (2009) Membrane Fusion: Grappling with SNARE and SM Proteins. Science 323:474-477.

Sugawara M, Murtie JC, Stankovic KM, Liberman MC, Corfas G (2007) Dynamic patterns of neurotrophin 3 expression in the postnatal mouse inner ear. J Comp Neurol 501:30-37.

Tracey WD, Jr., Wilson RI, Laurent G, Benzer S (2003) painless, a Drosophila gene essential for nociception. Cell 113:261-273.

Trapani JG, Nicolson T (2010) Physiological recordings from zebrafish lateral-line hair cells and afferent neurons. Methods Cell Biol 100:219-231.

Trapani JG, Nicolson T (2011) Mechanism of spontaneous activity in afferent neurons of the zebrafish lateral-line organ. J Neurosci 31:1614-1623.

Uthaiah RC, Hudspeth AJ (2010) Molecular anatomy of the hair cell's ribbon synapse. J Neurosci 30:12387-12399.

van Dijk P, Wit HP, Segenhout JM (1989) Spontaneous otoacoustic emissions in the European edible frog (Rana esculenta): Spectral details and temperature dependence. Hear Res 42:273-282.

von Bekesy G (1960) Experiments in Hearing. New York: McGraw-Hill.

Westerfield M (1993) The Zebrafish Book: A Guide for the Laboratory Use of Zebrafish (Brachydanio rerio), Second Edition. Eugene: University of Oregon Press.

Yu XL, Lewis ER, Feld D (1991) Seismic and auditory tuning curves from bullfrog saccular and amphibian papillar axons. J Comp Physiol A Neuroethol Sens Neural Behav Physiol 169:241-248.

Zakon H, Capranica RR (1981) An anatomical and physiological study of regeneration of the eighth nerve in the leopard frog. Brain Res 209:325-338.

Zampini V, Johnson SL, Franz C, Lawrence ND, Münkner S, Engel J, Knipper M, Magistretti J, Masetto S, Marcotti W (2010) Elementary properties of CaV1.3 Ca2+ channels expressed in mouse cochlear inner hair cells. J Physiol (Lond) 588:187-199.